

## **Project**

# **Passenger Aircraft towards Zero Emission with Hydrogen and Fuel Cells**

**Author:** Martin Gollnow

**Supervisor:** Prof. Dr.-Ing. Dieter Scholz, MSME

**Submitted:** 2022-11-16

*Faculty of Engineering and Computer Science  
Department of Automotive and Aeronautical Engineering*

DOI:

<https://doi.org/10.15488/xxxxx>

URN:

<https://nbn-resolving.org/urn:nbn:de:gbv:18302-aero2022-11-16.010>

Associated URLs:

<https://nbn-resolving.org/html/urn:nbn:de:gbv:18302-aero2022-11-16.010>

© This work is protected by copyright

The work is licensed under a Creative Commons Attribution-NonCommercial-ShareAlike 4.0 International License: CC BY-NC-SA

<http://creativecommons.org/licenses/by-nc-sa/4.0>



Any further request may be directed to:

Prof. Dr.-Ing. Dieter Scholz, MSME

E-Mail see: <http://www.ProfScholz.de>

This work is part of:

Digital Library - Projects & Theses - Prof. Dr. Scholz

<http://library.ProfScholz.de>

Published by

Aircraft Design and Systems Group (AERO)

Department of Automotive and Aeronautical Engineering

Hamburg University of Applied Science

This report is deposited and archived:

- Deutsche Nationalbibliothek (<http://www.dnb.de>)
- Repositorium der Leibniz Universität Hannover (<http://www.repo.uni-hannover.de>)
- Internet Archive (<https://archive.org>)  
Item: <https://archive.org/details/TextGollnow.pdf>

This report has associated published data in Harvard Dataverse:

<https://doi.org/10.7910/DVN/CURS1U>

## Abstract

**Purpose** – This project evaluates the feasibility of passenger aircraft designed for Top Level Aircraft Requirements (TLAR) of the Airbus A320 using liquid hydrogen (LH2) and fuel cells to achieve "zero emissions".

**Methodology** – An existing preliminary sizing tool for jet and propeller passenger aircraft (CS-25) is modified to include all elements for LH2 storage and fuel cell integration including electric motors and heat exchangers. Current and possible future technology parameters are determined from a literature review.

**Findings** – The first reference aircraft is the redesign of the A320. The second reference aircraft is a possible turboprop version of the A320 with a cruise Mach number of only 0.65. The turboprop version shows a fuel mass and Direct Operating Costs (DOC) of only 66.1% and 86.5% respectively. Related to the A320 redesign, the fuel cell aircraft has fuel energy and DOC higher by 140% and 221% based on current technology parameters. If plausible future technology parameters are considered, the same values are 74% and 146%. These results show that a fuel cell passenger aircraft is unfeasible with current technology and remains unlikely with future technology. Water emissions can neither be avoided by water storage in flight nor by discarding the water in flight in form of ice cubes.

**Research Limitations** – The impact of liquid water emissions during flight into the atmosphere needs to be investigated further, but seems not to be of major impact according to a recent publication.

**Practical Implications** – The new preliminary sizing tool for fuel cell passenger aircraft is made available and can be used for further studies.

**Social Implications** – So far large fuel cell passenger aircraft were seen as a possible solution to aviation's environmental problems. The general feasibility, energy requirements, environmental and economic impact of hydrogen-electric aircraft can now be discussed by the public.

**Originality** – It seems, there is so far no preliminary aircraft sizing tool for hydrogen-electric aircraft publicly available.

# Passenger Aircraft towards Zero Emission with Hydrogen and Fuel Cells

Task for a *Project*

## Background

According to the EU's "Green Deal", no more net greenhouse gas emissions should be released in 2050. All modes of transportation will have to contribute to this reduction. This includes also aviation. To keep things relatively simple here, the aircraft is considered the system boundary. This is called "tank-to-wake". The options to achieve "zero emission" flight (in these boundaries) are limited. Electric flight with batteries will be limited to short range for years to come. Burning hydrogen in jet engines would be a major step forward, but is clearly no solution to achieve "zero emissions", it emits NO<sub>x</sub> and water vapor. Electric flight with hydrogen and fuel cells could be an option. It has neither CO<sub>2</sub> nor NO<sub>x</sub> emissions. Furthermore, it releases water in liquid form. Discussed is a new short-medium range aircraft to the Top Level Aircraft Requirements (TLAR) of the Airbus A320. Liquid hydrogen (LH<sub>2</sub>) is considered as fuel. Tools for preliminary sizing of jet and propeller passenger aircraft (PreSTo-Classic) are available, but need to be modified for a fuel cell aircraft.

## Task

Task of this project is to determine the feasibility of a fuel cell passenger aircraft powered by LH<sub>2</sub>. The subtasks are:

- Review current aircraft projects with hydrogen and fuel cells.
- Describe and discuss the components of the hydrogen-electric powertrain.
- Summarize fundamentals of preliminary aircraft sizing.
- Show the necessary additions to a tool for preliminary aircraft sizing of propeller aircraft (CS-25) to allow sizing of a fuel cell aircraft.
- Show options how to deal with the emitted water. Can the water be collected in a tank and transported down? Can the water be transformed into ice cubes that are discarded over board? What would (most likely) be the consequences of emitting water depending on cruise altitude?
- Evaluate your designs: Compare the A320 jet with a related propeller aircraft, a hydrogen fuel cell aircraft sized with current technology parameters, and one sized with future technology parameters.

- Summarize the results, draw conclusions, and make recommendations for further research.

The report has to be written in English based on German or international standards on report writing.

# Table of Contents

	Page
List of Figures .....	9
List of Tables.....	12
List of Symbols .....	13
List of Abbreviations.....	18
List of Definitions .....	19
<b>1 Introduction</b> .....	<b>20</b>
1.1 Motivation .....	20
1.2 Title Terminology.....	21
1.3 Objectives .....	21
1.4 Literature Review .....	22
1.5 Structure of the Work .....	22
<b>2 State of the Art</b> .....	<b>23</b>
2.1 ZeroAvia.....	23
2.2 Project Fresson .....	24
2.3 H2Gear .....	26
2.4 FlyZero .....	29
2.5 EXACT.....	36
<b>3 Hydrogen-Electric Powertrain</b> .....	<b>38</b>
3.1 Fuel Containment System .....	38
3.1.1 Tank Shape and Configuration.....	39
3.1.2 Tank Wall Material .....	40
3.1.3 Tank Insulation.....	41
3.1.4 Dimensions of the Tank .....	44
3.1.5 Weight of the Tank.....	44
3.1.6 Hydrogen Fuel System .....	45
3.2 Fuel Cell .....	46
3.2.1 Basis Operating Principle of a Fuel Cell .....	47
3.2.2 Types of Fuel Cells.....	48
3.2.3 Implementation of the Fuel Cell.....	56
3.2.4 Weight of the Fuel Cell .....	57
3.2.5 Oversizing of the Fuel Cell .....	57
3.3 Balance of Plant.....	58
3.3.1 Heat Rejection System .....	59
3.3.2 Air Supply System.....	62
3.3.3 Fuel Conditioning System .....	62
3.3.4 Heat Exchanger System.....	63
3.3.5 Water Management System.....	67

3.3.6	Mass Budget for the Thermal Management System .....	70
3.4	Electric Propulsion and Thrust Devices .....	72
3.4.1	DC/DC Convertor.....	72
3.4.2	Inverter and Distribution .....	73
3.4.3	Electric Motor.....	73
3.4.4	Gearbox .....	74
3.4.5	Propeller .....	74
<b>4</b>	<b>Fundamentals of the Preliminary Sizing</b> .....	<b>76</b>
4.1	Landing.....	76
4.2	Take-off.....	78
4.3	Climb Rate during Second Segment .....	79
4.4	Climb Rate during Missed Approach.....	80
4.5	Cruise.....	81
4.6	Matching Chart.....	83
4.7	Maximum Take-off Mass .....	84
<b>5</b>	<b>PreSTo-Classic-Prop Implementation</b> .....	<b>87</b>
5.1	Preliminary Sizing I.....	87
5.2	Maximum Glide Ratio in Cruise .....	88
5.3	Wetted Area.....	89
5.4	Preliminary Sizing II .....	91
5.5	Matching Chart.....	91
5.6	Fuel Consumption .....	91
5.7	Fuel Containment System .....	93
5.8	Fuel Cell .....	95
5.9	Heat Exchanger .....	99
5.10	Electric Propulsion System .....	101
5.11	Thrust Device .....	102
5.12	Mass of the Hydrogen Powertrain.....	105
<b>6</b>	<b>Evaluation of the Hydrogen-Electric Aircraft</b> .....	<b>108</b>
6.1	Aircraft Requirements .....	108
6.2	Aircraft with Conventional Propulsion .....	108
6.2.1	Conventional Airbus A320.....	108
6.2.2	Turboprop A320 .....	109
6.2.3	Comparison of the Conventional Aircraft .....	110
6.3	Input Data Hydrogen Aircraft .....	112
6.4	Results .....	114
6.5	Evaluation of the Results.....	117
6.5.1	Operating Empty Mass .....	117
6.5.2	Equivalent Fuel Mass .....	119
6.5.3	Length of the Fuselage .....	119

6.5.4	Wingspan and Wing Area .....	120
6.5.5	Take-off Power.....	120
6.5.6	Maximum Take-off Mass .....	121
6.6	Direct Operating Costs .....	121
<b>7</b>	<b>Summary and Conclusions</b> .....	<b>123</b>
<b>8</b>	<b>Recommendation</b> .....	<b>125</b>
	<b>List of References</b> .....	<b>126</b>
	<b>Appendix A – Matching Chart Conventional A320</b> .....	<b>136</b>
	<b>Appendix B – Matching Chart Turboprop A320</b> .....	<b>137</b>
	<b>Appendix C – Matching Chart Hydrogen-Electric A320 Current Technology</b> .....	<b>138</b>
	<b>Appendix D – Matching Chart Hydrogen-Electric A320 Future Technology</b> .....	<b>139</b>

# List of Figures

<b>Figure 1.1</b>	Global carbon dioxide emissions from aviation (Ritchie 2022) .....	20
<b>Figure 2.1</b>	Piper Malibu with hydrogen tanks inside the cabin (Aviation Week 2020)	23
<b>Figure 2.2</b>	Hydrogen storage tank (Innovatus 2020).....	25
<b>Figure 2.3</b>	Heat exchanger (Reaction Engines 2022).....	25
<b>Figure 2.4</b>	Retrofitted Norman Island (Cranfield Aerospace Solutions 2022).....	26
<b>Figure 2.5</b>	19-seat passenger aircraft with hydrogen-electric propulsion (GKN Aerospace 2021) .....	27
<b>Figure 2.6</b>	48-seat passenger aircraft with hydrogen-electric propulsion (GKN Aerospace 2021) .....	27
<b>Figure 2.7</b>	Using liquid hydrogen as a fuel and a cryocooler (Noland 2021) .....	28
<b>Figure 2.8</b>	A fuel-cell system using cryocooling (Noland 2021) .....	28
<b>Figure 2.9</b>	Electric ducted fan (Gullers 2022).....	29
<b>Figure 2.10</b>	Regional aircraft concept (FlyZero 2022b).....	31
<b>Figure 2.11</b>	Location of the fuel cell system (FlyZero 2022b) .....	31
<b>Figure 2.12</b>	Details of the fuel cell system (FlyZero 2022b) .....	32
<b>Figure 2.13</b>	Fuel containment system (FlyZero 2022b).....	32
<b>Figure 2.14</b>	Engine nacelle equipped with electric motor and heat exchanger .....	33
<b>Figure 2.15</b>	General arrangement of the narrowbody concept (FlyZero 2022c).....	33
<b>Figure 2.16</b>	Fuel containment system of the narrowbody concept (FlyZero 2022c) .....	34
<b>Figure 2.17</b>	General Arrangement of the midsize aircraft concept (FlyZero 2022d).....	35
<b>Figure 2.18</b>	Location of the fuel tanks of the midsize aircraft concept (FlyZero 2022d) .....	36
<b>Figure 2.19</b>	Concept of a regional plane (Hartmann 2022).....	37
<b>Figure 3.1</b>	Comparison of specific energy and energy density for different fuels (US Department of Energy 2022) .....	38
<b>Figure 3.2</b>	Storage density of Hydrogen (Wikimedia 2022).....	39
<b>Figure 3.3</b>	Multilayer insulation concept (Khang 2022).....	42
<b>Figure 3.4</b>	Multi-layer vacuum insulation (Kim 2022).....	42
<b>Figure 3.5</b>	Foam Insulation (Khandelwal 2013) .....	43
<b>Figure 3.6</b>	Electrode reactions and charge flow for fuel cell with an acid electrolyte (Dicks 2018).....	48
<b>Figure 3.7</b>	Schematic of a PEMFC (O’Hayre 2016).....	50
<b>Figure 3.8</b>	Schematic of the water movement of a PEMFC (Dicks 2018).....	51
<b>Figure 3.9</b>	Schematic of a AFC (O’Hayre 2016) .....	52
<b>Figure 3.10</b>	Schematic of a PAFC (O’Hayre 2016) .....	53
<b>Figure 3.11</b>	Schematic of a MCFC (O’Hayre 2016).....	55
<b>Figure 3.12</b>	Schematic of a SOFC (O’Hayre 2016) .....	56
<b>Figure 3.13</b>	Balance of plant of a fuel cell propulsion system (FlyZero 2022f) .....	58
<b>Figure 3.14</b>	Fuel Cell cooling methods depending on stack power (FlyZero 2022e).....	60

<b>Figure 3.15</b>	Vapor pressure curve R1233 (Eyerer 2019) .....	60
<b>Figure 3.16</b>	T-S Diagram of vapor compression cycle (FlyZero 2022f).....	61
<b>Figure 3.17</b>	Details of fuel cell air pre-cooling and hydrogen pre-conditioning (FlyZero 2022f).....	63
<b>Figure 3.18</b>	Surface radiator (Stroman 2010).....	64
<b>Figure 3.19</b>	Compact heat exchanger (Stroman 2010).....	64
<b>Figure 3.20</b>	Wing mounted radiator (Hoerner 1965) .....	65
<b>Figure 3.21</b>	Condensers behind the propeller (FlyZero 2022f).....	66
<b>Figure 3.22</b>	Installation of the condenser (light blue) inside the nacelle (FlyZero 2022f) .....	66
<b>Figure 3.23</b>	Positions of the air inlet during flight phases (FlyZero 2022f).....	67
<b>Figure 3.24</b>	Estimation of water production of the fuel cell (FlyZero 2022e) .....	68
<b>Figure 3.25</b>	Hydrogen-electric powertrain with an ice machine (Fuhs 2016).....	70
<b>Figure 3.26</b>	Schematic of the thermal management system (FlyZero 2022f) .....	72
<b>Figure 3.27</b>	Schematic of the electric propulsion (FlyZero 2022b) .....	73
<b>Figure 3.28</b>	Specific power of current electric motors (Hepperle 2012).....	74
<b>Figure 4.1</b>	The preliminary sizing process (Scholz 2015).....	76
<b>Figure 4.2</b>	Definition of the landing field length (Scholz 2015).....	77
<b>Figure 4.3</b>	Definition of the balanced field length (Scholz 2015).....	78
<b>Figure 4.4</b>	Flight phases (Scholz 2015).....	79
<b>Figure 4.5</b>	Generic matching chart (Scholz 2015) .....	84
<b>Figure 4.6</b>	Typical flight phases of a civil transport flight mission (Scholz 2015).....	85
<b>Figure 5.1</b>	Worksheet "Abstract" .....	87
<b>Figure 5.2</b>	Worksheet "Max. Glide in Cruise" .....	88
<b>Figure 5.3</b>	Worksheet "Wetted Area".....	90
<b>Figure 5.4</b>	Worksheet "Fuel consumption" .....	92
<b>Figure 5.5</b>	Worksheet "Fuel Containment System" .....	93
<b>Figure 5.6</b>	Worksheet "Fuel Cell" .....	95
<b>Figure 5.7</b>	Worksheet "Heat Exchanger" .....	100
<b>Figure 5.8</b>	Worksheet "Electric Propulsion System" .....	101
<b>Figure 5.9</b>	Worksheet "Thrust Devices".....	103
<b>Figure 5.10</b>	Worksheet "Mass H2 Powertrain" .....	105
<b>Figure 6.1</b>	Comparison of the results of the preliminary sizing between the conventional and the turboprop version.....	111
<b>Figure 6.2</b>	Comparison of the results of the preliminary sizing between both versions of the hydrogen aircraft related to the turboprop aircraft.....	115
<b>Figure 6.3</b>	Comparison of the results of the preliminary sizing between both versions of the hydrogen aircraft related to the conventional aircraft.....	116
<b>Figure 6.4</b>	Operating empty mass of the hydrogen aircraft related to the reference aircraft.....	117
<b>Figure 6.5</b>	Composition of the operating empty mass of the hydrogen aircraft with current technology .....	118

<b>Figure 6.6</b>	Composition of the operating empty mass of the hydrogen aircraft with future technology .....	118
<b>Figure 6.7</b>	Fuel mass of the hydrogen aircraft related to the reference aircraft .....	119
<b>Figure 6.8</b>	Fuselage length of the hydrogen aircraft related to the reference aircraft .	119
<b>Figure 6.9</b>	Wingspan and Wing Area of the hydrogen aircraft related to the reference aircraft .....	120
<b>Figure 6.10</b>	Take-off Power of the hydrogen aircraft related to the reference aircraft .	120
<b>Figure 6.11</b>	Maximum Take-off Mass of the hydrogen aircraft related to the reference aircraft .....	121
<b>Figure 6.12</b>	DOC of the hydrogen aircraft related to the reference aircraft .....	122
<b>Figure A.1</b>	Matching Chart conventional A320 .....	136
<b>Figure B.1</b>	Matching Chart conventional A320 .....	137
<b>Figure C.1</b>	Matching Chart hydrogen A320 with current technology .....	138
<b>Figure D.1</b>	Matching Chart hydrogen A320 with future technology .....	139

## List of Tables

<b>Table 3.1</b>	Comparison by electrolyte of fuel cell types (O’Hayre 2016).....	49
<b>Table 3.2</b>	Comparison by operating temperature of fuel cell types (Dicks 2018) .....	49
<b>Table 3.3</b>	Comparison between PEMFC and SOFC (FlyZero 2022e) .....	57
<b>Table 3.4</b>	Mass estimation of the thermal management system (FlyZero 2022f).....	71
<b>Table 4.1</b>	Gradient of climb during second segment (EASA 2021) .....	80
<b>Table 4.2</b>	Mission segment mass fractions for regional turboprop (Scholz 2015) .....	85
<b>Table 6.1</b>	Basic requirements of the aircraft .....	108
<b>Table 6.2</b>	Parameter of the conventional A320.....	109
<b>Table 6.3</b>	Parameter of the turboprop aircraft (Johanning 2014).....	110
<b>Table 6.4</b>	Parameter of the conventional aircraft and the turboprop aircraft.....	111
<b>Table 6.5</b>	Adjusted values of the different aircraft version.....	112
<b>Table 6.6</b>	Values of the different hydrogen aircraft version (Kadyk 2018).....	112
<b>Table 6.7</b>	Parameter of the turboprop aircraft and the hydrogen aircraft .....	114
<b>Table 6.8</b>	Relative difference of the values of the hydrogen aircraft related to the turboprop version .....	115
<b>Table 6.9</b>	Parameter of the conventional aircraft and the hydrogen aircraft.....	116
<b>Table 6.10</b>	Relative difference of the hydrogen aircraft related to the conventional version.....	116

## List of Symbols

$A$	Aspect ratio
$a$	Speed of sound / Slope
$B$	Number of Blades
$b$	Wingspan
$B_S$	Breguet range factor
$B_t$	Breguet time factor
$c$	Constant
$C_D$	Drag coefficient
$C_L$	Lift coefficient
$c_p$	Specific heat coefficient
$D$	Drag
$d$	Diameter
$E$	Lift-to-drag ratio
$e$	Oswald factor
$f$	Factor
$g$	Earth acceleration
$h$	Altitude
$j$	Constant
$k$	Constant
$l$	Length
$L$	Lapse rate in troposphere
$m$	Mass
$\dot{m}$	Mass flow
$M_{ff}$	Mission fuel fraction
$N$	Quantity
$n$	Quantity
$of$	Oversizing factor
$P$	Power
$R$	Range
$p$	Pressure
$r$	Radius / Ratio
$t$	Time
$th$	Thickness
$S$	Surface / Distance
$Sr$	Sizing ratio
$T$	Temperature
$V$	Volume / Velocity
$\Delta H_{v,water}$	Latent heat vaporization

## Greek Symbols

$\gamma$	Gradient of climb
$\eta$	Efficiency
$\lambda$	Taper ratio
$\mu$	Friction coefficient
$\rho$	Density
$\sigma$	Relative density
$\phi$	Specific power
$\omega$	Rotational speed

## Indices

<i>0</i>	Initial value
<i>2<sup>nd</sup></i>	2 <sup>nd</sup> Segment
<i>A320</i>	Airbus A320
<i>air</i>	Air
<i>all</i>	All
<i>APP</i>	Approach
<i>AS,TMS</i>	Air system thermal management system
<i>ATTACH</i>	Attachments
<i>AWS</i>	air-water separator
<i>B</i>	Boiling
<i>C</i>	Condenser
<i>cabin</i>	Cabin
<i>CARGO</i>	Cargo
<i>CEL</i>	Compressor electric motor
<i>CFM56</i>	CFM56 powerplant
<i>CLB</i>	Climb
<i>CONV</i>	Electric converter
<i>cool</i>	Coolant
<i>CORE</i>	Core
<i>CP</i>	Coolant pumps
<i>cp</i>	Conventional propulsion
<i>CR</i>	Cruise
<i>CT</i>	Coolant tanks
<i>CY</i>	Cylindrical part of the fuel tank
<i>D</i>	Propeller disc
<i>DES</i>	Descent

<i>E</i>	Engine
<i>e</i>	Engine
<i>ELM</i>	Electric motor
<i>ELMcool</i>	Electric motor cooling
<i>ELPS</i>	Electrical propulsion system
<i>eng</i>	Engine
<i>EV</i>	Expansion valves
<i>EWH</i>	Excessive waste heat
<i>exf</i>	Excluding fuselage
<i>EXV</i>	Excess volume
<i>F</i>	Fuel / Fuselage
<i>FC</i>	Fuel cell
<i>FC,TMS</i>	Fuel cell thermal management system
<i>FCF</i>	Fuel cell feed
<i>FCS</i>	Fuel containment system
<i>FCSYS</i>	Fuel cell system
<i>fc</i>	Fuel cell
<i>FF</i>	Fuel flow
<i>flap</i>	Flap
<i>fuselage</i>	Fuselage
<i>F,erf</i>	Necessary fuel
<i>GEAR</i>	Landing gear / Gearbox
<i>H</i>	Horizontal tail
<i>H2</i>	Hydrogen
<i>hex</i>	Heat exchanger
<i>HPS</i>	Hydrogen propulsion system
<i>HX,air</i>	Heat exchanger air pre-cooler
<i>HX,LH2</i>	Heat exchanger LH2-refrigerant
<i>HX,LH2p</i>	Heat exchanger LH2 pre-cooler
<i>in</i>	Entering
<i>inlet</i>	Air inlet
<i>INS</i>	Insulation of the fuel tank
<i>concrete</i>	Concrete pavement
<i>L</i>	Landing
<i>LFL</i>	Landing field length
<i>LH</i>	Line heater
<i>LH2</i>	Liquid hydrogen
<i>LH2store</i>	Liquid hydrogen storage
<i>liq</i>	Liquid
<i>LOI</i>	Loiter
<i>loiter</i>	Loiter
<i>max</i>	Maximum

<i>md</i>	Minimum drag
<i>MA</i>	Missed approach
<i>ML</i>	Maximum landing
<i>MTO</i>	Maximum take-off mass
<i>MZF</i>	Maximum zero fuel mass
<i>nacelle</i>	Nacelle
<i>OE</i>	Operating empty mass
<i>P</i>	Profile / Propeller
<i>PC</i>	Pipes and coolant
<i>PEL</i>	Power electronics
<i>PL</i>	Payload
<i>PAX</i>	Passenger
<i>prop</i>	Propeller
<i>r</i>	Root
<i>r1233</i>	R1233 coolant
<i>res</i>	Reserves
<i>Rotor</i>	Main rotors
<i>RP</i>	Refrigerant and pipes
<i>RT</i>	Refrigerant tank
<i>S</i>	Stall / Single
<i>SA</i>	Seats abreast
<i>slat</i>	Slat
<i>std</i>	Standard flight
<i>stretch</i>	Stretched Version
<i>TANK</i>	Fuel tank
<i>TAXI</i>	Taxiing
<i>TDS</i>	Thrust devices
<i>TMS</i>	Thermal management system
<i>TO</i>	Take-off
<i>TOFL</i>	Take-off field length
<i>Total</i>	Total
<i>V</i>	Vertical tail
<i>vp</i>	Vapor
<i>W</i>	Wing
<i>water</i>	Water
<i>WH</i>	Waste heat
<i>WP</i>	Water pump
<i>WS</i>	Water system
<i>WT</i>	Water tank
<i>WW</i>	Waste water
<i>WWC</i>	waste water cooling
<i>WWD</i>	waste water discarding

*WWF* waste water freezing  
*wet* Wetted

## List of Abbreviations

AEA	Association of European Airlines
AFC	Alkaline Fuel Cell
CS	Certification Specifications
DC	Direct Current
DLR	Deutsches Zentrum für Luft- und Raumfahrt
DOC	Direct Operating Costs
ICAO	International Civil Aviation Organization
MCFC	Molten Carbonate Fuel Cell
NASA	National Aeronautics and Space Administration
PAFC	Phosphoric Acid Fuel Cell
PEMFC	Proton Exchange Membrane Fuel Cell
PreSTo	Preliminary Sizing Tool
SFC	Specific Fuel Consumption
SOFC	Solid Oxide Fuel Cell
TLAR	Top Level Aircraft Requirements
UN	United Nations

# List of Definitions

## **Airframe**

*“this structure is typically considered to include the fuselage, undercarriage, empennage and wings, and excludes the propulsion system”* (Wikipedia 2023c)

## **Balance of plant**

*“a term generally used in the context of power engineering to refer all the supporting components and auxiliary systems of a power plant to deliver the energy, other than the generating unit itself”* (Wikipedia 2023a)

## **Climate change**

*“changes in the world’s weather, in particular the fact it is believed to be getting warmer as a result of human activity increasing the level of carbon dioxide in the atmosphere”* (Cambridge Dictionary 2022)

## **Ducted fan**

*“consists of the prime mover and the drivetrain. The drivetrain is the group of components that deliver mechanical energy from the prime mover to the driven components”* (Wikipedia 2023b)

## **Efficiency**

*“is a thrust-generating mechanical fan or propeller mounted within a cylindrical duct or shroud”* (Wikipedia 2023d)

## **Fuel efficiency**

*“a measure of how much energy is produced by an engine in relation to the amount of fuel that it uses”* (Cambridge Dictionary 2022)

## **Heat exchanger**

*“is a system used to transfer heat between a source and a working fluid”* (Wikipedia 2023f)

## **Gravimetric energy density**

*“sometimes referred as specific energy is the available energy per mass unit of a substance”* (Energy Education 2023)

## **Power train**

*“consists of the prime mover and the drivetrain. The drivetrain is the group of components that deliver mechanical energy from the prime mover to the driven components”* (Wikipedia 2023b)

## **Turboprop**

*“is a turbine engine that drives an aircraft propeller”* (Wikipedia 2023e)

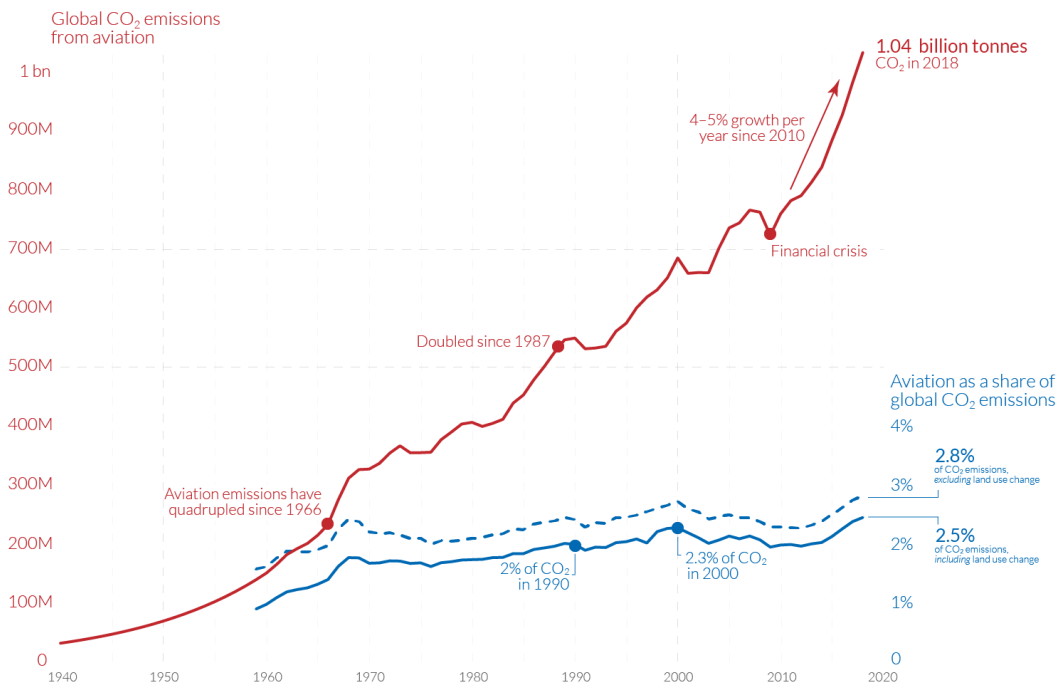
# 1 Introduction

## 1.1 Motivation

In recent years, the awareness of the climate change has become continuously more important to the public. The climate change can be investigated in long-term shifts in temperature and weather patterns. Since the 1800s human activities, especially the burning of fossils fuels, have been the main contributor to the climate change. This has resulted in rising temperature on the earth which led to intense draughts, water scarcity, rising sea levels, flooding, melting polar ice, storms, and declining biodiversity. To prevent this from happening half of the emission must be cut in 2030, and by 2050 net zero emission must be achieved (UN 2022).

### Global carbon dioxide emissions from aviation

Aviation emissions includes passenger air travel, freight and military operations. It does not include non-CO<sub>2</sub> climate forcings, or a multiplier for warming effects at altitude.



OurWorldinData.org - Research and data to make progress against the world's largest problems.  
 Source: Lee et al. (2020). The contribution of global aviation to anthropogenic climate forcing for 2000 to 2018; based on Sausen and Schumann (2000) & IEA.  
 Share of global emissions calculated based on total CO<sub>2</sub> data from the Global Carbon Project. Licensed under CC-BY by the author Hannah Ritchie.

**Figure 1.1** Global carbon dioxide emissions from aviation (Ritchie 2022)

One of the main contributors to CO<sub>2</sub> emissions is the transport sector as shown in Figure 1.1, which includes the aviation. The global aviation contributes 2.5% to the worldwide emission of CO<sub>2</sub> and 3.5% of effective radiative forcing. While the CO<sub>2</sub> emissions results to the burning of fuel, the effective radiative forcing results to the emission of water vapor, soot, and sulfur aerosols. The environmental impact of aviation caused mainly by non-CO<sub>2</sub> forcings to which contrails contribute the most (Ritchie 2022).

There are only two solutions for aviation which offer a reduction of all emissions to zero. The first one is a battery-electric propulsion, while the other one is hydrogen-electric propulsion. Compared to the battery-electric powertrain the hydrogen-electric powertrain offers quicker refueling times and a higher gravimetric density (Thomson 2020).

## 1.2 Title Terminology

### **Passenger**

The term *passenger* means “*a person who is travelling in a vehicle but is not driving it, flying it, or working on it*” (Cambridge Dictionary 2022). In the case of an aircraft, the passenger is not flying it.

### **Aircraft**

An *aircraft* is “*any vehicle, with or without an engine, that can fly, such as a plane or helicopter*” (Cambridge Dictionary 2022).

### **Zero-emission**

The term *zero-emission* refers to “*an engine, motor, process, or other energy source, that emits no waste products that pollute the environment or disrupt the climate*” (Wikipedia 2022).

### **Hydrogen**

*Hydrogen* is “*a chemical element that is the lightest gas, has no color, taste, or smell, and combines with oxygen to form water*” (Cambridge Dictionary 2022).

### **Fuel cell**

A *fuel cell* is “*a device that changes the chemical energy from a fuel into electricity*” (Cambridge Dictionary 2022).

## 1.3 Objectives

The objective of this project is to study the feasibility of a zero-emission propulsion of a passenger aircraft. The propulsion uses fuel cells as power source and hydrogen as propellant.

## 1.4 Literature Review

This calculation and the spreadsheet are based on the initial versions of PreSTo-Classic-Prop and SAS-Part25-Prop by Nita (2008).

The preliminary sizing of this work are mainly based on Scholz (2015) and Loftin (1980) with regard to the certification specifications (CS25) stated in EASA (2021).

In regards of the fuel containment system the work is based on the on “Hydrogen Aircraft Technology” (Brewer 1991). This book features detailed information about the fuel tank, the fuel tank insulation, and the subsystems of the fuel containment system.

The work regarding the fuel cell system, the electric propulsion system, and the thrust devices is based on the various reports of the FlyZero study (FlyZero 2022a ... h).

## 1.5 Structure of the Work

The structure of this work is as follows:

- Chapter 2** describes the existing studies of a hydrogen fueled aircraft.
- Chapter 3** explains the main components of the hydrogen-electric drivetrain.
- Chapter 4** covers fundamentals of preliminary sizing.
- Chapter 5** explains the implementation of a hydro-electric powertrain into PreSTo-Classic-Prop.
- Chapter 6** evaluates the results gained from PreSTo-Classic-Prop.

## 2 State of the Art

This section presents the current studies of hydrogen fueled aircraft and what the distinctive characteristics of those studies are.

### 2.1 ZeroAvia

ZeroAvia is a British-American aircraft developer which was founded in 2017. The focus of ZeroAvia is to develop a scalable hydrogen fuel cell powertrain which replaces conventional engines in existing airframes. The choice of a hydrogen-electric instead of a battery-electric powertrain was due to the better energy-to-weight ratio and the lower operating of the fuel cell (ZeroAvia 2020a).

In the project “HiFlyer I” a six-seat Piper Malibu was chosen to be refitted with a 250 kW hydrogen-electric power train as seen in Figure 2.1. The airframe was chosen because of its popularity, efficiency and it features enough room to house the conversion. The conversion itself was done by replacing the existing conventional engine with two electric motors in line that drive a single shaft. The electric motors were powered by two sets of fuel stacks (Boatman 2019).

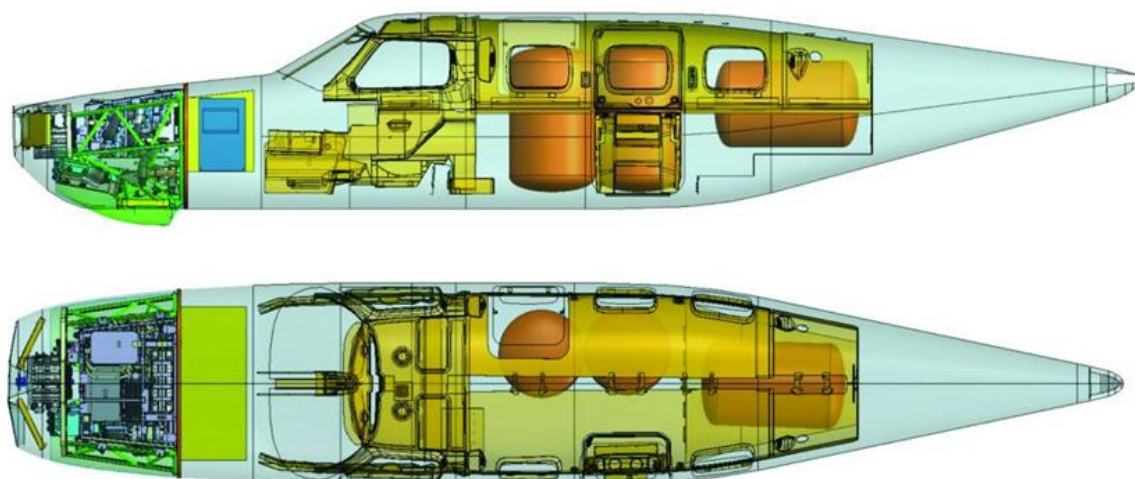


**Figure 2.1** Piper Malibu with hydrogen tanks inside the cabin (Aviation Week 2020)

On 23rd of June 2020 the first electric-powered flight took place with the converted airframe and on the 25th of September 2020 the first hydrogen-electric flight took place (ZeroAvia 2020b).

After the successful testing of the HiFlyer I project the HiFlyer II project was announced. For this project, a two-engine 19-seater Dornier was chosen to be retrofitted with two 600 kW hydrogen-electric powerplants (ZeroAvia 2021a). In the final configuration all components of the hydrogen-electric powertrain including the hydrogen fuel tanks will be carried under the wings. The tanks will hold up to 100 kg of compressed gaseous hydrogen which gives the aircraft a range of about 300 nm. This powertrain will be commercially available by 2024 (Perry 2021a).

Another more powerful hydrogen-electric powertrain ZA 2000 will be available by 2027. It will feature 2 MW and aims at full-size regional aircraft with 40 ... 80 passengers like the ATR 42/72 and the De Havilland Dash 8 (Perry 2021b).

In December 2022, a memorandum of understanding has been signed between ZeroAvia and De Havilland Aircraft of Canada to develop both a line-fit and a retrofit program using Zero Avia's hydrogen-electric powertrain (ZeroAvia 2021b). One of the first customer to enter this program will be the airline Ravn Alaska which placed an order for thirty of Zero Avia's ZA 2000 powertrain to retrofit the airline's De Havilland Dash 8 (ZeroAvia 2022a).

Besides providing hydrogen-electric powertrains for propeller driven aircraft ZeroAvia plans to convert Bombardier CRJ regional jets to hydrogen-electric propulsion (Perry 2021b). For this purpose, ZeroAvia cooperates with MHI RJ Aviation Group which is the world's largest CRJ Series Aircraft Maintenance, Repair and Overhaul company (ZeroAvia 2021c). In August 2022, a memorandum of understanding was signed between ZeroAvia and American Airlines in which American Airlines opts to order 100 of Zero Avia's hydrogen-electric powerplants to power the airline's regional jets (ZeroAvia 2022b).

## 2.2 Project Fresson

This project is being under the development of Cranfield Aerospace Solutions. The project aims at retrofitting a nine-seat Bitten-Norman Islander with a zero-emission powertrain. Initially it was planned to convert into a battery-electric powertrain, but in May 2021 the project shifted to a hydrogen-electric powertrain (Perry 2022a). This shift has been made due to improvements regarding the weight of the hydrogen tanks, the output of the fuel cells and the availability of hydrogen as fuel (Project Fresson 2021).

The fuel tanks which are developed and produced by the Scottish company Innovatus feature a multi-chamber composite design, which makes it lightweight, very high pressure capable and formable. This tank as seen in Figure 2.2 also features the world's highest gravimetric storage density of 10% allowing 5.4 kg of hydrogen storage (Innovatus 2020).



**Figure 2.2** Hydrogen storage tank (Innovatus 2020)

Regarding the fuel cells used in the project the British company Ricardo has developed a hydrogen fuel cell system while improving the balance of plant for a multiple stack layout. This fuel cell system features an efficiency improvement of 5% ... 15% compared to conventional systems (Project Fresson 2021).

With the shift to a hydrogen-electric powertrain the question of the thermal management also appeared (Perry 2021). This issue will be addressed by a heat exchanger from the British company Reaction Engines, as seen in Figure 2.3, which features a lightweight and low drag solution (Reaction Engines 2022).



**Figure 2.3** Heat exchanger (Reaction Engines 2022)

The final configuration of the retrofitted Britten-Norman Islander as seen in Figure 2.4 will be two external tanks, one under each wing, which stores gaseous hydrogen at seven hundred bars. The original two piston engines will be replaced by two 240 kW hydrogen fuel cell systems which will provide power to two 220 kW electric motors each driving a three-bladed propeller. The cooling of the powertrain will be provided by an advanced heat exchanger which is situated at the bottom of the engine nacelle (Cranfield Aerospace Solutions 2022).



**Figure 2.4** Retrofitted Norman Island (Cranfield Aerospace Solutions 2022)

In the next step of the project, which will take place in 2022, the conversion of a 19-seater plane, most likely a Cessna 208 or DHC Twin Otter, to a hydrogen-electric powertrain will be developed. Around 2023 in Phase 3 the design of a completely new 19-seater aircraft is planned. This design should be optimized to hydrogen-electric propulsion from the start of the design phase. In 2029 the final stage is to be taken by designing a completely new aircraft for seventy-five passenger which should feature a hydrogen-electric powertrain (Cranfield Aerospace Solutions 2022).

## 2.3 H2Gear

This program is led by GKN Aerospace, a multinational aerospace components company, from their Global Technology Centre in Bristol and supported by the UK Aerospace Technology Institute. The program aims at developing a liquid hydrogen propulsion system for a sub-regional aircraft that could be scaled up to a larger aircraft (HM Government 2021).

The first step in the program is to develop a 19-seater plane, as seen in Figure 2.5, with a 1 MW hydrogen-electric powertrain. Because of the simplicity of scaling the key elements, such as fuel cells, hydrogen storage tanks and electric motors, larger aircraft with up to 8 MW should be possible (Perry 2022b).

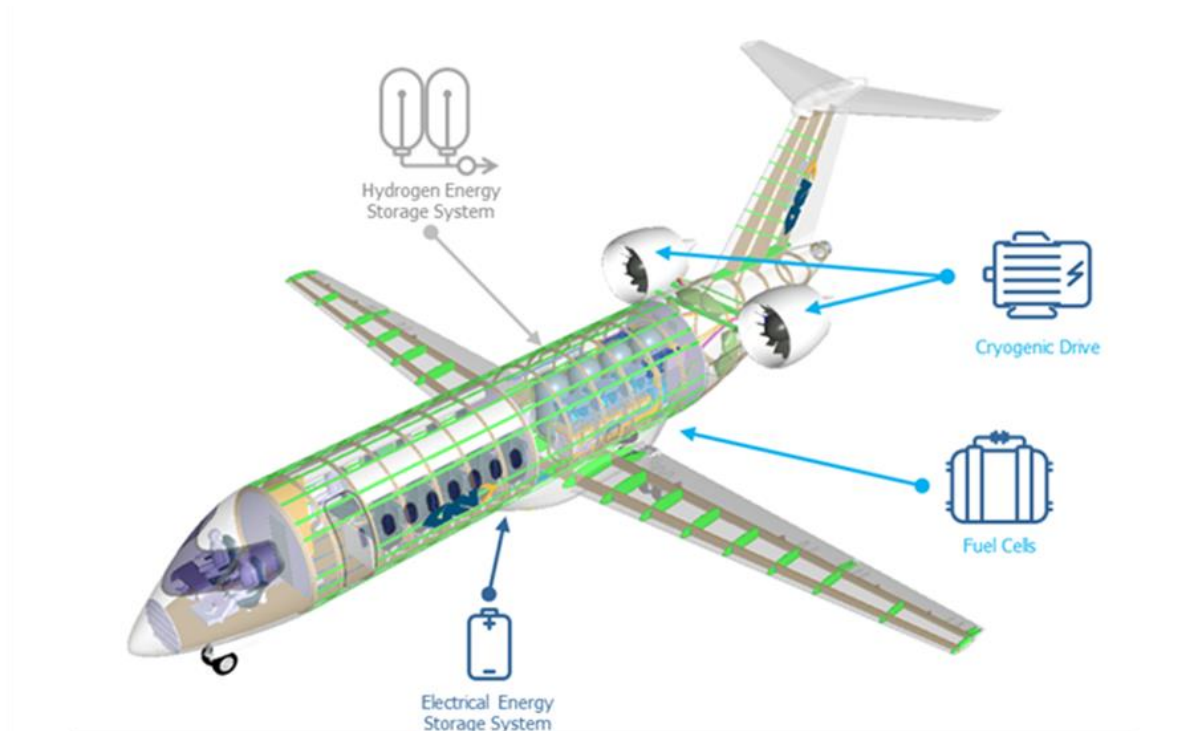


**Figure 2.5** 19-seat passenger aircraft with hydrogen-electric propulsion (GKN Aerospace 2021)

Based on this assumption there is a concept for a 48-passenger regional aircraft, as seen in Figure 2.6, with a range of 934 miles. This concept features a liquid hydrogen fuel system, fuel cell power system, optimized electrical network and cryogenic motor drive technology. To prevent the aircraft from emitting moisture because of water being the only byproduct due to the hydrogen-electric powertrain the aircraft will equipped with a GKN smart venting system (GKN Aerospace 2021).

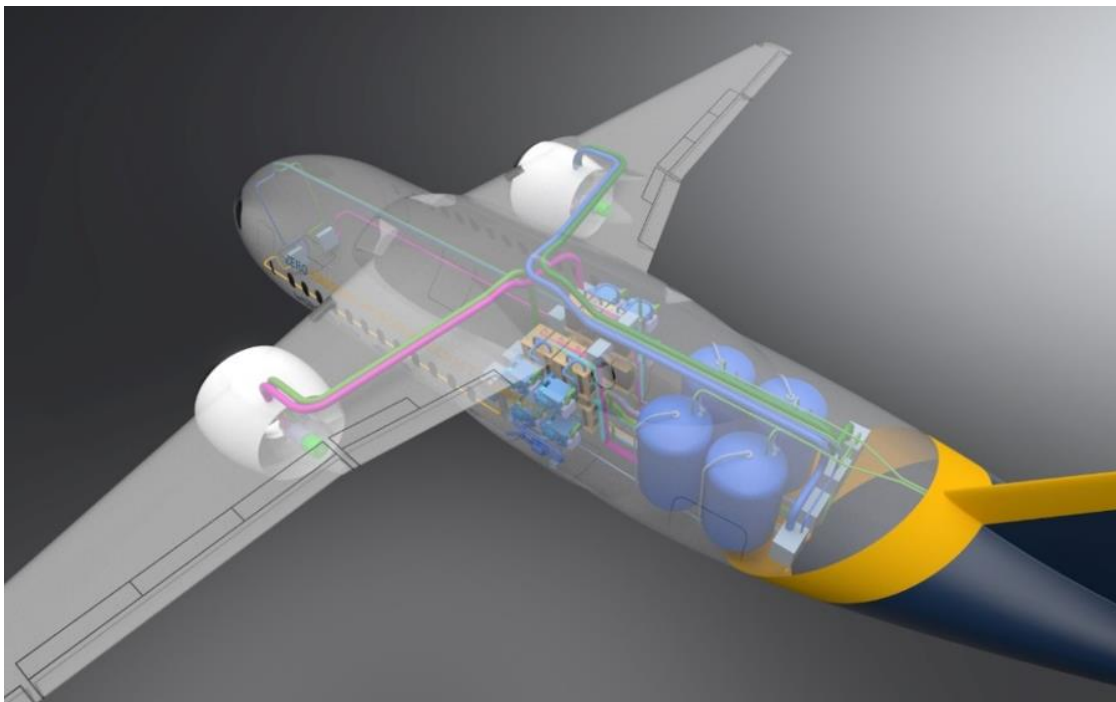


**Figure 2.6** 48-seat passenger aircraft with hydrogen-electric propulsion (GKN Aerospace 2021)

One outstanding feature in this project is development of the hyperconducting network and cryogenic motor technology. This system will use the stored liquid hydrogen as a heat sink for cooling the electrical conductors to temperature below  $-200\text{ }^{\circ}\text{C}$  which significantly reduce their electrical resistivity. This concept is seen in Figure 2.8. This facilitates electrical power distribution leading to lighter electric cables and lighter electric motors with higher efficiency (GKN Aerospace 2002).

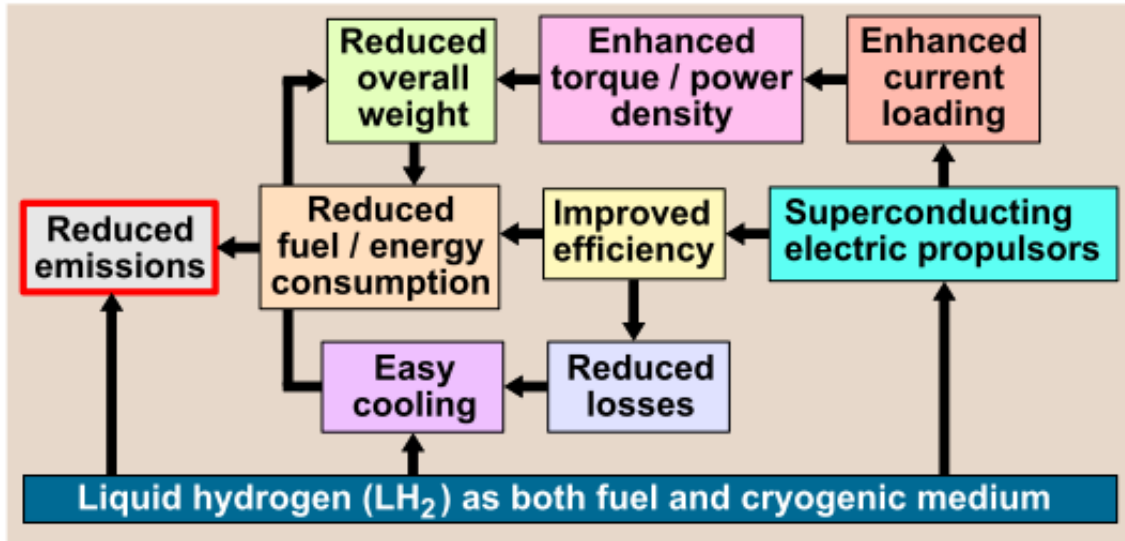


**Figure 2.7** Using liquid hydrogen as a fuel and a cryocooler (Noland 2021)

This weight reduction is significant when remembering that all-electric aviation also implements the need of replacing the conventional propulsors with electric motors. Such a configuration is seen in Figure 2.9. Today's electric machinery in the multimewatt range is about 50 to 100 times too heavy for aircraft applications. But the weight of the electric equipment can be significantly reduced by using the onboard liquid hydrogen both as fuel and cryogenic cooling medium. The temperature of the evaporation of liquid hydrogen is also the temperature needed for superconducting machines. Due to having no electrical resistance superconducting machines can manage massive amounts of current and cause only minimum amounts of dissipating heat which results in an ultrahigh efficiency and a power-to-weight ratio at least two to three times higher compared to conventional components (Noland 2021).

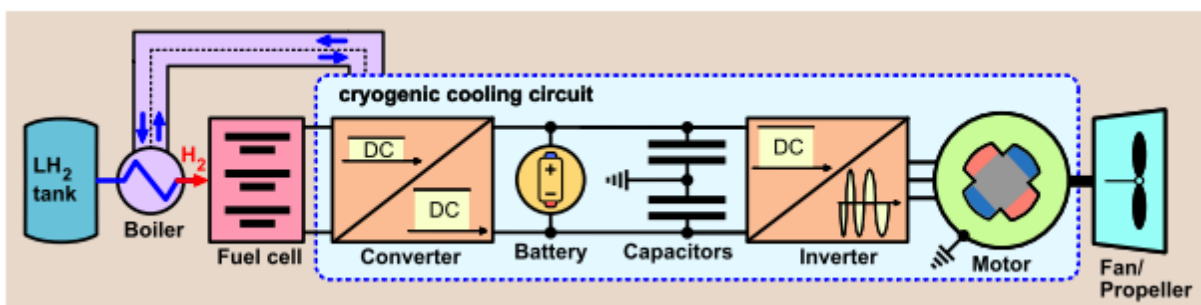


**Figure 2.8** A fuel-cell system using cryocooling (Noland 2021)

Unlike the hyperconducting systems superconducting systems exhibits no electrical resistance but hyperconducting systems do use more conventional conductor materials which make them more feasible in the next future (GKN Aerospace 2021).

The final part of the propulsion system is a low pressure-ratio ducted fan (GKN Aerospace 2022) as seen in Figure 2.10. This fan is being developed in the EleFanT project in cooperation with the Swedish Royal Institute of Technology. The project aims at researching the aerodynamic design performance, noise and manufacturing technology for a ducted fan powered by electricity (Sampson 2021).

Compared to a propeller-driven configuration a ducted fan emits less noise, is easier to integrate on the fuselage, as it would not be limited to wing-mounted configurations. A fan is also safer in the event of an engine failure due to the nacelle (Gullers 2022).



**Figure 2.9** Electric ducted fan (Gullers 2022)

Another issue which is getting more important when enlarging the system is thermal management, the larger the aircraft becomes the more difficult is the removal of the heat which is generated by the hydrogen-electric powertrain. GKN is looking at solutions to dissipate the waste heat through aircraft structures and other systems like heat exchangers (Perry 2022).

## 2.4 FlyZero

This study is in-depth to develop a zero-carbon emission aircraft until 2030. The study is led by the Aerospace Technology Institute and funded by the UK government (HM Government 2021).

The study aims at assessing the design challenges, manufacturing demands, operational requirements, and market opportunities of different zero-carbon emission aircraft concepts. Concerning these issues, the study identified thirteen technology topics which were fundamental for realizing hydrogen fueled aircraft (FlyZero 2022a).

Six of these topics were fundamental technologies:

- hydrogen gas turbine and thrust generation,
- electric propulsion system,
- fuel cells,
- cryogenic hydrogen fuel system and storage,
- thermal management,
- aerodynamic structures.

Another seven topics were critical to ensure that hydrogen aircraft are commercially and operationally enabled (FlyZero2022a):

- aircraft systems,
- airport, airlines, airspace,
- materials,
- lifecycle impact,
- sustainable cabin design,
- compressed design and validation,
- manufacturing.

Based on these criteria three different concepts have been implemented (FlyZero 2022a):

- a regional aircraft, which should demonstrate the feasibility of fuel cell aircraft. The main focus of this concept was the aircraft performance and cost relative to a kerosene or SAF fueled aircraft as well as the integration of the fuel cell,
- a narrowbody concept which focus on turnaround time, aircraft utilization and flexibility,
- a midsize concept was made longer haul flights regarding the view that SAF was deemed more appropriate for long-haul flight.

The regional market segment is regarded as the entry point for hydrogen fueled aircraft. For this concept, the ATR 72-600 has been chosen as the reference aircraft. According to the typical characteristics of a regional aircraft the requirements for the concept as seen in Figure 2.11 were set at eight hundred nautical miles range and a cruise speed of 325 knots while carrying 75 passengers (FlyZero 2022a).



**Figure 2.10** Regional aircraft concept (FlyZero 2022b)

The concept features a hydrogen-electric powertrain. During the analysis of this concept the feasibility of this concept for this powertrain in the regional segment has been proven while consuming 10% more energy than the reference aircraft.

Regarding the components of the powertrain the sizing of the fuel cells is being oriented at the peak power demand which is during take-off. Regarding the fact that fuel cell efficiency increases if the power is reduced relative to maximum an oversizing of the fuel cells might be beneficial in terms of fuel consumption and reduced weight of the thermal management system at the cost of increased fuel cell weight. The fuel cells and its system component are located under the rear cabin floor in an unpressurized area as seen in Figure 2.12 with details in Figure 2.13 (FlyZero 2022b).

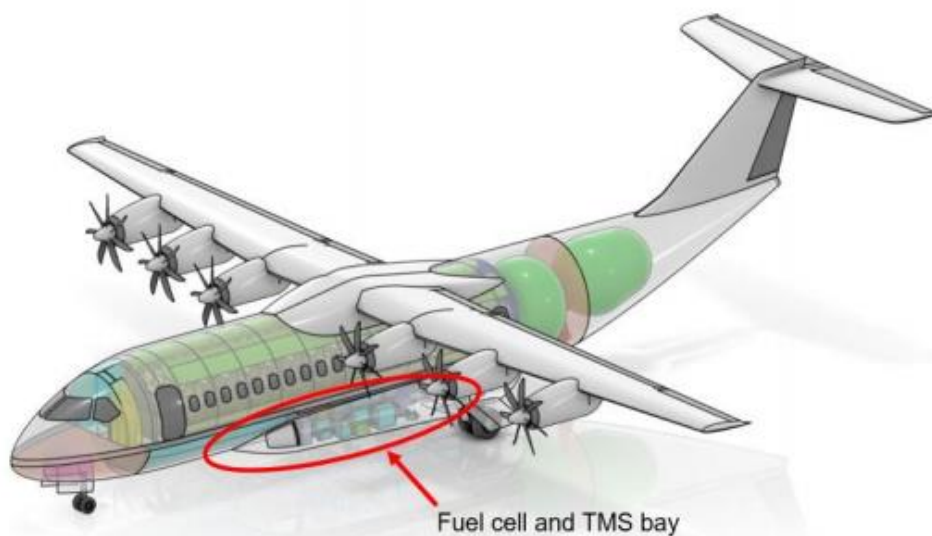


**Figure 2.11** Location of the fuel cell system (FlyZero 2022b)

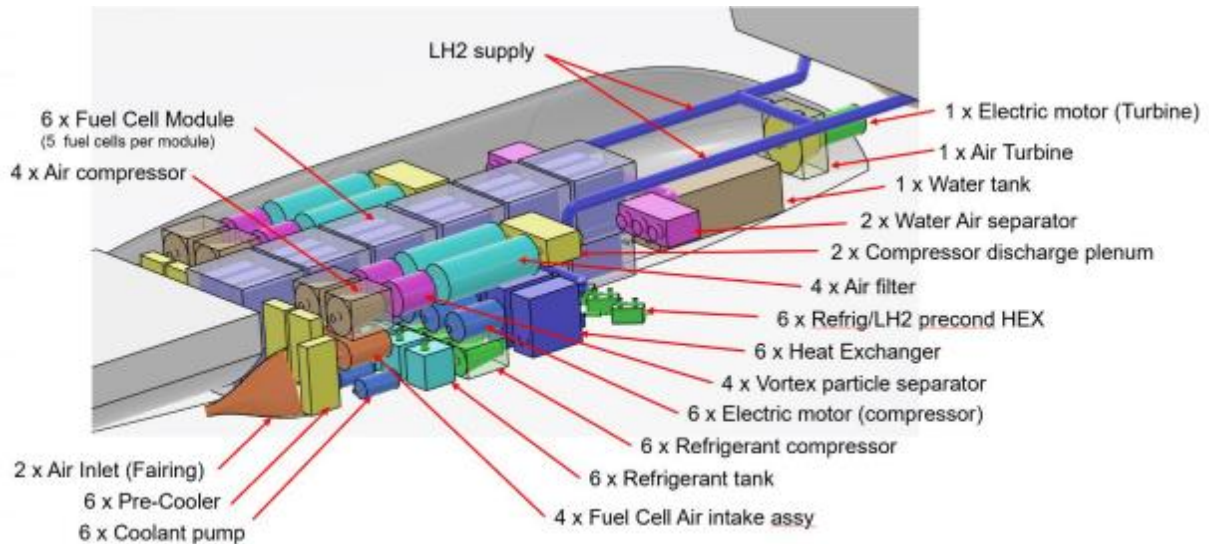


**Figure 2.12** Details of the fuel cell system (FlyZero 2022b)

The hydrogen storage tanks are in the rear of the fuselage as seen in Figure 2.14. To make the hydrogen storage more efficient the diameter of the fuselage has been increased. It was chosen to use a vacuum insulation instead of a foam insulation due to the additional space required by a foam insulation to prevent a further increasing of the fuselage's diameter (FlyZero 2022b).

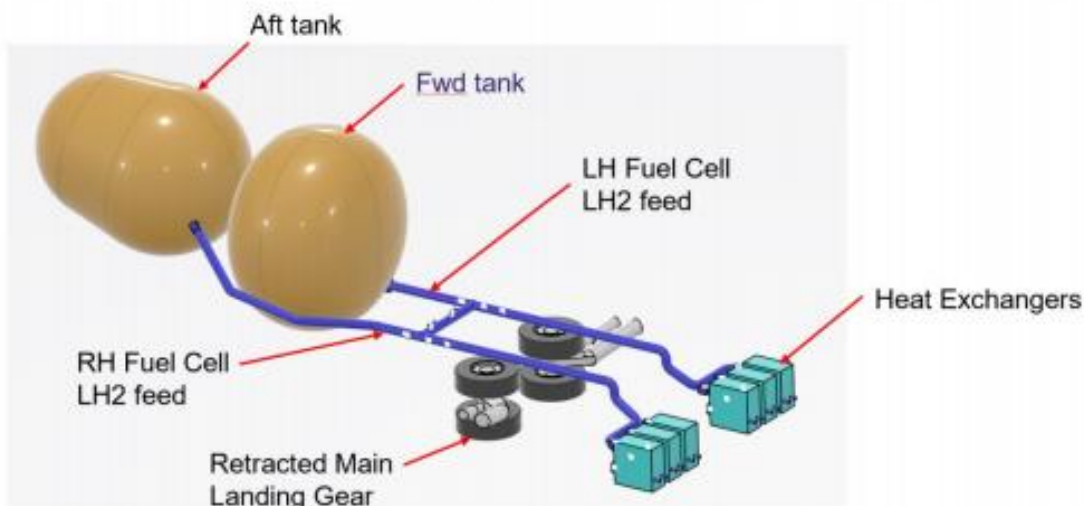


**Figure 2.13** Fuel containment system (FlyZero 2022b)

The propulsion system includes six electric motors each housed in a nacelle driving propellers as seen in Figure 2.15. Each of these nacelles also included heat exchangers which are part of the electrical and thermal management system (FlyZero 2022b).

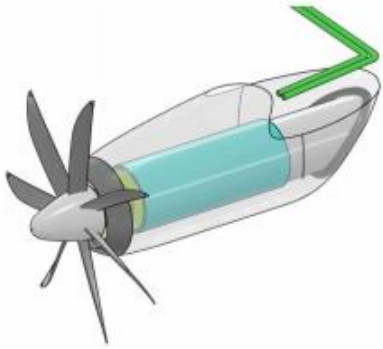


**Figure 2.14** Engine nacelle equipped with electric motor and heat exchanger

It is also noted that the thermal management system is significantly important for the overall weight of the system. Due to the hydrogen-electric powertrain water will be the only byproduct. As the emission of water must be avoided during the flight phase of take-off and initial climb because water would reduce runway friction a storage tank for the water being produced by the fuel cells has been added (FlyZero 2022b).

The narrowbody market segment makes up 67% of new commercial aircraft acquisitions between 2030 and 2050. But this segment is very unlikely to be the entry point of hydrogen fueled aircraft. The Airbus A 320-200 has been chosen as the reference aircraft for this concept, as seen in Figure 2.16, and accordingly the range was set at 2400 nautical miles at a cruising speed of 450 knots while carrying 180 passengers (FlyZero 2022a).

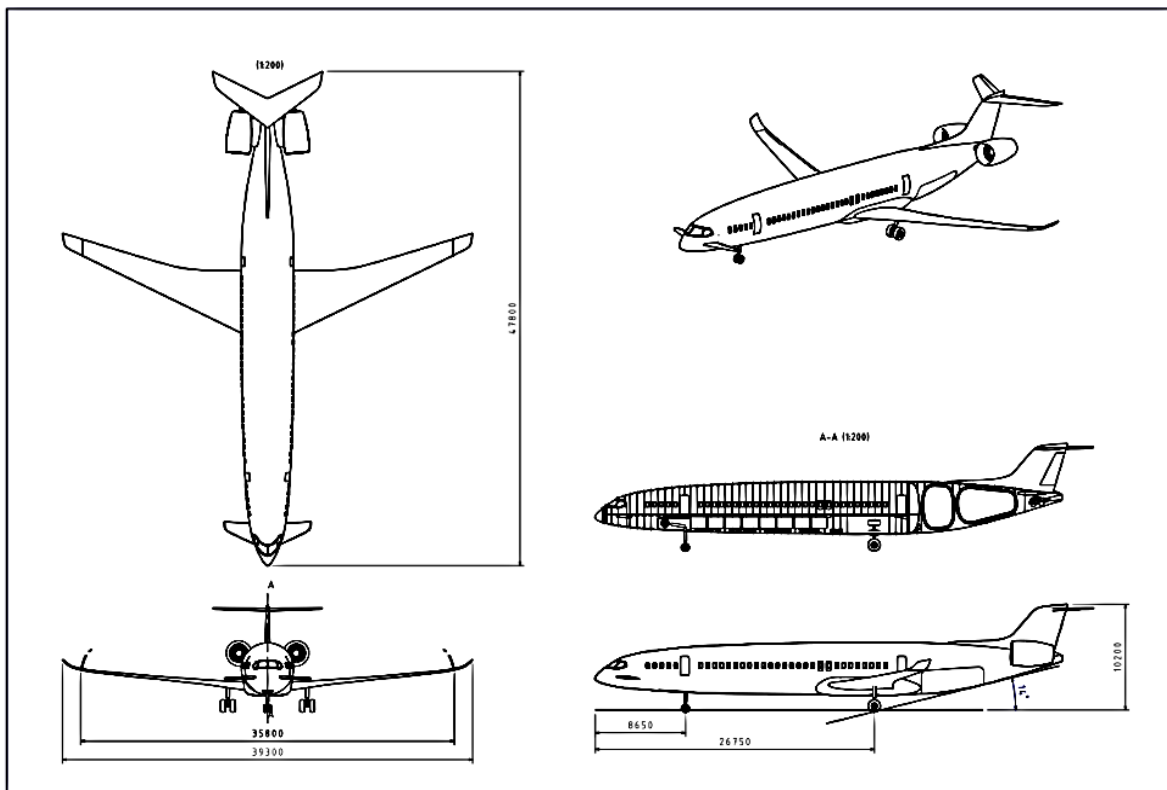


**Figure 2.15** General arrangement of the narrowbody concept (FlyZero 2022c)

The propulsion is a hydrogen-combustion powertrain. This includes two hydrogen tanks, fuel systems and jet engines. The propulsion and fuel system are located at the rear of the fuselage which results in a more compact layout than a layout with a wing mounted propulsion. This configuration also results in minimizing the pipe length of the hydrogen fuel lines which reduces the area of the aircraft containing hydrogen and the risk of a hydrogen leak. On the other hand, can such a configuration cause center of gravity issues which might imply aerodynamical changes to the control surfaces (FlyZero 2022a).

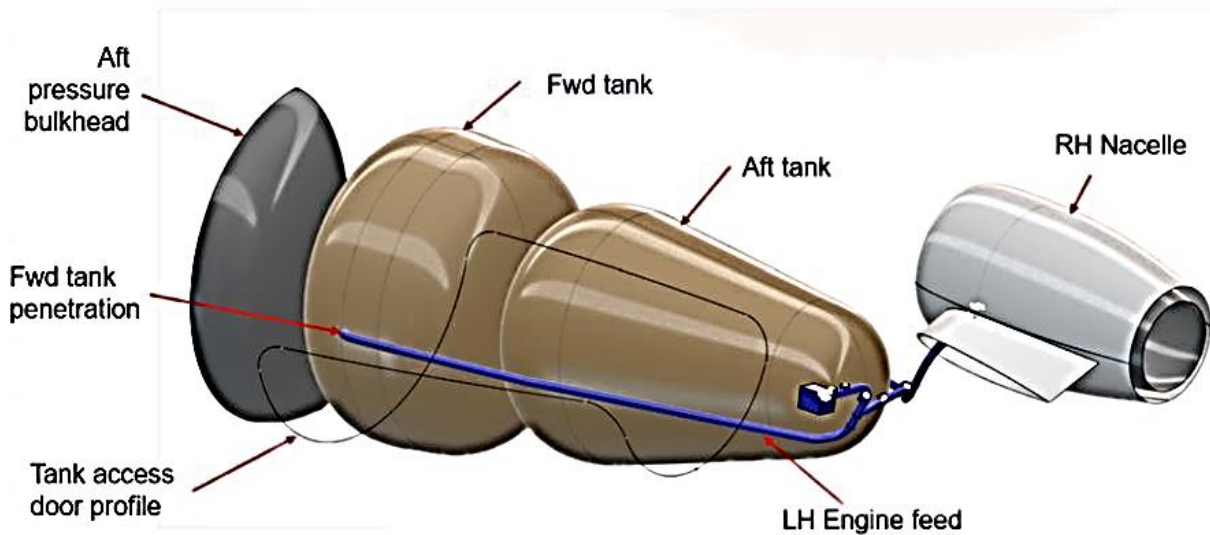


**Figure 2.16** Fuel containment system of the narrowbody concept (FlyZero 2022c)

Due to the hydrogen storage tanks in the rear of the fuselage and the absence of wing mounted propulsion devices there is a possibility to optimize the wings for wing loading and aeroelastic purposes (FlyZero 2022a).

Regarding the fuselage diameter which has been constant in the regional concept for the narrowbody concept a diameter has been chosen which was getting wider at the rear of the fuselage where the hydrogen storage tanks are situated. This configuration would improve natural laminar flow and therefore reduce drag (FlyZero 2022a).

The third and last concept is a midsize plane as seen in Figure 2.18. Due to the higher development costs the market availability of hydrogen fueled aircraft in this segment is unlikely to happen in the foreseeable future. The reference aircraft is the Boeing 767-200 ER which is a long-range widebody aircraft. The design range for the concept was set at 5750 nautical miles at a cruise speed of 460 knots while carrying 280 passengers. The powertrain is hydrogen-combustion which includes two jet engines located one under each wing (FlyZero 2022a).

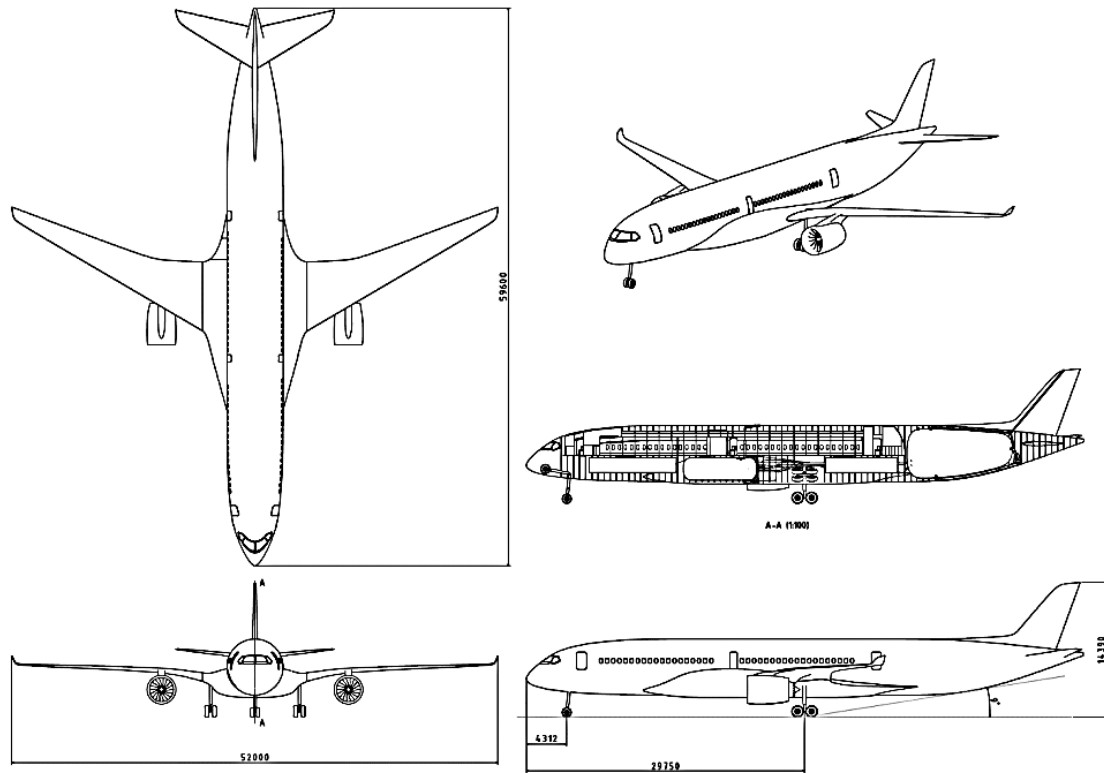


**Figure 2.17** General Arrangement of the midsize aircraft concept (FlyZero 2022d)

The location of the hydrogen tank has been identified as a main issue regarding the aircraft architecture. It was chosen to install one tank in the aft of the fuselage and two forward tanks forward the wing beneath the cabin floor which are all unpressurized areas of the plane as seen in Figure 2.19. The configuration has been chosen to address weight and balance issues (FlyZero 2022a).

Like all other concepts the fuselage diameter is linked to the hydrogen storage tank diameter. As the hydrogen storage becomes more efficient the tank diameter increases there is a need to increase the fuselage diameter. This comes at the expense of increased drag. Another issue due to the tank in the rear and the wing mounted propulsion units is the length of the hydrogen fuel lines. Because leakage can occur it is critical to have the fuel lines in unpressurized areas (FlyZero 2022a).

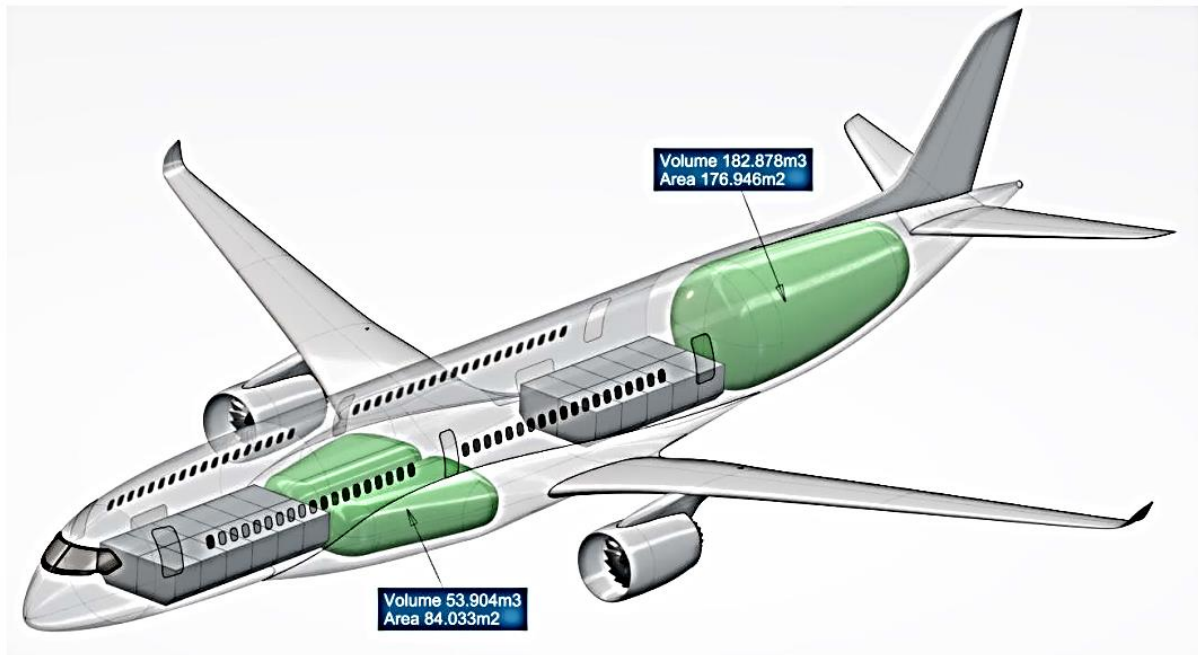


**Figure 2.18** Location of the fuel tanks of the midsize aircraft concept (FlyZero 2022d)

## 2.5 EXACT

The German Aerospace Center abbreviated DLR is also conducting a study to develop an ecologically efficient medium-haul aircraft into commercial service by 2040. This study is part of the Exploitation of Electric Aircraft Concepts and Technologies (“EXACT”) project which includes twenty institutes of the DLR from the fields of aeronautics, energy, and atmospheric research. This project aims at combining environmental impacts with economic necessities from the concept phase onwards. It also regarded as a core understanding that conventional aircraft engines have no or little room to be optimized for further reduction of carbon dioxide emissions. Because of this an innovative approach is being made by the introduction of new propulsion concepts which utilizes hydrogen and electric components (Hoidis 2020).

To put these efforts into reality in the first different hydrogen-electric concepts and plane configurations will be assessed. It also will be evaluated how the different concepts cope with the infrastructure of airports and how the propulsion concepts effect the environment especially their climatical impact will be noted (DLR 2021).

A concept, which is pictured in Figure 2.19, has been made for this project is a regional plane with a range of 1000 nautical miles at a cruising speed of about 600 km/h while carrying seventy passengers. The aircraft features a hydrogen-electric powertrain with a distributed propulsion that consists of ten propulsion units. Each propulsion unit is housed in a nacelle beneath the wing and includes a propeller, electrical motor, PEM fuel cell, battery, heat exchanger and power electronics. The battery will provide additional power during phases of

peak power demands like take-off. The implementation of a battery could result in a smaller and lighter fuel cell because the size of the fuel has not been oriented at the peak power demand. When comparing the energy consumption of this fuel cell powertrain to the jet engine power train of a regional jet a 20% less energy consumption of this concept can be noted. On the system level of the whole plane the hydrogen-electric concept has a 10% higher power consumption when compared to a conventional aircraft. This higher power consumption results due to the subsystems of the hydrogen-electric powertrain especially the thermal management system and the fuel containment system (Hartmann 2022).

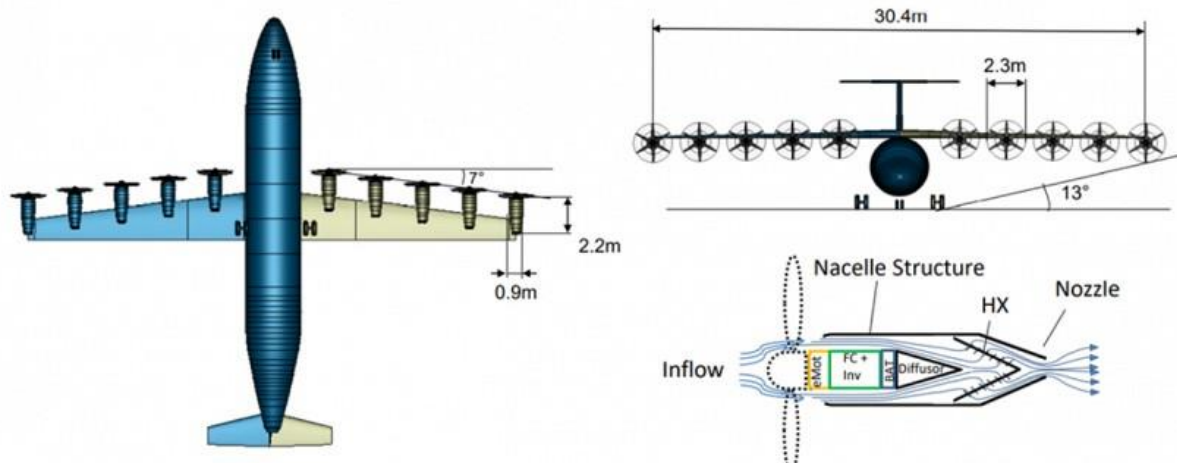


**Figure 2.19** Concept of a regional plane (Hartmann 2022)

For evaluating innovative approaches in electric powertrains, the DLR has acquired a Dornier 228 in cooperation with MTU Aero Engines. This plane will be used as a testbed for the components of the powertrain concepts and in later stages it is planned to replace one of the two conventional powerplants by a 600 kW hydrogen-electric propulsion unit. In this configuration the electrical motor will be mounted in the nacelle beneath the wing. The fuel cell and the hydrogen storage tank will be located inside the fuselage. There is also the need of the implementation of a cooling system due to the heat being produced by the fuel cells (DLR 2021).

This project is unlike other retrofit programs not limited to the retrofit of an existing aircraft; the focus is working as a testbed to gain practical knowledge about the powertrain concepts. This makes the conclusions drawn from this project transferable to other projects in the field of hydrogen-electric aviation. It also gives the opportunity to assess questions of aviation law and registration issues. (Sebayang 2022).

### 3 Hydrogen-Electric Powertrain

In this section the parts of the hydrogen-electric of the hydrogen-electric powertrain will be explained and how the various parts are implemented in an aircraft.

#### 3.1 Fuel Containment System

One major difference between a conventional kerosene fueled aircraft and a hydrogen fueled aircraft is the fuel storage. In kerosene fueled airliners the fuel is stored in integral tanks inside the wings or the fuselage. The fuel itself is stored in liquid state at ambient temperatures. Kerosene has a gravimetric energy content of 42.8 MJ/kg and a volumetric energy content of 35 MJ/L. Hydrogen gas at ambient conditions a gravimetric energy of 120 MJ/kg and a volumetric energy content of 0.01005 MJ/kg. Compared to the energy contents of kerosene the gravimetric energy content is about 2.8 times which significantly reduces the fuel weight. The volumetric energy content at ambient conditions is vastly inferior to those of kerosene. This will result in significantly larger storage volume when hydrogen is stored at ambient condition (Verstraete 2010). This comparison between hydrogen and other propellants can be seen in Figure 3.1.

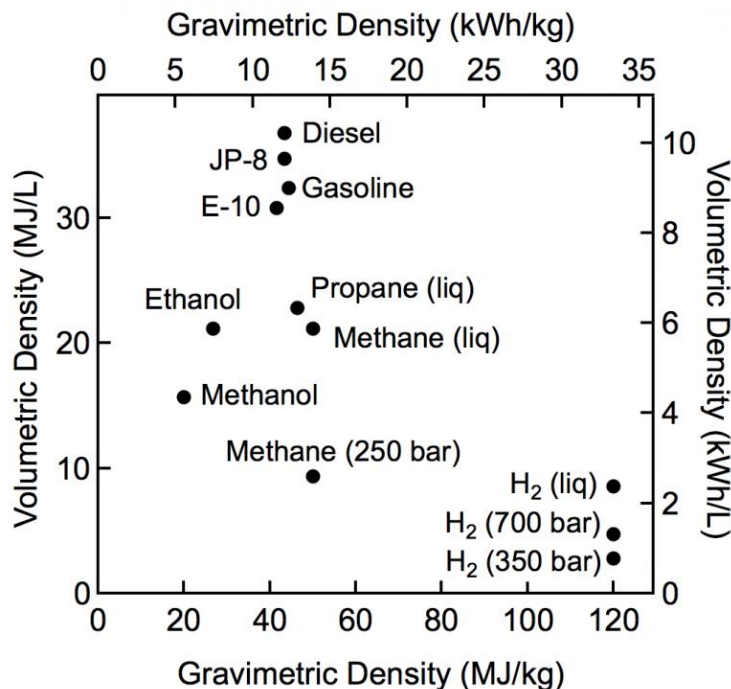


**Figure 3.1** Comparison of specific energy and energy density for different fuels (US Department of Energy 2022)

Therefore, the major challenge is to achieve the highest volumetric density possible. There are two conventional methods of storage, by storing hydrogen as a compressed gas or as a cryo-

genic liquid. For the use in an aircraft the cryogenic hydrogen storage allows to almost double the volumetric capacity compared to the storage as a compressed gas. This significantly reduces the mass of the tank (Verstraete 2010).

When stored as a cryogenic liquid the hydrogen is stored in a liquid state at a temperature of around  $-260\text{ °C}$  at a density of  $71\text{ kg/m}^3$  as seen in Figure 3.2. Regarding the hydrogen storage temperature, the tanks themselves need to be insulated to reduce the boil-off of the liquid hydrogen and to keep the stored hydrogen at cryogenic temperatures. The tanks also need to be sealed off from the atmosphere to prevent air from entering. If the air enters the tanks the stored hydrogen will freeze and block the flow lines. The tanks must be kept at a constant pressure usually around  $1.45 \cdot 10^5$  to minimize boil-off (Colozza 2002).

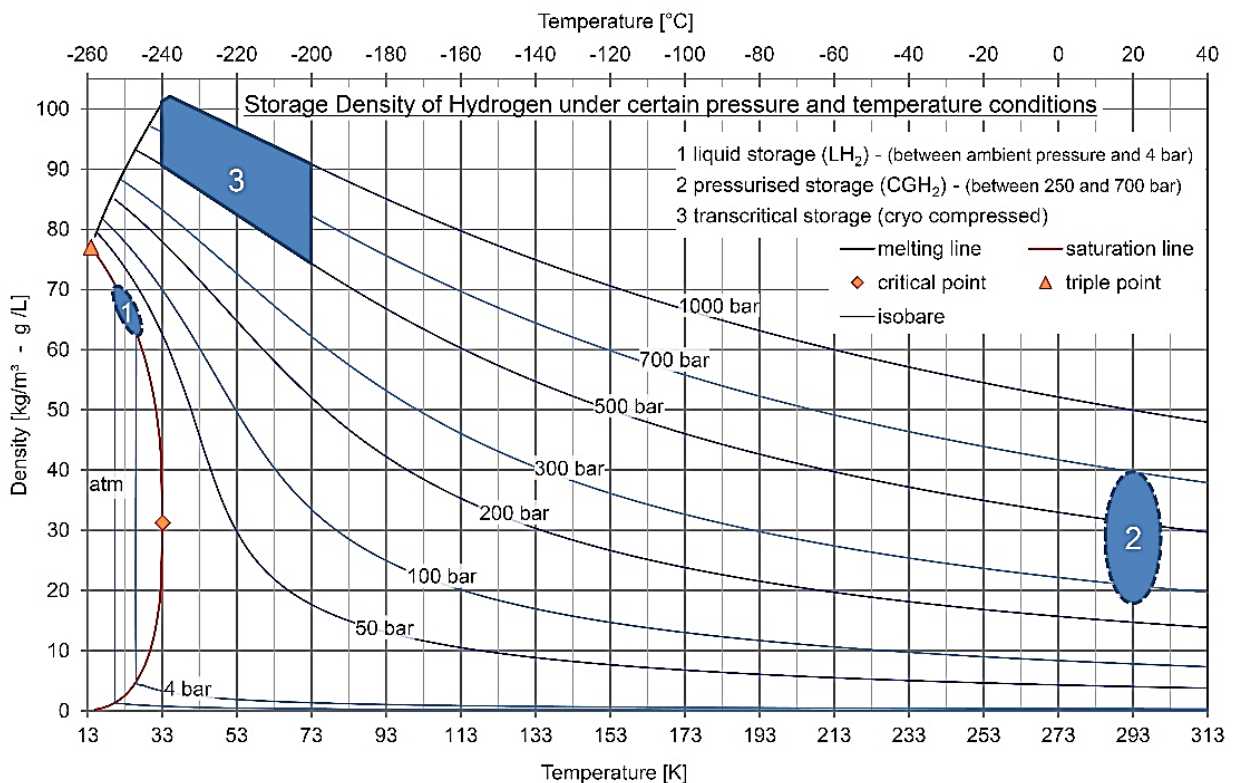


**Figure 3.2** Storage density of Hydrogen (Wikimedia 2022)

### 3.1.1 Tank Shape and Configuration

As mentioned earlier due to larger volume needed for storing hydrogen the configuration of the fuel tank needs to have an innovative approach as the conventional way of storing the fuel inside the wing is no more suitable.

From the load perspective there are two options: integral and non-integral structures of the airframe. Integral tanks are a structurally integrated part of the airframe and as such it must

resist the loads to which the supporting structure of the aircraft is exposed (Winnefeld 2018). Because the fuel containment system is located inside the fuselage it is also limited in its geometry by the fuselage this can result in decreased efficiency of the hydrogen storage (Khandelwal 2013). Non-integral tanks are subject to the load of their fuel containment. The tanks are located outside the fuselage which causes drag and integration problems (Khandelwal 2013).

Comparing both options, the space inside the fuselage can be better used when installing an integral tank and the ease of maintenance of an integral tank is inferior compared to a non-integral tank (Brewer 1991).

The tank shape itself could be spherical or cylindrical. A spherical tank would have less surface area for a given volume which also results in lesser passive heat flux compared to a cylindrical tank. The cylindrical tank is easier to produce and to integrate in the mostly cylindrical fuselage of the aircraft which results in a better volumetric efficiency (Khandelwal 2013).

Regarding the number of the tanks a single tank offers the lowest weight because the surface of the tank is less than a configuration with more than one tank. Because of the passenger cabin a hydrogen tank can only be installed in front or in aft of the fuselage. The usage of only one tank will result in a change of the point of gravity of the aircraft during operations because of fuel consumption. This could cause difficulties in balancing the plane which would make a larger horizontal and vertical tail necessary. This could also be solved by installing two tanks in front and aft of the passenger cabin (Verstraete 2010).

### **3.1.2 Tank Wall Material**

The material of the tank will face different issues which relate to its usage inside a plane but also due to the storage conditions of the hydrogen. For the use inside a plane weight consideration are important a low density of the material is desired. Due to pressure loading of the high strength, high fracture toughness and high stiffness must be archived to prevent fatigue. But also, the cryogenic storage temperature will make a lot of material getting brittle and some materials are porous to hydrogen. Under these circumstances a tank made of aluminum seems to be the best option as aluminum resists hydrogen embrittlement and features low density and high strength (Verstraete 2010). For future aircraft application the monolithic metals could be replaced by composite materials which offer significant weight savings (Winnefeld 2018).

### 3.1.3 Tank Insulation

The insulation is necessary to reduce the amount of boil-off from the storage tanks. The boil-off itself occurs when the liquid boils and changes from liquid state into gaseous form. The boil-off is being caused by heat transfer and permeation from the outside. The insulation reduces the thermal conductivity and prevents the air from permeating. Without a proper insulation the use of liquid hydrogen would be impossible (Verstraete 2010).

The insulation could be attached to the outside or the inside of the hydrogen storage tank. If the insulation is located inside the tank it is exposed to liquid hydrogen at cryogenic temperatures. Due to the heat transfer from the outside liquid hydrogen situated at the boundaries turn into gaseous hydrogen and diffuses into the tank wall which results in an increase in thermal conductivity which creates additional heat transfer and therefore boil-off. To prevent this the insulation must be impermeable to gaseous hydrogen. The external insulation is attached to the outside of the tank. Due to the low temperatures needed for cryogenic storage the tank significantly contracts and expands during operations which causes attachment issues as well as thermal leaks. Therefore, the insulation must be impermeable to air to prevent cryopumping and also being protected against mechanical damage (Khandelwal 2013).

As a material impermeable to liquid hydrogen is not to be found an external insulation is favorable. To prevent attachment issues the tank must kept in cooled conditions except during maintenance (Verstraete 2010).

### Multilayer Insulation

This insulation consists of several alternating layers of a low conductivity spacer and a low emission foil as seen in Figure 3.3. The foil is made of metal and the spacer are of insulating material like glass fiber, polyester etc. This combination function as a thermal radiation shields perpendicular to the direction of the heat flow. The optimal number of layers is around 60 ... 100, a further increase in layers will result in additional heat transfer due to conduction (Khandelwal 2013). Another import issue is the degrading performance if the multilayer insulation is operated at pressures higher than 0.001 mbar. This makes a vacuum shielding of the insulation necessary. In the case of a vacuum leak the insulation would lose its thermal insulation which would result in a massive boil-off of the stored hydrogen. This would removing the boiled-off hydrogen necessary to prevent the tank from bursting. A massive loss of propellant would cause an emergency during a flight mission (Verstraete 2010).

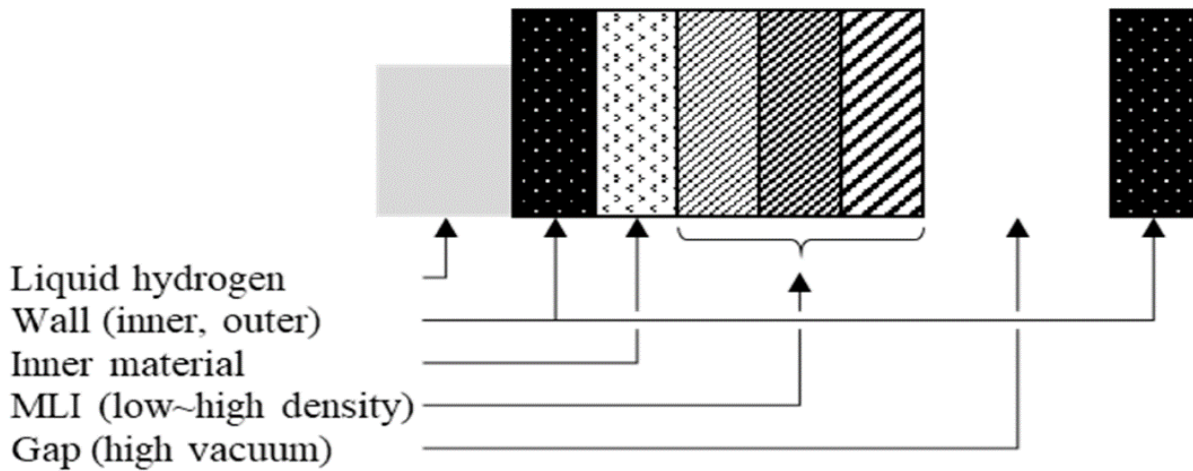


**Figure 3.3** Multilayer insulation concept (Khang 2022)

### Vacuum Insulation

As a vacuum has an extremely low thermal conductivity it could be beneficial for the fuel containment system. This insulation consists of vacuum jacket around the hydrogen storage tank as seen in Figure 3.4. On the inner wall of the vacuum jacket sealing material must be attached to prevent air from entering the tank. This air would freeze inside the tank and eventually blocking the fuel lines. To prevent the jacket from buckling due to the pressure difference between the ambient pressure and the vacuum inside the jacket the wall an outside wall and stiffeners between the inside and outside wall must be implemented. Both drive up the weight of the fuel containment system. Another issue is to attain the vacuum during operations. For this task venting equipment is required at the expense of weight and energy needed (Khandelwal 2013).

Like the multilayer insulation the vacuum also poses a safety concern as a vacuum leak leads to the massive loss of propellant.

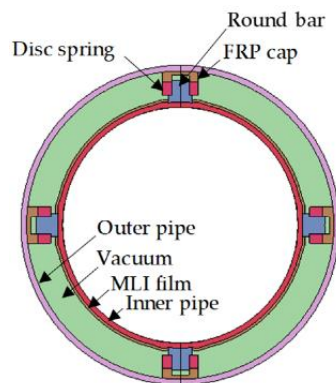


**Figure 3.4** Multi-layer vacuum insulation (Kim 2022)

## Foam Insulation

This insulation consists of a jacket made of foam around the outside wall of the hydrogen storage tank. On the outside of the foam insulation a thin metal-walled enclosure is attached to maintain its integrity and to protect the insulation from external forces (Khandelwal 2013).

There are different foams which differ in the materials and characteristics. The focus on choosing a foam is the weight and the thermal conductivity. The two most promising solutions by now are a rigid closed-cell polymethacrylimide and closed-cell polyurethane. The polyurethane itself offers excellent thermal conductivity and a low density, but it is not thermoformable and due to the open cells cyropumping might be an issue. The rigid closed-cell polymethacrylimide offers a slightly better thermal conductivity at a significantly higher density compared to the open-cell polyurethane, it is thermo-formable and due to the closed cells cyropumping is not an issue (Verstraete 2010).

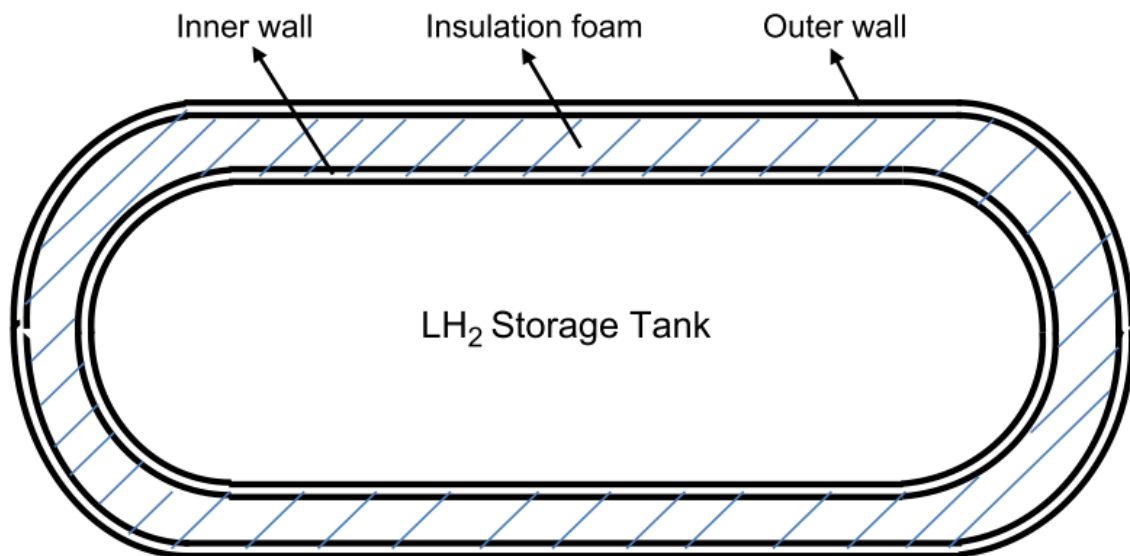


**Figure 3.5** Foam Insulation (Khandelwal 2013)

Compared with the other types of insulation a foam insulation has a higher thermal conductivity which results in a thicker insulation. This is compensated that only single tanks walls are needed as there is no vacuum jacket included. The absence of a vacuum jacket makes the foam insulation immune to the risk of a massive loss of propellant due to a vacuum leak. This makes the foam insulation low cost, lightweight and easy to implement (Verstraete 2010).

### 3.1.4 Dimensions of the Tank

The volume of the tank can be estimated by the following equation

$$V_{F,erf} = \frac{m_{F,erf} \cdot (1 + f_{EXV})}{\rho_F} . \quad (3.1)$$

As for our task the needed fuel mass is being calculated by the preliminary sizing and by solving the equation above the needed tank volume can be estimated. This calculation also includes an excess volume factor  $f_{EXV}$  of about 7.2% which provides additional space for the boil-off (Colozza 2002). Also, with  $m_{F,erf}$  as the needed fuel mass provided by the worksheet “Preliminary Sizing II” and  $\rho_F$  as the fuel density which will be set at 71 kg/m<sup>3</sup>.

The length of the cylindric part of the tank can be calculated with the following equation

$$l_{TANK,CY} = \frac{V_{F,erf} - \frac{4 \cdot \pi \cdot r_{TANK}^3}{3}}{\pi \cdot r_{TANK}^2} . \quad (3.2)$$

For this equation, the radius  $r_{TANK}$  of the tank is given by the boundaries of the aircraft’s fuselage. It should be kept in mind, that the thickness of the tank and the insulation adds up to the radius and the length of the tank. The wall thickness of the tank itself is not significant, but according to Verstraete the insulation thickness can be up to 15 cm.

The overall length of the tank can be calculated by the following equation

$$l_{TANK} = l_{TANK,CY} + 2 \cdot r_{TANK} . \quad (3.3)$$

The surface of the tank can be calculated by the following equation:

$$S_{TANK} = 2 \cdot \pi \cdot r_{TANK} \cdot l_{TANK,CY} + 4 \cdot \pi \cdot r_{TANK}^2 . \quad (3.4)$$

### 3.1.5 Weight of the Tank

The final design for the fuel containment system will be an integral spherical tank made from aluminum 2014-T6 insulated with polyurethane foam. The thickness of the insulation is 15 cm.

The weight of the tank and the insulation can be calculated by the following two equations (Seeckt 2010)

$$\frac{m_{TANK}}{S_{TANK}} = 3 \text{ kg/m}^2 \quad (3.5)$$

$$\frac{m_{INS}}{S_{TANK}} = 5 \text{ kg/m}^2 \quad (3.6)$$

### 3.1.6 Hydrogen Fuel System

The purpose of the fuel system is to pump, manage and deliver fuel to from the fuel containment system to the propulsion system. The fuel systems include all the systems which connect with either the fuel containment system or the propulsive system. Therefore, the fuel system consists of fuel pumps, a vent system, insulated fuel supply lines, heat exchangers, fuel quantity gauging equipment, refueling, and defueling systems and a fuel jettison system (Brewer 1991).

#### Boost Pumps

This electronically drive centrifugal pump is located in the bottom of the fuel tank (FAA 2018). It provides a steady flow of fuel and can also be used to transfer fuel between the tanks or to dump fuel. Each tank will have three boost pumps located in a surge box to ensure a sufficient flow of fuel during take-off and to prevent fuel starvation during flight maneuvers with low fuel levels (Brewer 1991).

#### Engine Fuel Delivery Lines

The purpose of these lines is to carry the fuel from the fuel containment system to the propulsion system. The main issue is to insulate the fuel lines to prevent the liquid hydrogen from freezing while flowing through the fuel lines. The insulation would be made from a rigid closed-cell polyurethane foam on the outside of the inner tube which carries the fuel. The inner tube is made of stainless steel (Brewer 1991). A cross feed valve will ensure that each tank is able to provide propellant to the fuel cells (FlyZero 2022b).

## Engine Fuel Control System

To ensure the proper flow rate of fuel to the propulsion system the whole fuel system has to be monitored. For these functions different inputs regarding the propulsion system and fuel containment system have to be collected, processed, and output parameters have to be used to adjust the fuel system (Brewer 1991).

## Fueling and Defueling System

To refill the liquid hydrogen at the airport using the ground supply systems fueling adapters have to be attached to the fuselage of the aircraft. These could be located at the aft end of the fuselage below the vertical tail. In the case of using two tanks which are located in the front and the aft of the fuselage there has to be a fuel line running from the aft end of the fuselage to the tank in the front of the aircraft. To prevent over pressurization during the refill process a shut-off valve must be included in the system (Brewer 1991).

## Tank Vent and Pressurization System

As mentioned before regarding the fuel containment system the tank need to be kept at a constant pressure. Every tank needs to have a pressurization and venting system (Brewer 1991).

## Fuel System Weight Prediction

According to the Cryoplane Project (Westenberger 2003) the weight can be estimated by the following equation

$$\frac{m_{ATTACH}}{V_{TANK}} = 12 \text{ kg/m}^3 \quad . \quad (3.7)$$

## 3.2 Fuel Cell

Another key component for a zero-emission plane is the fuel cell. The fuel cell is the part of the propulsion system in the chemical energy of a fuel is converted into electrical energy without any combustion. This electricity would provide power to the other components of the propulsion systems and therefore replace the jet engine on conventional planes. This is essential important because even the hydrogen combustion in a modified jet engine would

eliminate CO<sub>2</sub>, CO, SOX but not NOX and water vapor emission, which makes this option zero-carbon, but not zero-emission. The use of a fuel cell combined with an electric propulsion would eliminate all CO<sub>2</sub>, NOX, SOX, CO, HC, and soot emissions. The use of a fuel cell in a hydrogen-electric powertrain also offers an increase of efficiency of 20% ... 40% compared to a hydrogen-combustion powertrain due to the more efficient energy conversion (Thomson 2021).

The electric based propulsion also benefits to the trend of the substitution of pneumatic and hydraulic systems by electric powered systems as seen in the last generation of airliners, which offers reduction in weight and enhanced reliability (Renouard 2012).

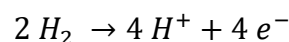
Another advantage of a fuel is the absence of moving parts, which makes it very dependable and therefore ideal for long-lasting systems. The fuel cell also itself emits no noises. Compared to a battery the fuel has a higher energy density, which makes it more efficient at larger sizes, and is quicker refueled while the battery needs to be recharged (Dicks 2018).

The volumetric power density is inferior to those of a combustion engine. The fuel itself poses issues regard to availability, storage and the lower volumetric power density compared to other types of fuel like gasoline. (O'Hayre 2016)

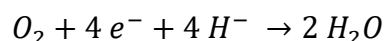
### 3.2.1 Basis Operating Principle of a Fuel Cell

A fuel cell is an electrochemical cell that converts the chemical energy of a fuel as in put into electricity as output (O'Hayre 2016). The fuel cell consists of an anode, a cathode, and an electrolyte. There are several types of fuel cells which vary on the sort of the electrolyte. The reaction inside the fuel cell will be explained at the example of a phosphoric acid fuel cell, which was the first type of a fuel cell to commercialized and is widely used today. The electrolyte highly concentrated or pure liquid phosphoric acid ( $H_3PO_4$ ) saturated in a silicon carbide matrix. The electrodes are made of carbon paper coated with dispersed platinum catalyst.

At the anode hydrogen is oxidized and releases electrons and heat and creates  $H^+$  ions.



At the cathode oxygen with electrons from the electrode and  $H^+$  ions from the electrolyte creates into water (Dicks 2018).



The electrons are forced due to spatial separation to flow through an external circuit in which electric current is produced. This spatial separation is being done by the electrolyte which allows the flow the ions, but not of electrons (O'Hayre 2016). The basic principle of a fuel cell can be seen in Figure 3.6.

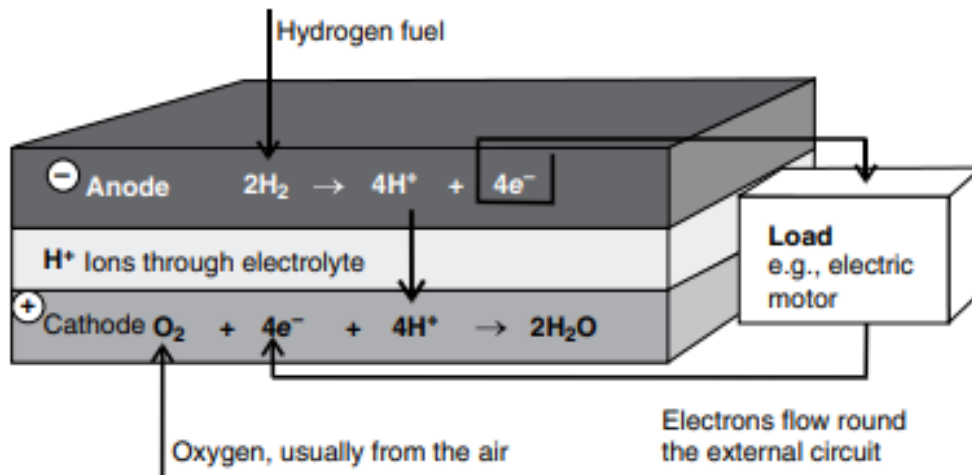


**Figure 3.6** Electrode reactions and charge flow for fuel cell with an acid electrolyte (Dicks 2018)

### 3.2.2 Types of Fuel Cells

The several types of fuel cell can be distinguished primarily by the electrolyte that is being used and secondly by the operating temperature. The several types of fuel cells and their characteristics can be seen in Table 3.1 and 3.2.

**Table 3.1** Comparison by electrolyte of fuel cell types (O'Hayre 2016)

Fuel Cell Type	Electrolyte	Catalyst	Fuel	Ion
Proton-exchange membrane (PEMFC)	Polymer electrolyte membrane	Platinum	Pure $H_2$	$H^+$
Alkaline (AFC)	Aqueous alkaline solution	Platinum	Pure $H_2$	$OH^-$
Phosphoric acid (PAFC)	Immobilized liquid phosphorus acid in SiC	Platinum	$H_2$ , low CO, low S	$H^+$
Molten carbonate (MCFC)	Immobilized liquid molten Carbonate in $LiAlO_2$	Electrode material	$H_2$ , hydrocarbon fuels	$CO_3^{2-}$
Solid oxide (SOFC)	Ceramic ionic conduction	Electrode material	$H_2$ , hydrocarbon fuels	$O^-$

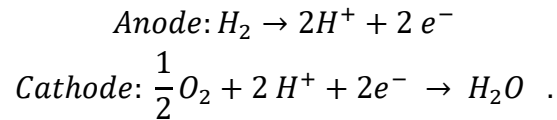
**Table 3.2** Comparison by operating temperature of fuel cell types (Dicks 2018)

Fuel Cell Type	Temperature (°C)	Power density (mW/cm <sup>2</sup> )	Power (kW)	Efficiency (%)	Application
Proton-exchange membrane (PEMFC)	50 ... 100 125 ... 200	500 ... 2500	0.001 ... 500	40 ... 60	Vehicle, mobile applications
Alkaline (AFC)	65 ... 220	150 ... 400	10 ... 200	60 ... 70	Space vehicles
Phosphoric acid (PAFC)	205	150 ... 300	< 10.000	50 ... 55	CHP systems
Molten carbonate (MCFC)	650	100 ... 300	<100.000	45 ... 65	Medium to large CHP systems
Solid oxide (SOFC)	600 ... 1000	250 ... 500	<100.000	50 ... 65	All sizes of CHP systems

## Proton Exchange Membrane Fuel Cell (PEMFC)

This fuel cell is also known as Polymer Electrolyte Membrane Fuel Cell. It is the most successful commercially by now (Dicks 2018). By now all major car companies focusing almost their entirely development efforts on this type of fuel cell.

This fuel cell consists of a proton conducting polymer electrolyte membrane. It is coated on either side with a thin layer of platinum-based catalyst and porous carbon electrode support material. Therefore, the anode and cathode reactions are



The operating temperature of this fuel cell depends on the membrane used. In most cases a polymer membrane is used, which must be hydrated with liquid water to maintain adequate conductivity. In this case the operating temperature is limited to 90 °C. There are also high temperature PEMFC in which polybenzimidazole (PBI) is used as membrane. In both cases the relatively low reaction temperature requires a sophisticated catalyst and electrode. This makes the use of platinum as catalyst necessary. The platinum catalyst itself is prone to carbon monoxide and sulfur poisoning. To prevent this only pure hydrogen as fuel could be used. During operation water will be produced at the cathode (O'Hayre 2016). The basic operation principle of this fuel cell can be seen in Figure 3.7.

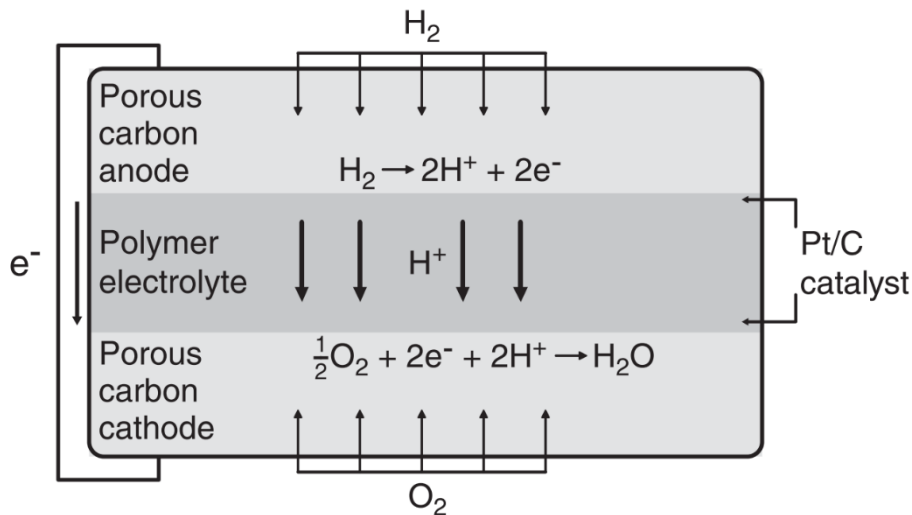


**Figure 3.7** Schematic of a PEMFC (O'Hayre 2016)

The amount of water in the fuel is critical to the efficiency of the fuel cell. The water is needed in the polymer electrolyte to maintain high proton conductivity. While excess water is produced at the cathode this may lead to flooding of the fuel cell. If the membranes are not correctly humidified the proton conductivity decreases and therefore the resistance of the fuel cell increases which leads to efficiency losses. To prevent this a water management of the fuel cell is needed (Spiegel 2017). The water movement inside the fuel cell can be seen in Figure 3.8.

The advantages of this type of fuel cell are

- very high power density,
- good start-stop capabilities,
- low operation temperature.

The disadvantages of this type of fuel cell are

- expensive Materials,
- water management is required,
- poor CO and S tolerance.

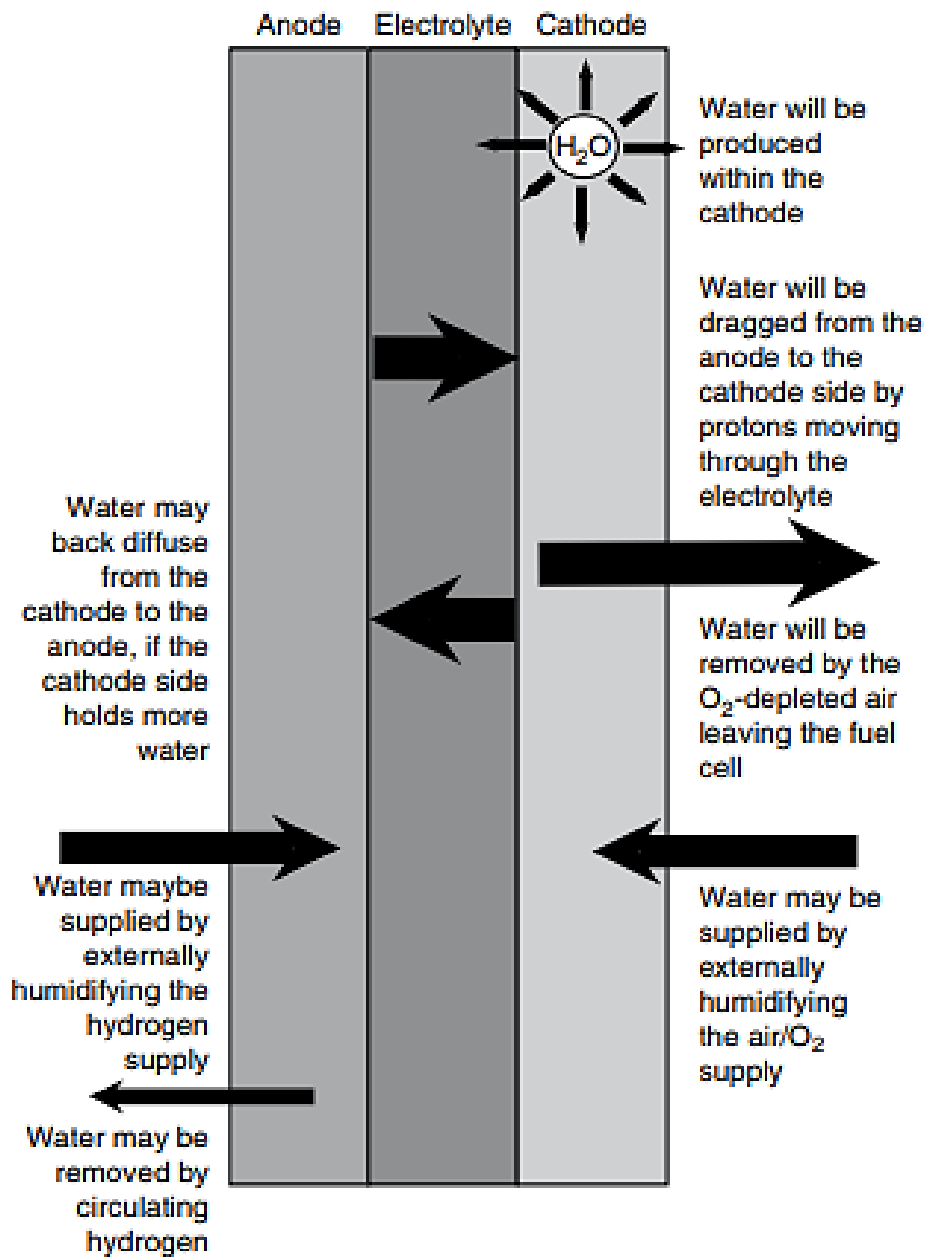
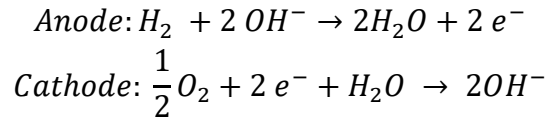


**Figure 3.8** Schematic of the water movement of a PEMFC (Dicks 2018)

## Alkaline Fuel Cell (AFC)

This type of fuel cell has been used in the Apollo and Space Shuttle program (Dicks 2018). This fuel cell employs an aqueous potassium hydroxide electrolyte.



During its operation water is produced and must be removed. Otherwise, the electrolyte will be diluting and therefore the performance of the fuel cells degrades. The AFC requires pure hydrogen and oxygen during operations because it is prone to poisoning by carbon dioxide. Even atmospheric levels of carbon dioxide will reduce the electrolyte conductivity. This makes these fuel cells unsuitable for terrestrial conditions (O'Hayre 2016). The operating principle can be seen in Figure 3.9.

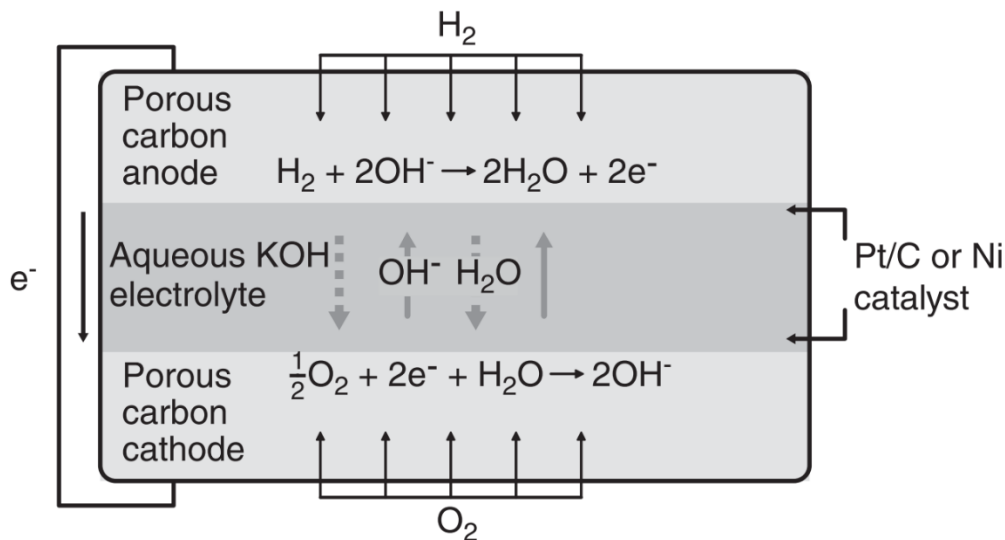


**Figure 3.9** Schematic of a AFC (O'Hayre 2016)

The advantages are

- improved cathode performance,
- inexpensive materials.

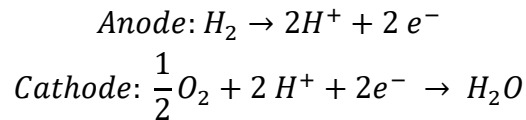
The disadvantages are

- needs pure  $H_2$ ,  $O_2$  as fuel,
- electrolyte needs replenishment,
- water management required.

## Phosphoric Acid Fuel Cell (PAFC)

This was the first type of fuel cell to be commercialized and see widespread terrestrial use since the 1980s (Dicks 2018).

This fuel cell consists of a liquid phosphoric acid in a thin SiC matrix between two porous graphite electrodes coated with a platinum catalyst. Hydrogen is used as the fuel while air is being used as oxidant.



Due to the electrolyte the operating temperature must be in the range of 42 °C ... 210 °C with optimal performance between 180 °C ... 210 °C. During the operation, the electrolyte must be constantly replenished due to evaporation. It shares the need of pure hydrogen as fuel for the same reasons as the PEMFC (O'Hayre 2016). The basic operating principle can be seen in Figure 3.10.

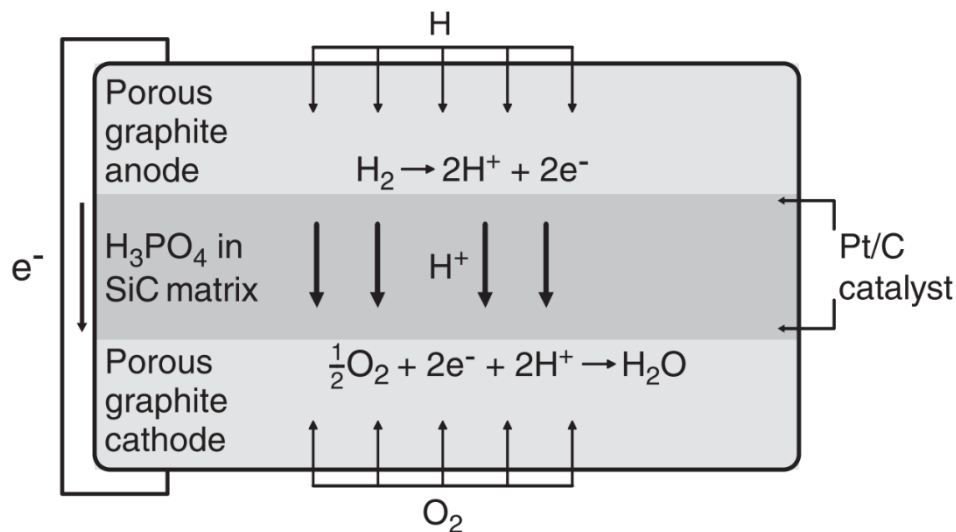


**Figure 3.10** Schematic of a PAFC (O'Hayre 2016)

The advantages of this type of fuel cell are

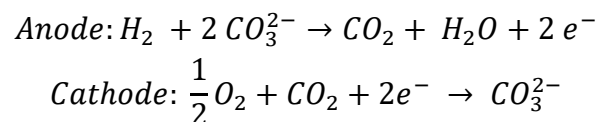
- proven technology,
- excellent reliability,
- unexpensive electrolyte.

The disadvantages are

- expensive catalyst,
- prone to CO and S poisoning,
- replenishment of electrolyte,
- corrosive electrolyte.

### **Molten Carbonate Fuel Cell (MCFC)**

This fuel cell uses an electrolyte composed of a molten mixture of alkali carbonates suspended in a porous, chemically inverted ceramic matrix. The electrodes are nickel based.



This type of fuel cell requires carbon dioxide to be fed to the cathode. Its high operating temperature results in a good reaction rate and an inexpensive catalyst can be used. The electrolyte is prone to stresses by freeze-thaw cycles which occur when the system is powered off or on. In result this type of fuel cell is unsuitable for mobile applications (O'Hayre 2016). The basic operating principle can be seen in Figure 3.11.

The advantages of this type of fuel cell are

- inexpensive catalyst,
- useable waste heat for cogeneration applications,
- fuel flexibility.

The disadvantages are

- expensive materials for electrodes,
- corrosive electrolyte,
- degradation resulting in lifetime issues.

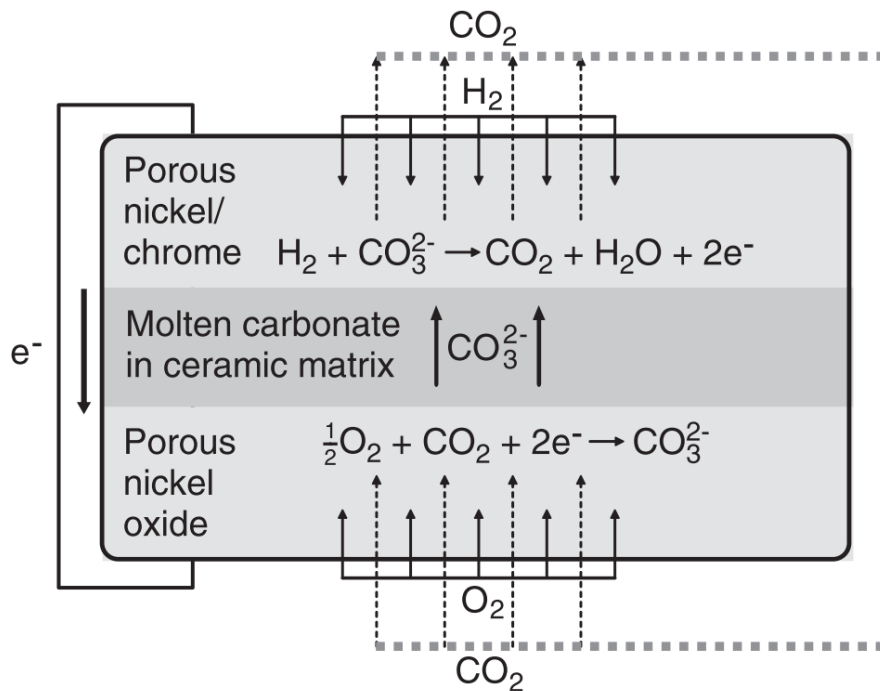
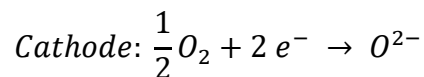
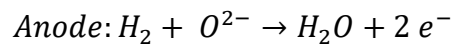


**Figure 3.11** Schematic of a MCFC (O'Hayre 2016)

### Solid Oxide Fuel Cell (SOFC)

This fuel cell uses a solid ceramic electrolyte. The material for the anode is nickel mixed with ceramic while the cathode is made of ceramic material.



The SOFC is operating at high temperature, which makes it efficient and produces useable waste heat. But the high temperature causes high material requirements and reliability issues (O'Hayre 2016). The basic operating principle can be seen in Figure 3.12.

The advantages of this type of fuel cell are

- fuel flexibility,
- usable waste heat,
- high power density.

The disadvantages are

- high temperature material issues,
- expensive components.

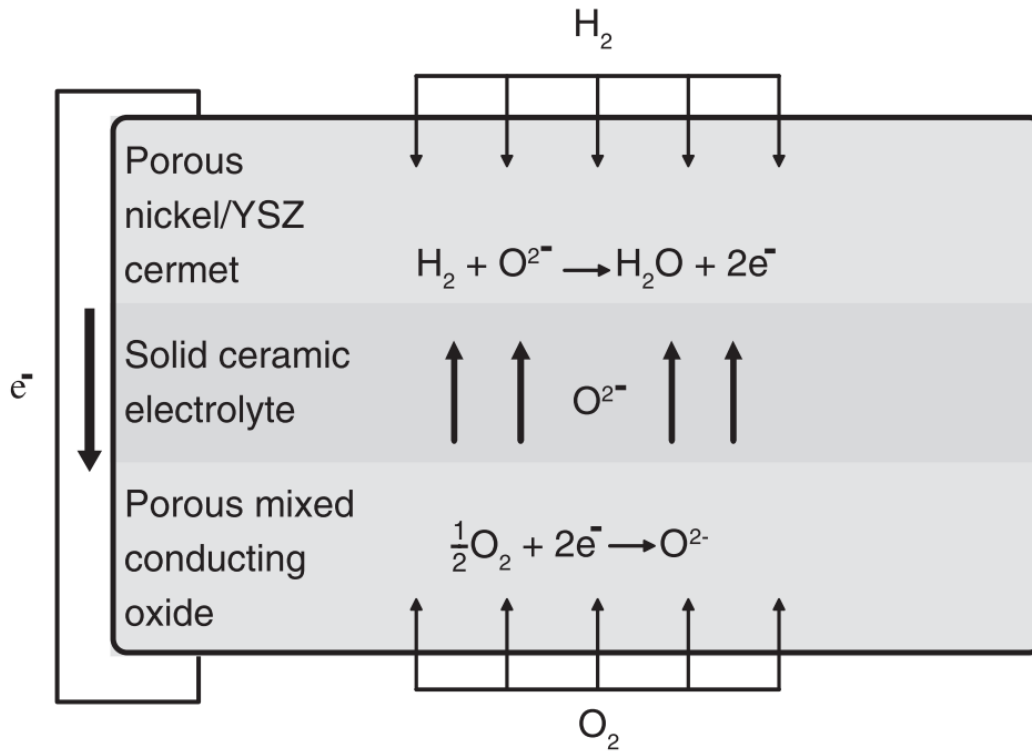


**Figure 3.12** Schematic of a SOFC (O'Hayre 2016)

### 3.2.3 Implementation of the Fuel Cell

Considering the advantages and disadvantages of the different types of fuel cells there are only two types of fuel cells which could be considered for the use as part of the aircraft propulsion system. These are the PEMFC and the SOFC. A comparison of both types is shown in the Table 3.3.

The PEMFC offers the highest power density and a relatively low operating temperature combined with better start-up times. The main drawback is the need for a water management system. The SOFC offers a better fuel flexibility, but the higher operating temperature poses significant problems in material and sealing issues. Also due to the high operating temperature of the SOFC the cooling will be more of an issue compared to the PEMFC.

Due to inferior start-up times and power density, the PEMFC is selected for aviation applications (FlyZero 2022e).

**Table 3.3** Comparison between PEMFC and SOFC (FlyZero 2022e)

Parameter	PEM fuel cell	SOFC
Operating temperature	50 °C ... 100 °C	500 °C ... 1000 °C
Typical stack size	1 kW ... 100 kW	1 kW ... 2 MW
Gravimetric power density	System: 0.5 kW/kg ... 1.5 kW/kg Stack: 3 kW/kg ... 5 kW/kg	System: 0.02 kW/kg... 0.25 kW/Kg Stack 0.17 kW/kg ... 0.47 kW/kg
Volumetric power density	System: 0.2 kW/l ... 0.4 kW/l Stack: 3 kW/l ... 5.5 kW/l	System: 0.1 kW/l ... 0.25 kW/l Stack: 1 kW/l ... 1.2 kW/l
Efficiency	60%	60%
Fuel	$H_2$	$H_2$ + reformed hydrocarbons
Waste products	Water and heat	Water and heat
Applications	Portable power, transportation, backup power, distributed generation	Electric utility, auxiliary power, large-scale distributed generation
Start-up	Fast (10s of seconds)	15 ... 30 min

### 3.2.4 Weight of the Fuel Cell

To estimate the weight of the fuel cell the needed power during the most power crucial part of the flight should be used. This is take-off power which is provided by the Preliminary Sizing. In a first step the weight can be calculated with the following equation

$$m_{fc} = \frac{P_{s,TO}}{\phi_{fc}} \quad (3.8)$$

The specific power of a PEMFC  $\phi_{fc}$  can be estimated at 1.6 kW/kg for current technology and 8 kW/kg for future technology (Kadyk 2018).

### 3.2.5 Oversizing of the Fuel Cell

Besides the power density of the fuel cells the efficiency is crucial for aircraft design as the efficiency determines the weight of the fuel needed. The efficiency of a fuel cell can be optimized by operating at partial load or oversizing the fuel cells. A slightly oversized fuel cell is always preferable (Kadyk 2018). According to FlyZero 2022e the oversizing factor is set to

18% which offers increased propulsion system efficiency while being weight neutral due to the impact on the thermal management system.

### 3.3 Balance of Plant

The balance of plant as seen in Figure 3.13 includes all subsystems that support the operation of the fuel cell in an aerospace environment. This includes (FlyZero 2022f):

- the heat rejection system,
- the air supply system,
- the fuel conditioning system,
- the heat exchanger system,
- the water management system.

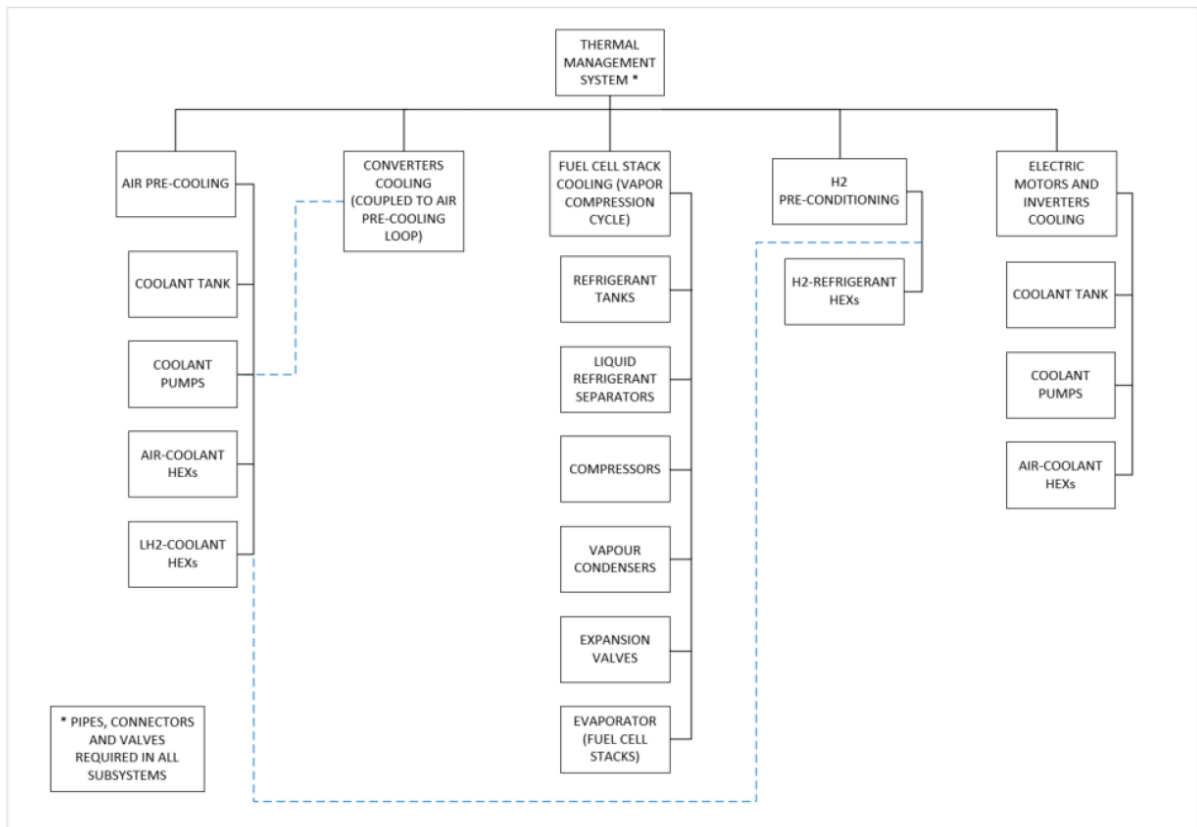


**Figure 3.13** Balance of plant of a fuel cell propulsion system (FlyZero 2022f)

### 3.3.1 Heat Rejection System

As low temperature PEM fuel cells have been chosen as part of the powertrain their requirement for a proper temperature control and heat management must be assessed. Their optimal operating temperature is about 80 °C (FlyZero 2022e).

As a fuel cell is about 30% ... 60% electrically efficient and the remaining energy is emitted as heat without removing of the excess heat the fuel cell can overheat. This results in the rising of thermal gradients which have a negative effect on the performance and decrease the durability of the fuel Cell (O'Hayre 2016).

There are different methods of cooling available. For application up to 2 kW air cooling is possible, above 5 kW liquid cooling is necessary (Dicks 2018)).

The basic method of liquid cooling is to pump coolant through the cooling channels of the bipolar plate. The coolant absorbs the heat within the fuel cell stacks and then emits the heat with the help of a radiator or heat exchanger. The coolant is now pumped back to repeat the cooling loop (Dicks 2018).

While in liquid cooling the coolant stay in liquid stage all the time another possibility is to evaporate the coolant. In this method the coolant evaporates, and the energy required to evaporate the coolant is absorbed by the coolant (FlyZero 2022e).

As the fuel cells the subsystems must designed to the peak power demand. When it comes to the cooling the dimensions of the cooling system have to consider a take-off during hot day ambient conditions (ISA+40). In this case the liquid cooling method would only offer a temperature difference between the ambient air and the fuel cell stack of less than 25 °C which would result in a large heat transfer area and therefore an increase in weight and drag of the system. The vapor compression cycle would offer an increase of the heat rejection temperature to about 100 °C which makes it superior in mass and induced drag. The vapor compression cycle uses R1233zd as coolant, which offers thermodynamic properties for the vapor compression cycle (Zulawski 2021).

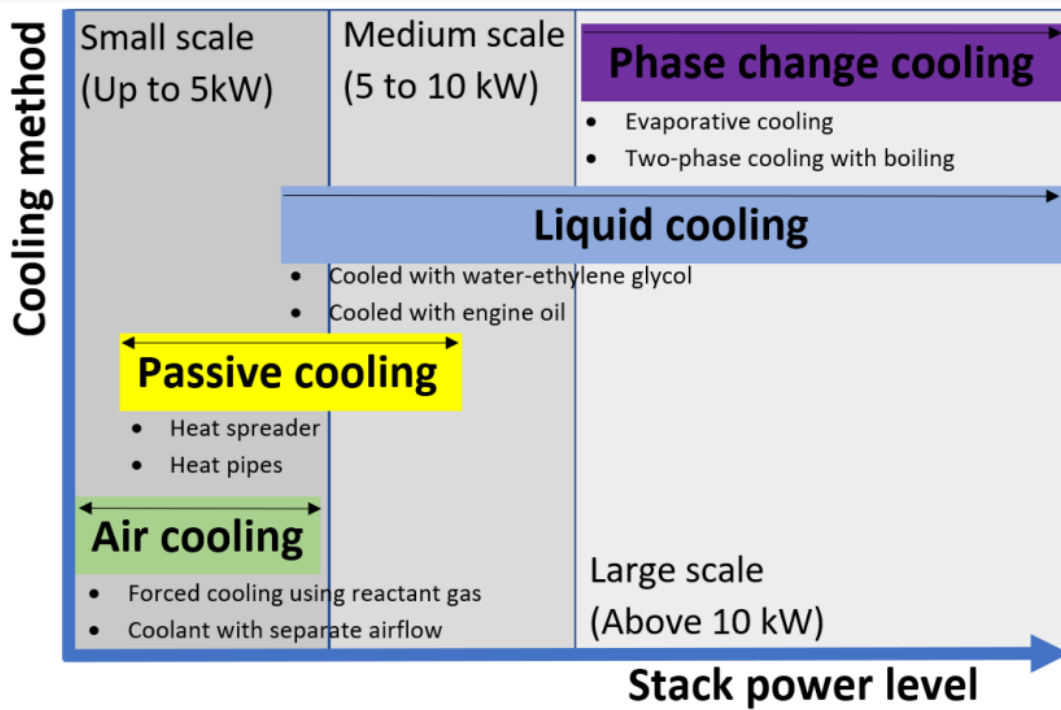


Figure 3.14 Fuel Cell cooling methods depending on stack power (FlyZero 2022e)

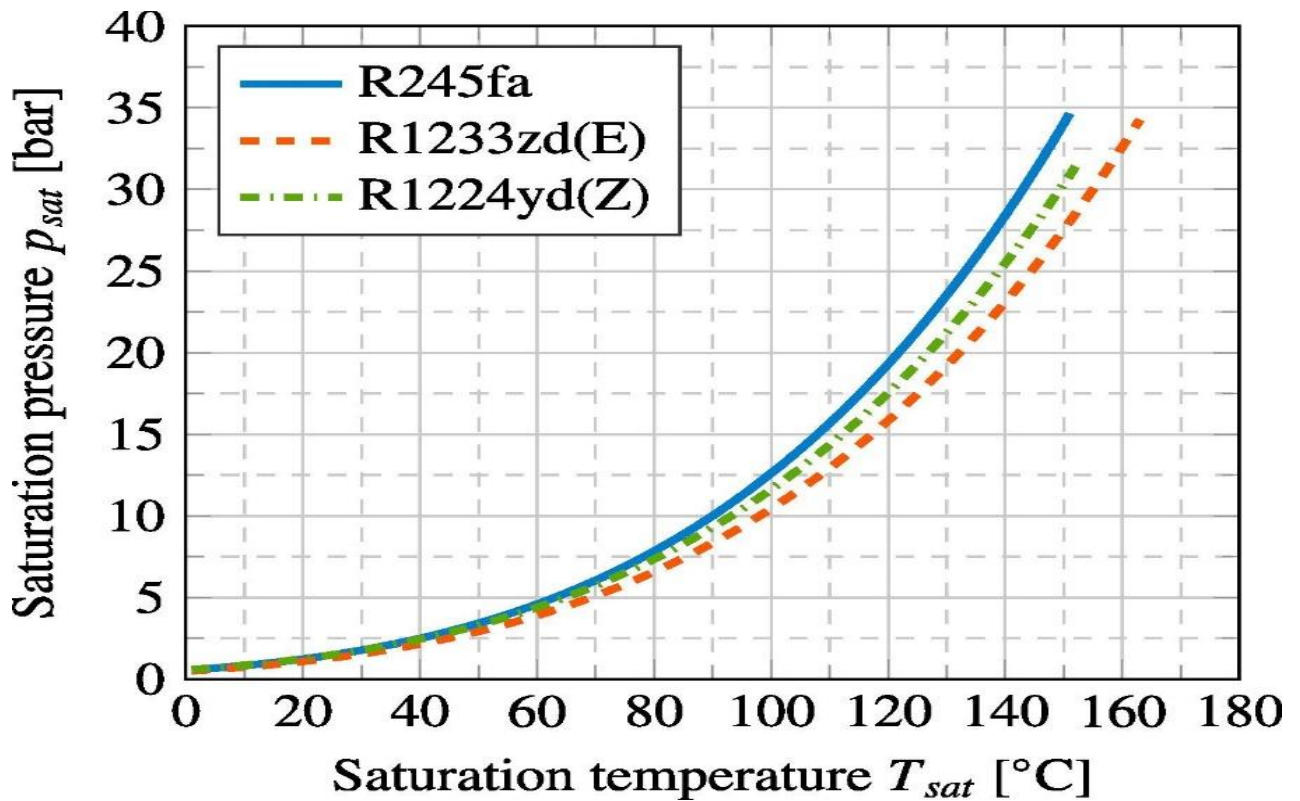
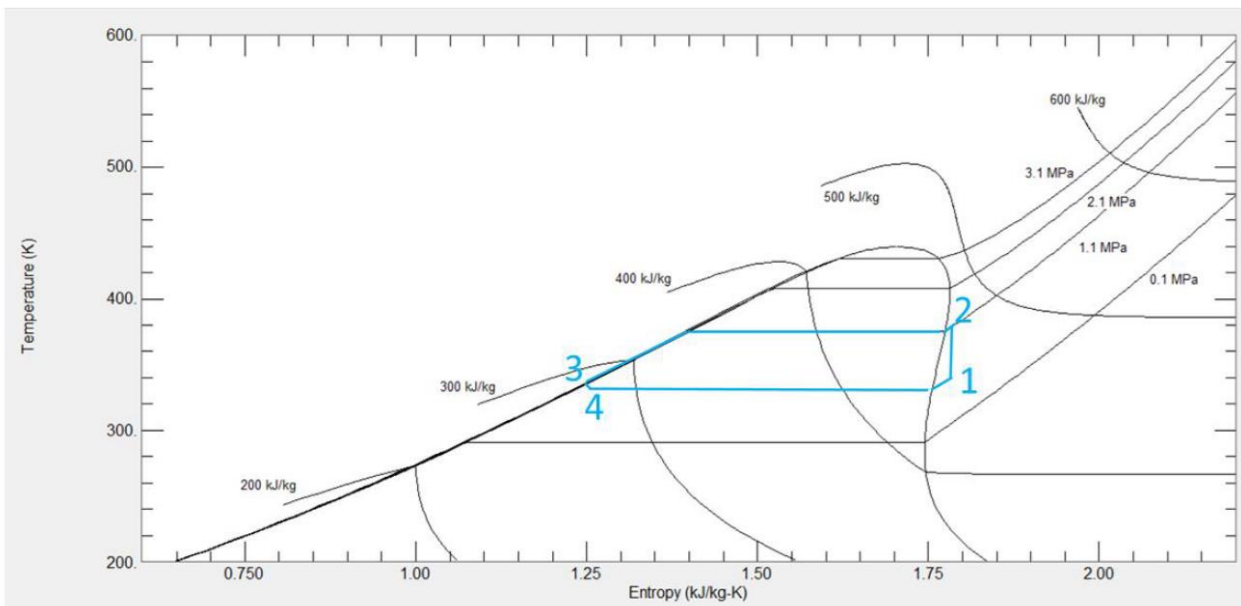


Figure 3.15 Vapor pressure curve R1233 (Eyerer 2019)

The main phases with their pressures and temperatures of the vapor compression cycle as shown in Figure 3.16 are (FlyZero 2022f):

- compression of superheated vapor (point 1 to 2),
  - compressor inlet,
    - pressure < 3 bar,
    - temperature ~ 67 °C,
- condensation of refrigerant plus further subcooling (point 2 to 3),
  - condenser inlet,
    - pressure ~ 11 bar,
    - temperature ~ 107 °C (with main isothermal heat rejection ~ 100 °C),
- expansion of refrigerant through isenthalpic valve (point 3 to 4),
  - valve inlet,
    - pressure < 11 bar,
    - temperature ~ 62 °C (subcooled liquid),
- evaporation process takes place though fuel cell stack (point 4 to 1),
  - evaporator inlet,
    - pressure ~ 3 bar,
    - temperature ~ 57 °C.



**Figure 3.16** T-S Diagram of vapor compression cycle (FlyZero 2022f)

### 3.3.2 Air Supply System

This system provides the fuel cell with the right amount of air to ensure the performance of the fuel cells. It also regulates the pressure, temperature, cleanliness, and humidity of the air to meet the requirements of the fuel cell. The air supply system includes heating, cooling, humidification, and filtering devices (Zulawski 2021).

The air fed to the fuel cell stack needs to be compressed to meet the requirements of the fuel stacks. When the air is being compressed it is getting warmer and the temperature is exceeding the operational temperature of the fuel cells. This results in the need to cool the ambient air before it enters the compressor. The low temperatures of the hydrogen fuel feed will be used as a heat sink for the compressed air via using the energy inside the refrigerant cycle of the vapor compression cycle. This also increases the temperature of the hydrogen propellant which must be delivered at operating temperature to the fuel cells. Therefore, the objective of the air pre-cooler heat exchange sizing is to maximize the heat extracted from the air stream and to minimize the temperature of the air feed before it enters the air compressor. It also must be noted that the temperature of the air entering the compressor must be above 0 °C to avoid the frosting of atmospheric moisture. Due to the high air mass flow rates a spiral involute architecture is selected. (FlyZero 2022f).

### 3.3.3 Fuel Conditioning System

This system must ensure that the fuel cell is provided with fuel of the right amount, pressure, and temperature (FlyZero 2022e).

The liquid hydrogen is stored at cryogenic temperature (-253 °C) and must be supplied to the fuel cell at its operating temperature. Using the propellant at this temperature would cause the freezing of other fluids inside the fuel cell resulting in excessive thermal gradients and eventually the fuel cell would become inoperable. The liquid hydrogen can be heated with two different heat sources (FlyZero 2022e):

- by consuming the heat of the air which is fed to the fuel cells. This is especially critical during take-off with hot day ambient conditions,
- via heat exchanger with the coolant from the vapor compression cycle.

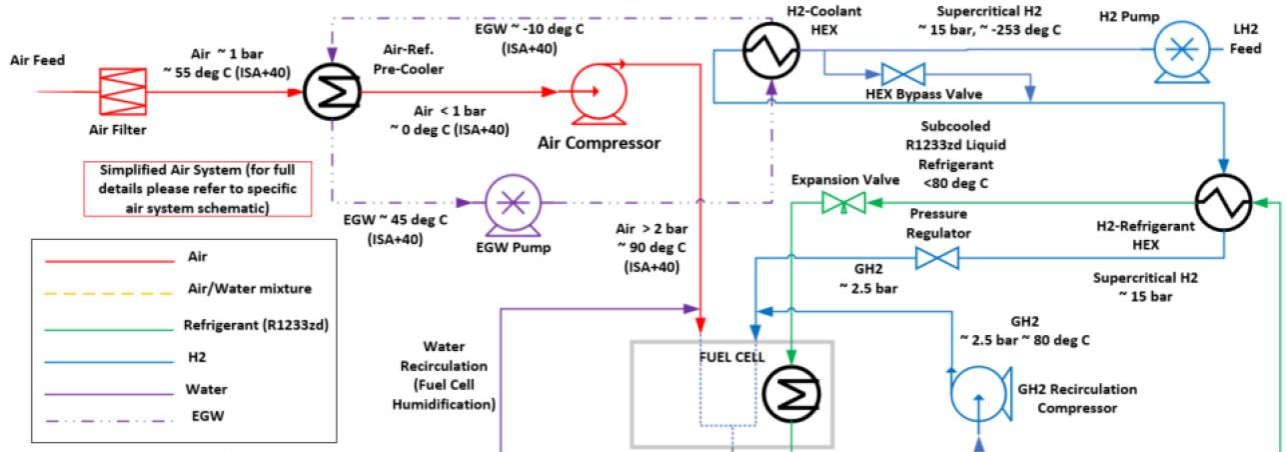


**Figure 3.17** Details of fuel cell air pre-cooling and hydrogen pre-conditioning (FlyZero 2022f)

### 3.3.4 Heat Exchanger System

The purpose of this system is to dissipate the heat being produced during the operation of the fuel cells. This can be done by either emitting the heat to the ambient air or putting the heat to practical use in form of providing energy to other systems of the aircraft (Dicks 2018).

There are two types of radiators which can be used to dissipate the heat to the ambient air (Stroman 2010):

- surface radiators,
- compact heat exchanger.

The surface radiator as seen in Figure 3.18 uses existing aircraft surfaces for the heat transfer. The main motivation is the low aerodynamic drag and low weight added to the aircraft compared to a conventional cooling method based on a heat exchanger (Kellerman 2019).

While conventional methods require additional equipment that add drag and weight the surface cooling method only consists of a flat panel which is attached to the surface of the aircraft. While the aircraft is moving the air flows over the surface radiator which emits heat to ambient air (Stroman 2010).

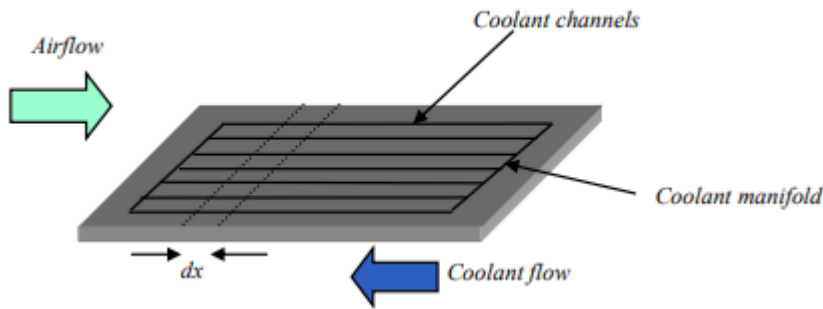


**Figure 3.18** Surface radiator (Stroman 2010)

A surface radiator may also be beneficial in reducing drag by emitting heat into the aircraft's boundary layer. This effect of reducing skin friction drag is only present in fully turbulent flow regions. If the heat is dissipated in a laminar flow region this results in an increase in skin friction. This also reduces the useable surface area where heat can be dissipated (Kellerman 2019).

This conclusion is critical in combination with the findings of another study in which the cooling potential of both surface and heat exchanger cooling solutions have been evaluated. It was noted that the heat transfer coefficient of the surface radiators was unsuitable for aviation use. The surface area that would have been necessary for cooling was above the aircraft's surface (Stroman 2010).

The compact heat exchanger as seen in Figure 3.19 mainly differentiates to surface radiators is the direction of the airflow which is perpendicular to the radiator area with air ducted through the heat exchanger. This type aims at high efficiency and durability instead of the low aerodynamic drag of the surface radiator (Stroman 2010.).

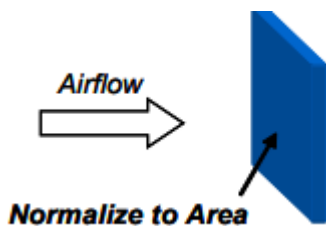


**Figure 3.19** Compact heat exchanger (Stroman 2010)

As the method of cooling the fuel cell is a vapor compression cycle which bases on the evaporation of the coolant there is a need for a condenser. After the coolant is evaporated it is necessary to condensate the coolant to repeat the cooling loop. The condensation is done inside the condensers which will emit the energy of the coolant to the ambient air. The condensers must be sized to the conditions of peak power demand during take-off and ISA+40 ambient temperatures (FlyZero 2022f).

The condensers could be house inside the fuselage, inside the wings or wing mounted. Due to the large heat exchanger dimension the wing mounted configurations is preferable (Kozulovic 2020). An example for such a wing mounted shown in the Figure 3.20.

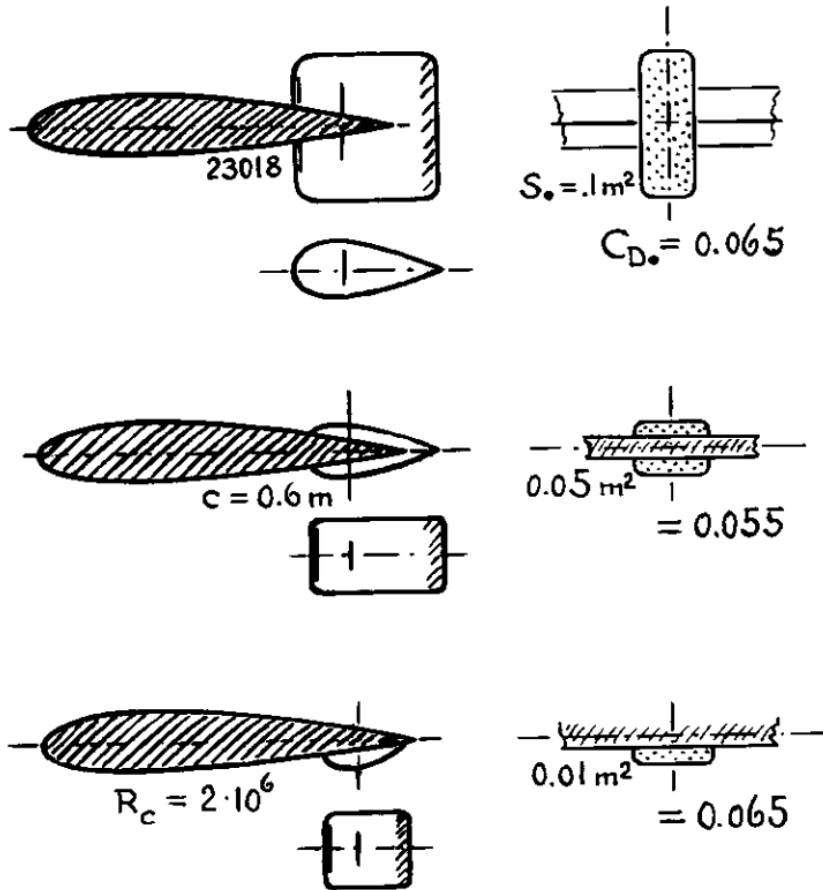


**Figure 3.20** Wing mounted radiator (Hoerner 1965)

The type of installation has been chosen in FlyZero's Regional Aircraft concept is to house the condensers inside the nacelle of the propulsion system with an array of microtubes perpendicular to the air flow. This configuration is shown in Figure 3.21. Because the heat exchangers would be housed behind the propeller blades, they would benefit from the additional dynamic head from the blades (FlyZero 2022f) as shown in Figure 3.22.

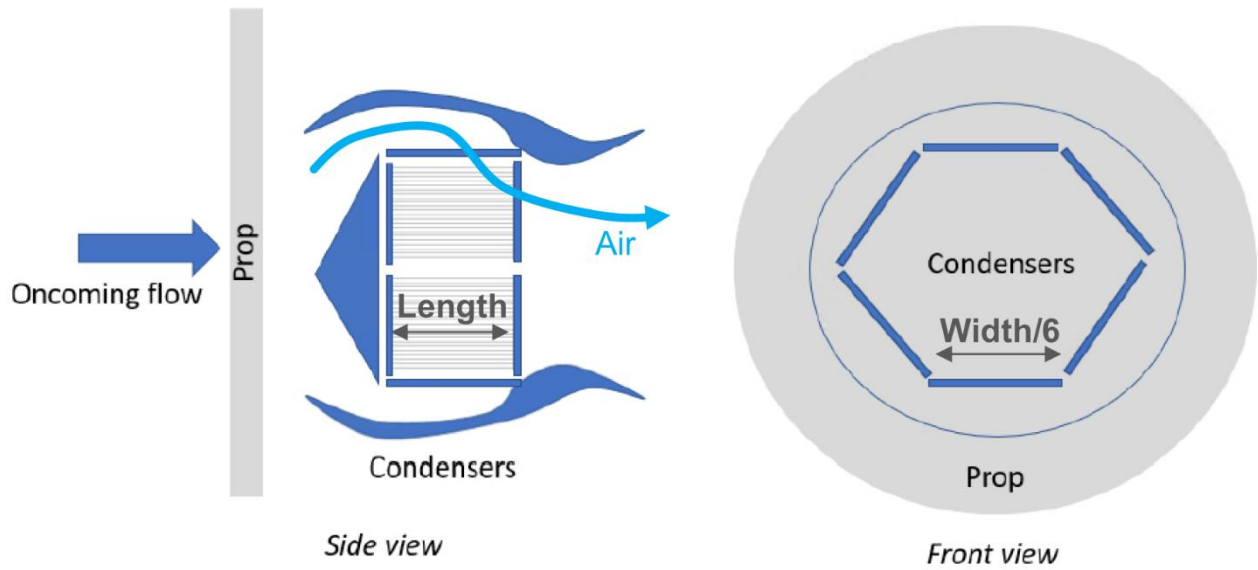


**Figure 3.21** Condensers behind the propeller (FlyZero 2022f)

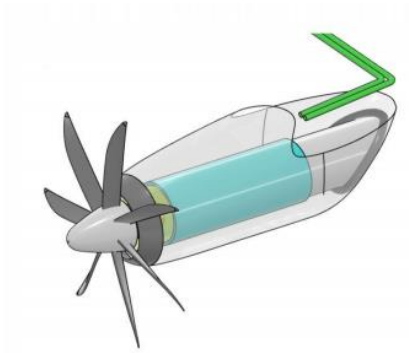


**Figure 3.22** Installation of the condenser (light blue) inside the nacelle (FlyZero 2022f)

Additionally, these heat exchangers could be optimized with a variable inlet to adjust the air flow to different stages of a flight mission as shown in Figure 3.23. During peak power demand there is a need for higher flow rate of air compared to cruise flight. With a variable inlet the aerodynamical drag could reduce significantly (FlyZero 2022f).

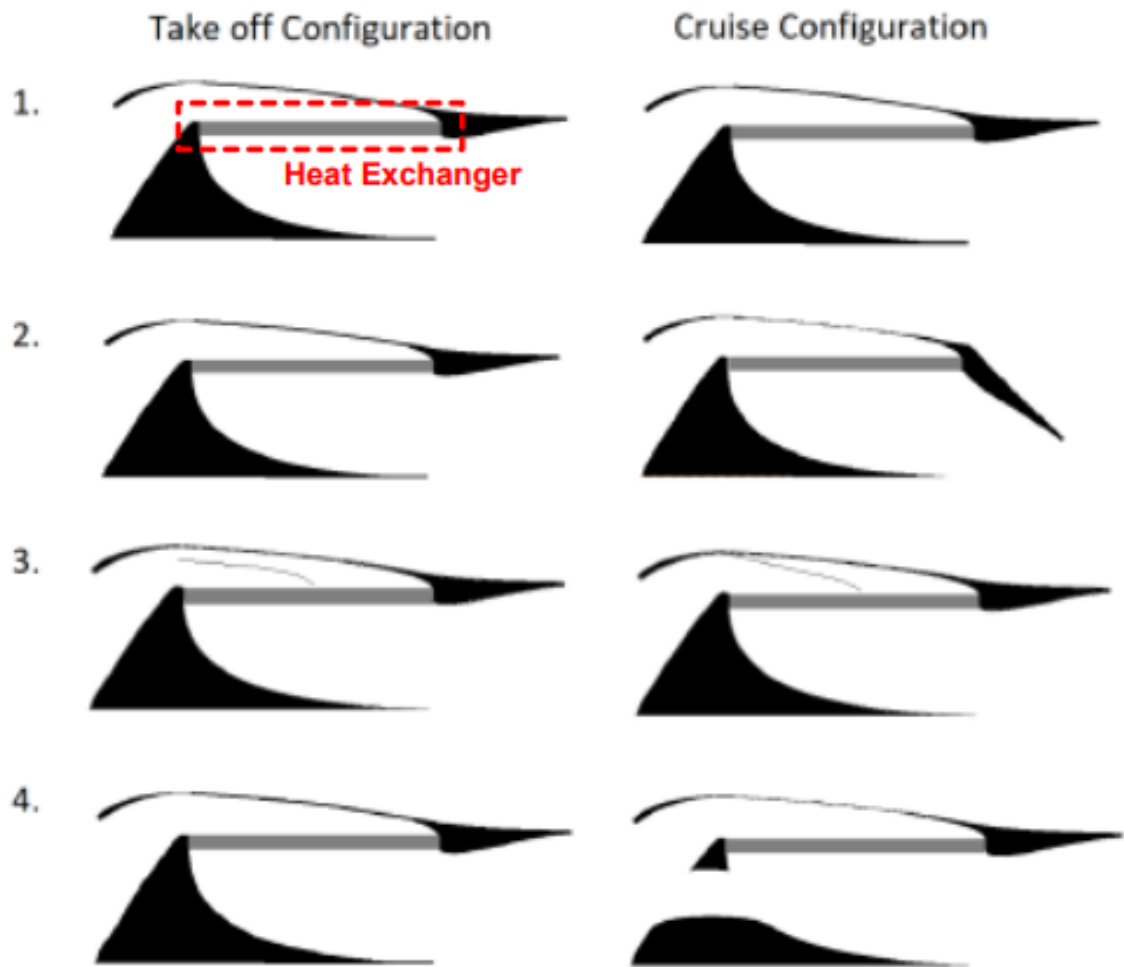


**Figure 3.23** Positions of the air inlet during flight phases (FlyZero 2022f)

### 3.3.5 Water Management System

During the operation of a fuel cell water is constantly produced proportional to the power output as shown in Figure 3.24.

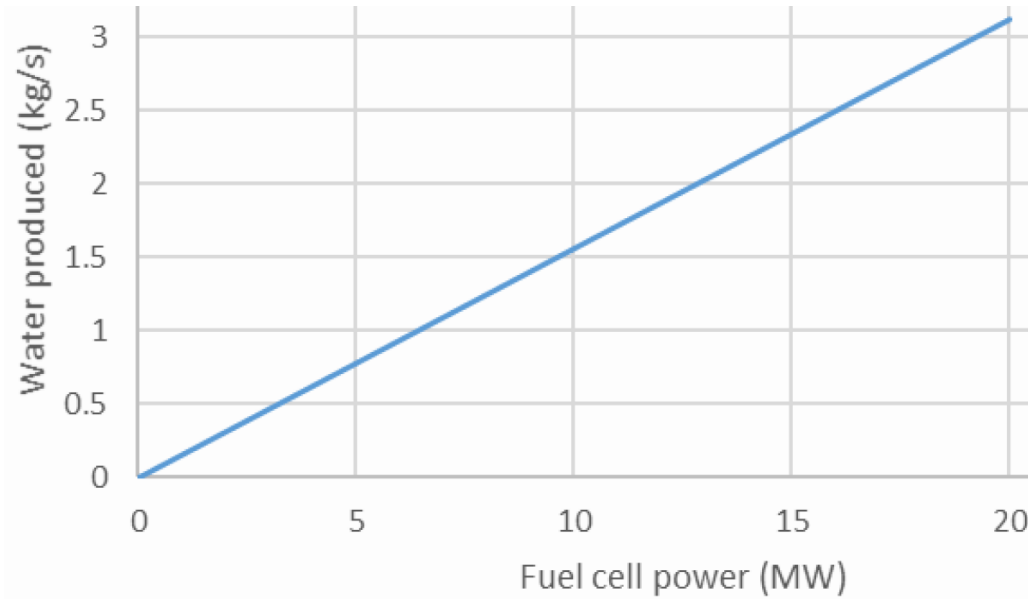


**Figure 3.24** Estimation of water production of the fuel cell (FlyZero 2022e)

Emitting this water into the atmosphere may form contrails which can form ice crystals and contrails at high altitude that may block outward infrared radiation. This can contribute to the global warming. To prevent this contrail management should be included.

The first option would be to store the water being produced during the flight to dispose the water at the airport after the plane has landed. Considering that 1 kg of hydrogen consumed would result in 8.94 kg of water (Scholz 2022). Given a propulsive demand of about 14 MW for a narrowbody plane during cruise flight this would result in 2.1 kg/s or 7500 kg of water being produced per hour (FlyZero 2022e). This additional weight could compromise the fuel economy and the total mass capacity of the plane. Therefore, this option is unacceptable.

The next option would be to continuously release the water after being produced. This option would benefit the weight of the plane by reducing the weight carried and making additional equipment for water storage unnecessary. But it would also take away the possibilities to manage the water disposal. As mentioned earlier at least for the phase of take-off and initial climb water storage must be installed to prevent the runway from getting sprayed with the exhaust water. This would result in reduced runway friction.

The third option would be to store a certain amount of water onboard the aircraft and to release it at certain conditions during the flight (FlyZero 2022e).

These conditions can be identified if the basic process behind the formation of contrails is kept in mind. Contrails form during the mixing of two air masses, one the exhaust gases which are warm and moist and the ambient air which is colder and drier. This mixing can result in a supersaturated state and droplets can form, which may freeze if the ambient air is sufficiently cold. This result in a contrail formation threshold temperature. This spontaneous

freezing limit for small droplets is around  $-38\text{ }^{\circ}\text{C}$  and if the ambient air is warmer the droplets remain liquid. This results in a contrail formation at cruise flight altitudes, but these contrails are only persistent within ice supersaturated air. Most of the contrails formed by a fuel cell aircraft should be not persistent which makes them without impact on the climate (Gierens 2021).

Another study implies that the effect of water to global warming emitted into the atmosphere decreases by decreasing the cruise altitude by avoiding the formation of contrails (Svensson 2004).

Another option of releasing the water during the flight would be to freeze the wastewater before it is emitted to the atmosphere. This system would prevent the creation of contrails completely.

When the water is frozen the ice cubes were discarded into the atmosphere. The ice cubes will melt before hitting the ground. The entire process should be monitored in regards of the ambient weather conditions to determine the size of the ice cubes and due to safety issues to prevent damage to other planes when dropping the ice cubes (Fuhs 2016).

The wastewater leaves the fuel cell at a temperature of about  $80\text{ }^{\circ}\text{C}$ . To meet the requirement of the ice machine the water must be precooled. The power needed to cool the water to meet this requirement is calculated by

$$P_{WWC} = c_{p,water} \cdot \dot{m}_{WW} \cdot (T_{WW} - 273,15\text{ K}) \quad . \quad (3.9)$$

With the specific heat capacity of water  $c_{p,water}$  set at  $4.2\text{ kJ/kg/K}$ , the mass flow of wastewater  $\dot{m}_{WW}$  according to assumption of a narrowbody aircraft set at  $2.1\text{ kg/s}$  and the needed cooling temperature which is the temperature difference between the wastewater temperature  $T_{WW}$  and the freezing point. This results in a needed power  $P_{PWC}$  of  $705.6\text{ kW}$ .

After being precooled the water enters the ice machine to be frozen. The power needed to freeze the water is calculated by

$$P_{WWF} = \Delta H_{v,water} \cdot \dot{m}_{WW} \quad . \quad (3.10)$$

With the latent heat vaporization of water  $\Delta H_{v,water}$  of  $334\text{ kJ/kg}$ . This results in an additional needed power  $P_{WWF}$  of  $701.4\text{ kW}$ .

Now the power for the whole process of producing ice cubes can be calculated by

$$P_{WWD} = P_{WWC} + P_{WWF} \quad . \quad (3.11)$$

This results in the total power needed of 1407 kW for the cooling and the freezing of the wastewater which is produced by the fuel cells. It has to be noted, that this method also takes the possibility away to discard waste heat with releasing warm water to the ambient air.

Due to the task of producing ice cubes an industrial ice cube maker is needed. According to Icemac 2023 such an ice machine can make up to 3000 kg of ice in 24 h. This machine has a mass of 700 kg and takes 3,808 m<sup>3</sup> of space. Considering the amount of ice produced by the fuel cells of about 7500 kg/h this would result in an ice machine with a mass of 42000 kg and a required space of 228,48 m<sup>3</sup>. This would increase the operating empty weight of the aircraft significantly and also exceeds the cargo capacity of any narrowbody aircraft.

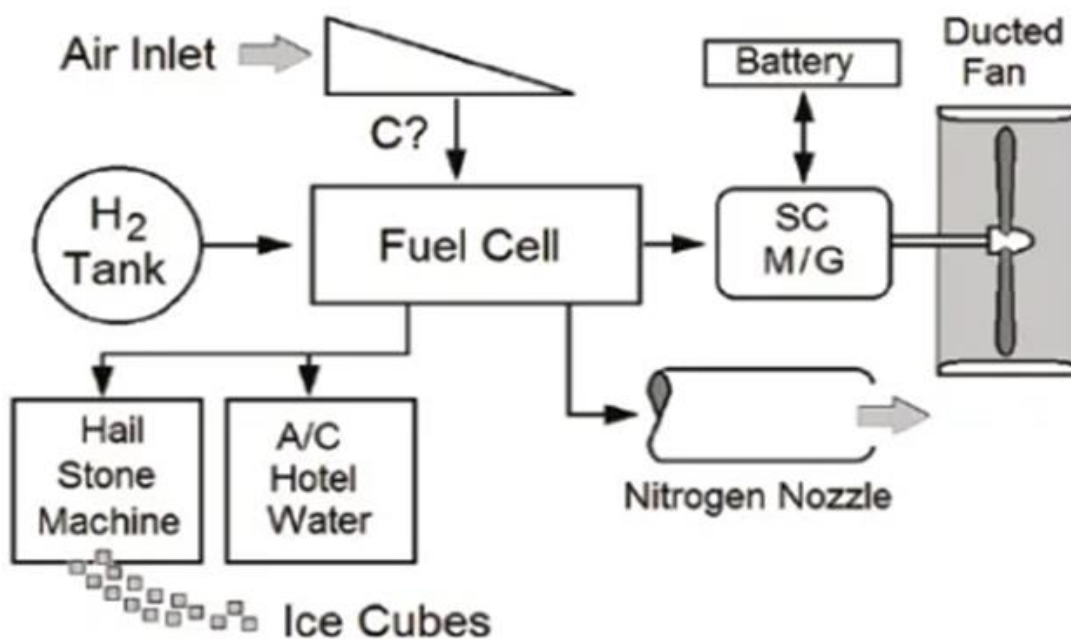


**Figure 3.25** Hydrogen-electric powertrain with an ice machine (Fuhs 2016)

### 3.3.6 Mass Budget for the Thermal Management System

This mass budget has been made by FlyZero to address the mass estimates of different components of the thermal management system of the regional plane concept. This concept featured a heat rejection of 5.1 MW at peak power demand during conditions ISA+40. The mass budget of the thermal management system except the water management system is shown in Table 3.4.

**Table 3.4** Mass estimation of the thermal management system (FlyZero 2022f)

Component	Subsystem	Total mass [kg]	Rejected heat/ weight [kW/kg]}
Condensers	Fuel cell stack cooling	510	10
Refrigerant compressors	Fuel cell stack cooling	153	33.3
Compressor electric motors	Fuel cell stack cooling	107	47.7
Refrigerant tanks	Fuel cell stack cooling	30	170
Refrigerant and pipes	Fuel cell stack cooling	95	53.7
Hydrogen-Refrigerant pre-conditioning heat exchangers	Fuel cell stack cooling	90	56.7
Expansion valves	Fuel cell stack cooling	3	1700
Total mass fuel cell Thermal management system		988	5.2
Air pre-cooler ambient air heat exchanger	Air system cooling	93	54.9
Air pre-cooler hydrogen heat exchanger	Air system cooling	37	137.8
Coolant pumps	Air system cooling	74	68.9
Coolant tanks	Air systems cooling	37	137.8
Pipes and coolant	Air system cooling	30	170
Total mass air system thermal management system	Air system cooling	271	18.8
Total mass thermal management system		1259	4

The schematics of the thermal management system is shown in Figure 3.26.

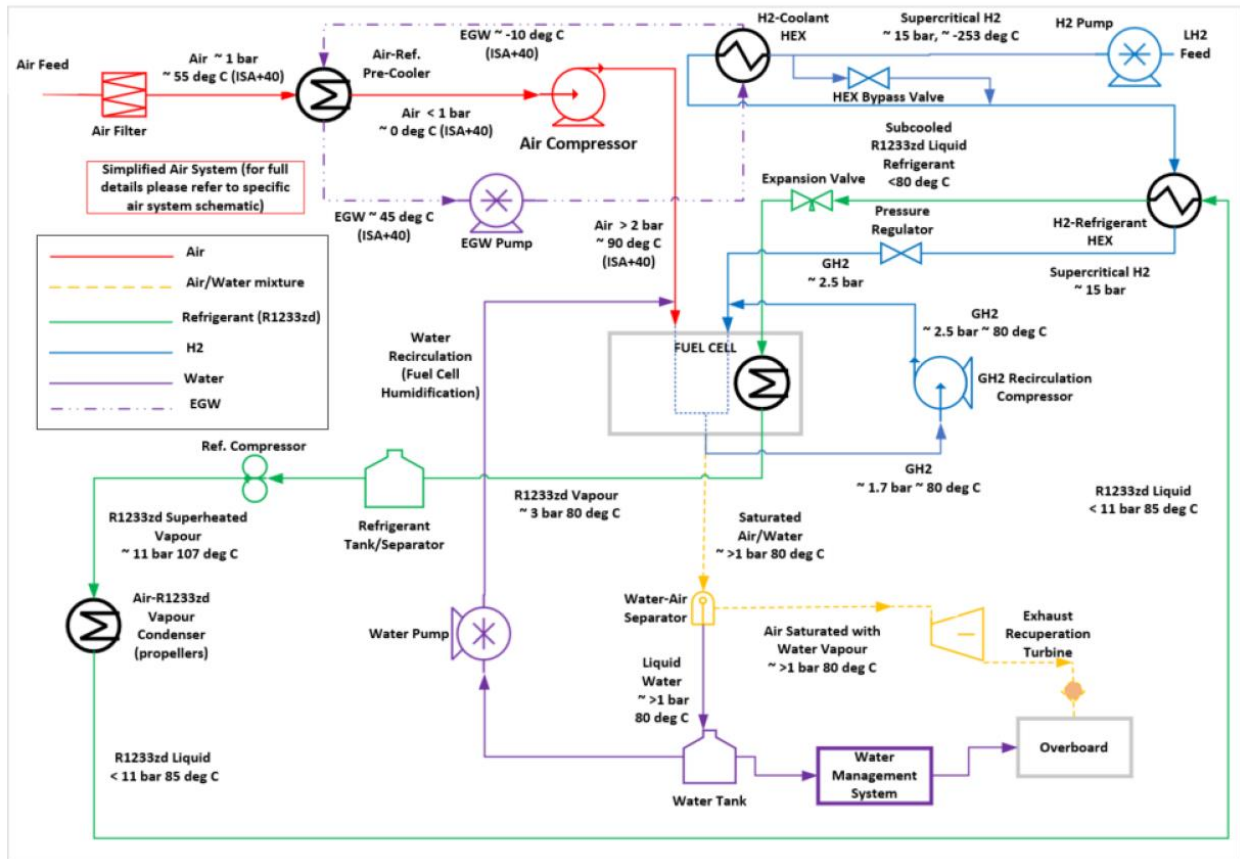


Figure 3.26 Schematic of the thermal management system (FlyZero 2022f)

### 3.4 Electric Propulsion and Thrust Devices

The final part of the hydrogen-electric powertrain is the electric propulsion system. This system is provided with electric energy by the fuel cells which is converted into shaft power. The shaft power is being transferred to a thrust device which generates the propulsive thrust. The schematic of the electric propulsion system including the thrust devices can be seen in Figure 3.27.

#### 3.4.1 DC/DC Convertor

These converters are used to manage the voltage from the fuel stack to fit the needs of the electric motor. This is necessary due to the voltage drop of the fuel cell when the power produced by the fuel cell increases (FlyZero 2022g).

These converters are a major contributor to the weight of the electric propulsion with a specific weight of 19 kW/kg ... 26 kW/kg (Jansen 2017) and an efficiency of 0.975 (Gesell 2012).

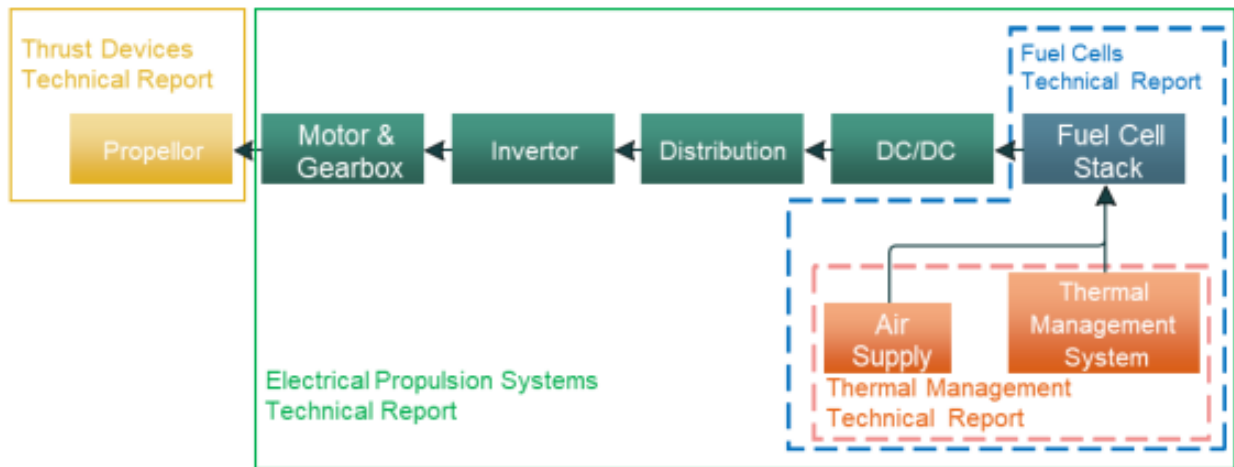


**Figure 3.27** Schematic of the electric propulsion (FlyZero 2022b)

### 3.4.2 Inverter and Distribution

These devices are the parts of the power electronics which are used for the power conversion and power distribution. The DC power is converted into AC current, and the rotation speed of the motor is controlled (FlyZero 2022f).

By now the power electronics features a power density of 14.3 kW/kg with an efficiency of 0.975 (Gesell 2018).

### 3.4.3 Electric Motor

The electric motor converts the electrical power into shaft power. It should be lightweight and highly efficient. Therefore, permanent magnet motors which run at about 15000 rpm are selected (FlyZero 2022f).

The power-to-weight ratio is about 5.2 kW/kg ... 9.5 kW/kg (Gesell 2018) and will be around 10 kW/kg in the near future (Kadyk 2018). The efficiency of the electric motor will be estimated at 0.95 (Hepperle 2012). The specific power of various electric motors in comparison to internal combustion engines can be seen in Figure 3.28.

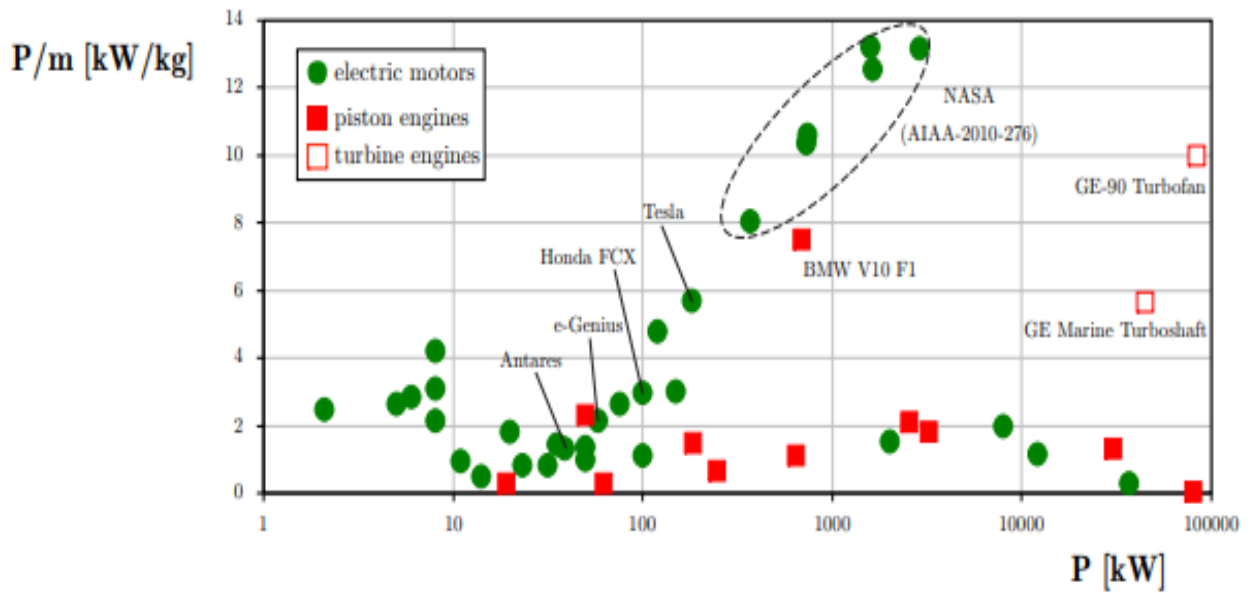


Figure 3.28 Specific power of current electric motors (Hepperle 2012)

### 3.4.4 Gearbox

The gearbox is necessary to adjust the output revolution per minute of the electric motor to the required value of the thrust device.

Its weight in lb  $m_{gb}$  will be calculated by the following equation (Teeuwen 2017)

$$m_{gb} = 95.7634 \cdot N_{rotor}^{0.38553} \cdot P_{Dslimit}^{0.78137} \cdot \frac{\omega_{eng}^{0.09899}}{\omega_{rotor}^{0.80686}} \quad (3.12)$$

With  $P_{Dslimit}$  as the drive system power limit which is the required take-off power in hp,  $N_{rotor}$  representing the number of rotors, and the rotation speed of the electric engine  $\omega_{eng}$  and the rotation speed of the rotor  $\omega_{rotor}$  both in rpm. The efficiency of the gearbox will be estimated at 0.98 (Hepperle 2012).

### 3.4.5 Propeller

The propeller has chosen as the thrust device due to the high efficiency during take-off which is identified as the phase of peak power demand. A high efficiency during this phase helps to significantly lower the weight of the hydrogen-electric powertrain (FlyZero 2022h).

The drawback of the propeller is its inferior efficiency at higher cruise speeds compared to other thrust devices. This results in longer flight times due to the lower cruise speed of the propeller.

The weight of the propeller in kg  $m_{prop}$  can be calculated with the following equation

$$m_{prop} = 1.1 \cdot (D_p \cdot P_{max} \cdot \sqrt{B})^{0.52} . \quad (3.13)$$

With  $D_p$  as the propeller diameter in m,  $P_{max}$  as the maximum propulsion power in kW and  $B$  as the number of propeller blades (Teeuwen 2017).

## 4 Fundamentals of the Preliminary Sizing

The stage of preliminary sizing is one of the most important stages during the process of designing a new aircraft. The stage itself follows the Method introduced by Loftin pictured in Figure 4.1.

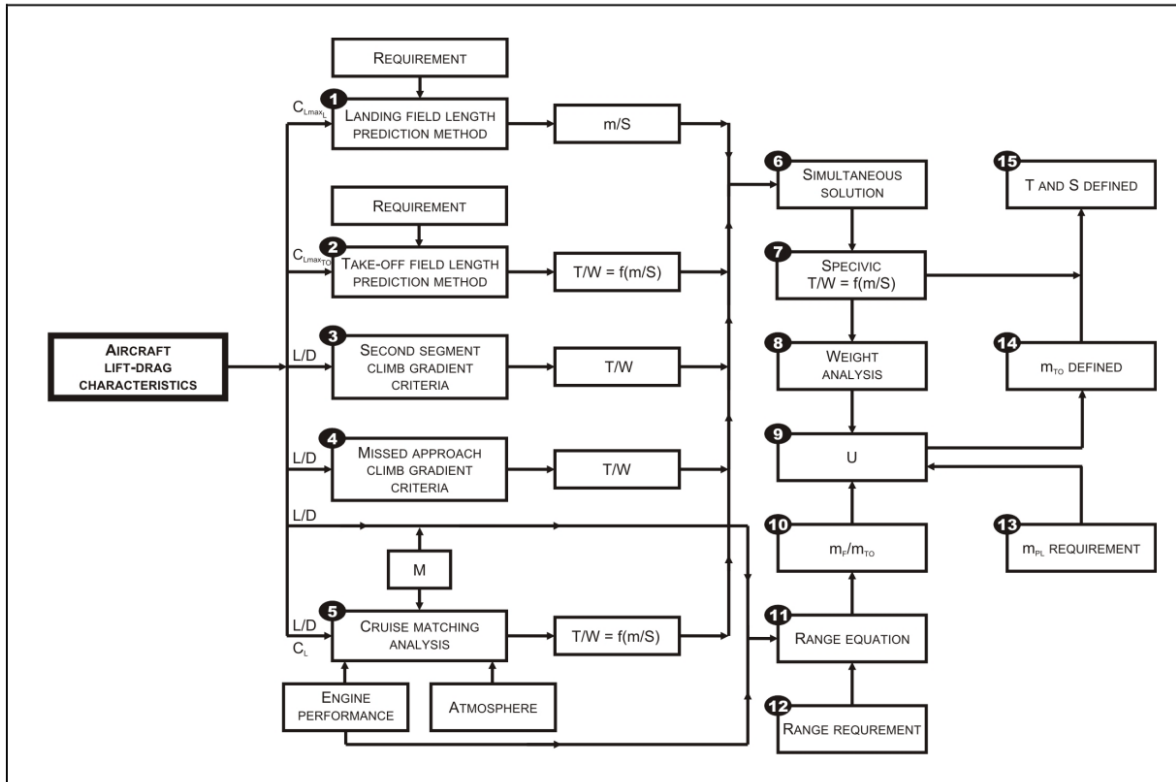


**Figure 4.1** The preliminary sizing process (Scholz 2015)

The method is divided into topics which relate to different flight phases: landing, takeoff, second segment, missed approach, and cruise. The different values of those flight phases attribute to the matching chart. This chart leads to the final step in which the maximum takeoff mass is calculated.

### 4.1 Landing

For the analysis of the landing distance, it is necessary to consider the regulation found in CS 25. A plane is allowed to land if the landing distance divided by a safety factor is shorter than the landing field length. This safety factor is 0.7 as the factor for propeller planes is being used. The landing field length is described in Figure 4.2.

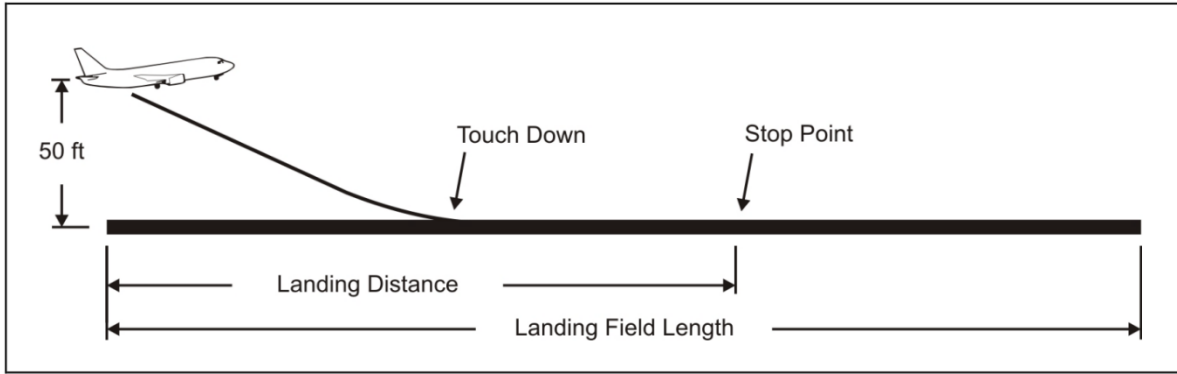


**Figure 4.2** Definition of the landing field length (Scholz 2015)

In a first step the relation of the approach speed  $V_{APP}$  and the landing field length  $S_{LFL}$  is defined as

$$V_{APP} = k_{APP} \sqrt{S_{LFL}} \quad . \quad (4.1)$$

With the Factor  $k_{APP}$ .

To evaluate the wing loading at maximum landing mass  $\frac{m_{MTO}}{S_W}$  conditions at sea-level with the relative density  $\sigma$  set at 1 will be estimated. The approach speed or the landing field length must be known as well as the maximum lift coefficient  $C_{L,max,L}$ .

$$\frac{m_{ML}}{S_W} = k_L \cdot \sigma \cdot S_{LFL} \cdot C_{L,max,L} \quad . \quad (4.2)$$

With the Factor  $k_L$  set at  $0.137 \text{ kg/m}^3$ .

Finally, the wing loading can be calculated with the following equation

$$\frac{m_{MTO}}{S_W} = \frac{m_{ML}/S_W}{m_{ML}/m_{MTO}} \quad . \quad (4.3)$$

With the mass ratio of landing and take-off  $m_{ML}/m_{MTO}$ .

## 4.2 Take-off

For the analysis of the take-off distance the regulations found in CS-25 apply. The take-off field length is defined as 115% of the distance the plane needs to fly over an obstacle of 35 feet. In case of a failed engine there are two options. If the engine fails before the plane reaches the decision speed the pilot must abort the take-off. The distance to stop the aircraft is called the accelerated stop distance. If the engine fails after the decision speed the take-off must be proceeded. This distance is called the take-off distance one engine inoperative. The distance which is larger becomes the balanced field length. The balanced field length is shown in Figure 4.3.

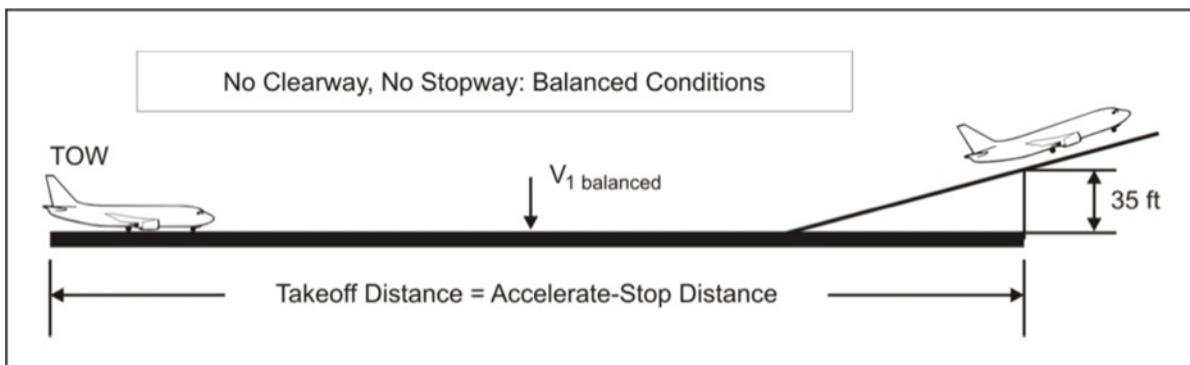


Figure 4.3 Definition of the balanced field length (Scholz 2015)

The power-to-weight-ratio is defined as

$$\frac{P_{S,TO}/m_{MTO}}{m_{MTO}/S_W} = \frac{k_{TO} \cdot 1.2 \cdot g \cdot V_{S,1}}{S_{TOFL} \cdot \sigma \cdot C_{L,max,TO} \cdot \eta_{P,TO} \cdot \sqrt{2}} \quad (4.4)$$

The maximum lift coefficient during take-off  $C_{L,max,TO}$  is derived from statistics or can be estimated with

$$C_{L,max,TO} = 0.8 \cdot C_{L,max,L} \quad (4.5)$$

With the stall speed during landing

$$V_{S,0} = \frac{V_{APP}}{1.23} \quad (4.6)$$

The stall speed  $V_{S,1}$  during take-off can be calculated with the following equation

$$V_{S,1} = V_{S,0} \cdot \sqrt{\frac{C_{L,max,L}}{C_{L,max,TO}}} \quad (4.7)$$

With  $k_{TO}$  as a factor set at 2,25 m<sup>3</sup>/kg,  $S_{TOFL}$  as the take-off field length in m and  $\eta_{P,TO}$  as the propeller efficiency during take-off.

### 4.3 Climb Rate during Second Segment

The flight phases following the take-off are shown in Figure 4.4. During the climb phase the power of the remaining engines must be sufficient to overcome the drag and a portion of the weight of the plane. The plane is still in take-off condition and one engine is inoperable while the other engines are at maximum power.

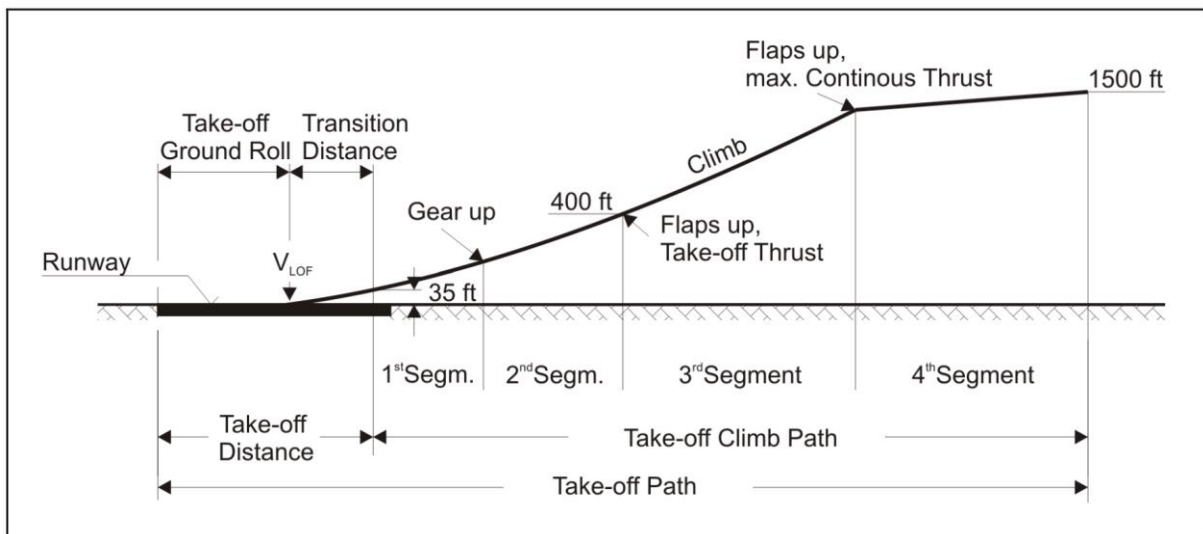


**Figure 4.4** Flight phases (Scholz 2015)

The lift coefficient during take-off is

$$C_{L,TO} = \frac{C_{L,max,TO}}{1.2^2} \quad (4.8)$$

The lift-to-drag ratio can be calculated with

$$E_{TO} = \frac{C_{L,TO}}{C_{D,P} + \frac{C_{L,TO}^2}{\pi \cdot A \cdot e}} \quad (4.9)$$

with an Oswald factor  $e$  of 0.7 due to the take-off configuration and the aspect ratio  $A$ . The profile drag coefficient  $C_{D,P}$  depends on the zero-lift drag, the drag caused by the high lift system and the drag of the landing gear.

$$C_{D,P} = C_{D,0} + \Delta C_{D,flap} + \Delta C_{D,slat} + \Delta C_{D,gear} \quad (4.10)$$

with

$$\Delta C_{D,flap} = 0.05 \cdot C_{L,TO} - 0.055 \quad . \quad (4.11)$$

According to Loftin 1980  $C_{D,0}$  can be set to 0.02 for a normal passenger aircraft,  $\Delta C_{D,slat}$  is neglectable and  $\Delta C_{D,gear}$  is zero due to the landing gear being retracted.

The power-to-weight ratio in the second segment by adapting the condition of engine failure is calculated by

$$\frac{P_{S,TO}}{m_{MTO}} = \left( \frac{n_e}{n_e - 1} \right) \cdot \left( \frac{1}{E_{TO}} + \sin \gamma \right) \cdot \left( \frac{V_2 \cdot g}{\eta_{P,2nd}} \right) \quad . \quad (4.12)$$

With  $n_e$  as the number of engines,  $\sin \gamma$  as the climb gradient during the second segment and  $\eta_{P,2nd}$  as the propeller efficiency during the second segment.

The take-off speed  $V_2$  is defined as

$$V_2 = 1.2 \cdot V_{S,1} \quad . \quad (4.13)$$

The climb of gradient is given by EASA 2021 dependent on the number of engines.

**Table 4.1** Gradient of climb during second segment (EASA 2021)

Number of Engines	Gradient of Climb	$\sin \gamma$
2	2.4%	0.024
3	2.7%	0.027
4	3.0%	0.03

## 4.4 Climb Rate during Missed Approach

In this phase the aircraft is in the process of the final approach before landing. Due to various circumstances the decision is made to abort the landing. The engines are set to take-off thrust and the plane climbs to make a new landing approach. The aircraft is still in landing configuration with the flaps in landing positions which causes considerable drag. The landing gear is still extended according to FAR 25 but not to CS 25.

The maximum lift coefficient is determined by the maximum lift coefficient in landing

$$C_{L,L} = \frac{C_{L,max,L}}{1.3^2} . \quad (4.14)$$

While the aircraft is still in landing configuration the lift-to-drag-ratio is to be calculated. An Oswald factor  $e$  of 0.7 is used due to the landing configuration.

$$E_L = \frac{C_{L,L}}{C_{D,P} + \frac{C_{L,L}^2}{\pi \cdot A \cdot e}} \quad (4.15)$$

Like in the second segment the profile drag is calculated by

$$C_{D,P} = C_{D,0} + \Delta C_{D,flap} + \Delta C_{D,slat} + \Delta C_{D,gear} \quad (4.16)$$

with

$$\Delta C_{D,flap} = 0.05 \cdot C_{L,TO} - 0.055 . \quad (4.17)$$

According to **Loftin 1980**  $C_{D,0}$  can be set to 0.02 for a normal passenger aircraft,  $\Delta C_{D,slat}$  is neglectable and  $\Delta C_{D,gear}$  is 0.015 if the landing gear is being retracted and 0.015 if the landing gear is still extended.

The power-to-weight-ratio is also like the ratio calculated during the second segment.

$$\frac{P_{S,TO}}{m_{MTO}} = \left( \frac{n_e}{n_e - 1} \right) \cdot \left( \frac{1}{E_{TO}} + \sin \gamma \right) \cdot \left( \frac{V_2 \cdot g}{\eta_{P,2nd}} \right) \cdot \frac{m_{ML}}{m_{MTO}} \quad (4.18)$$

## 4.5 Cruise

In this flight phase a stationary straight flight is assumed. The wing loading and the power-to-weight ratio are calculated separately as a function of altitude.

The calculation of the power-to-weight ratio follow the equations that drag is equal to thrust is defined as

$$\frac{P_{S,TO}}{m_{MTO}} = \frac{V_{CR} \cdot g}{\frac{P_{CR}}{P_{S,TO}} \cdot E \cdot \eta_{P,CR}} . \quad (4.19)$$

With the cruise speed  $V_{CR}$  and the propeller efficiency during cruise  $\eta_{P,CR}$ .

The lift-to-drag ratio needs to be calculated. The maximum lift-to-drag ratio is being determined by the following equation

$$E_{max} = k_E \cdot \sqrt{\frac{A}{S_{wet}/S_W}} \quad (4.20)$$

The factor  $k_E$  is chosen with a value of 11.22 for large propeller aircraft. The relative wetted area  $S_{wet}/S_W$  is commonly found in the range from 6.0 to 6.2 but because of the additional fuselage length which is caused by the hydrogen storage tanks this value might be incorrect. To get the correct value for the relative wetted area of the airplane this value will be calculated based on the data of the reference aircraft.

The dependance between the actual lift coefficient and the lift coefficient for flight with minimum drag can be calculated by

$$\frac{C_L}{C_{L,md}} = \frac{1}{\left(\frac{V}{V_{md}}\right)^2} \quad (4.21)$$

The ratio  $\left(\frac{V}{V_{md}}\right)$  could be set at 1 ... 1.316. Finally, the actual lift-to-drag ratio in cruise is defined as

$$E = \frac{2 \cdot E_{max}}{\left(\frac{C_L}{C_{L,md}}\right) + \frac{C_L}{C_{L,md}}} \quad (4.22)$$

Due to the use of an electric propulsion system, there is no altitude related change in the power of the airplane. Therefore, this ratio is set to 1 for all altitudes.

For the wing loading we follow the second equation about a stationary straight flight that lift equal weight

$$\frac{m_{MTO}}{S_W} = \frac{C_{L,CR} \cdot M_{CR}^2}{g} \cdot \frac{\gamma}{2} \cdot p(h) \quad (4.23)$$

With the lift coefficient during cruise  $C_{L,CR}$ , the mach number during cruise  $M_{CR}$  and the adiabatic index  $\gamma$  set at 1.4. The pressure  $p(h)$  is dependent on the height. The lift coefficient in cruise is defined by

$$C_{L,CR} = \frac{C_{L,md}}{\left(\frac{V}{V_{md}}\right)^2} \quad (4.24)$$

with

$$C_{L,md} = \frac{\pi \cdot A \cdot e}{2 \cdot E_{max}} \quad (4.25)$$

Finally, the separate result of wing loading, and power-to-weight ratio are entered in a chart in which the altitude varies. The different datapoints can be used to form a line in the matching chart.

## 4.6 Matching Chart

The matching chart solves a two-dimensional problem graphically. There are two variables:

- power-to-weight ratio,
- wing loading.

Every flight phase attributes a line to the matching chart which form the boundaries for the optimization.

The priority is to achieve the lowest power-to-weight ratio inside the boundaries possible. The second priority is to get the highest wing loading possible. Regarding these priorities a design point will be chosen. A generic matching chart is shown in Figure 4.5.

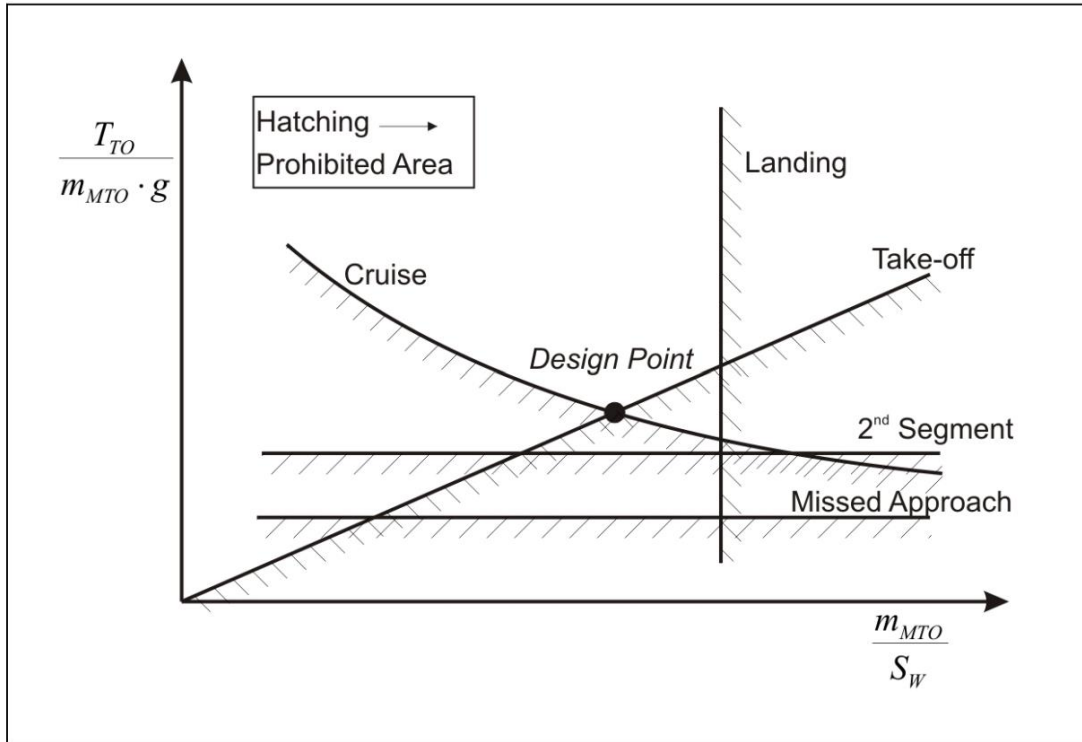


Figure 4.5 Generic matching chart (Scholz 2015)

## 4.7 Maximum Take-off Mass

The maximum take-off mass  $m_{MTO}$  is the total of the operating empty mass  $m_{OE}$ , the fuel mass  $m_F$ , and the mass of the maximum payload  $m_{MPL}$ .

$$m_{MTO} = \frac{m_{MPL}}{1 - \frac{m_F}{m_{MTO}} - \frac{m_{OE}}{m_{MTO}}} \quad (4.26)$$

The relative operating empty mass can be entered in a first step with the values of the reference aircraft. The relative fuel mass will be calculated with the total mission fuel fraction  $M_{ff}$ .

$$\frac{m_F}{m_{MTO}} = (1 - M_{ff}) \quad (4.27)$$

which consists of total fuel fraction

$$M_{ff} = M_{ff,std} \cdot M_{ff,res} \quad (4.28)$$

which itself is defined by the standard flight fuel fraction

$$M_{ff,std} = M_{ff,TO} \cdot M_{ff,CLB} \cdot M_{ff,CR} \cdot M_{ff,DES} \cdot M_{ff,L} \quad (4.29)$$

and the fuel fraction for all reserves

$$M_{ff,res} = M_{ff,RES} \cdot M_{ff,loiter} \cdot M_{ff,CLB} \cdot M_{ff,DES} \cdot \quad (4.30)$$

The standard flight fuel fraction is defined by the mass ratio for each flight phase. These flight phases are shown in Figure 4.6 with their segment mass fraction shown in Table 4.2.

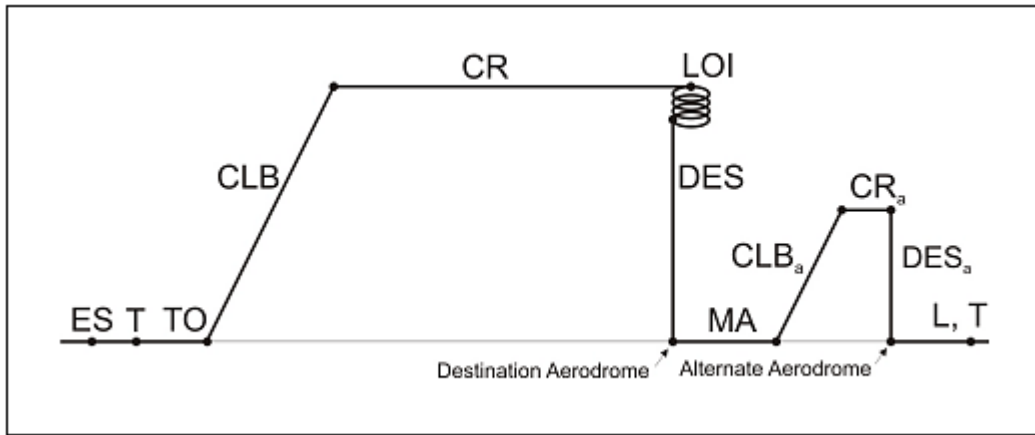


**Figure 4.6** Typical flight phases of a civil transport flight mission (Scholz 2015)

**Table 4.2** Mission segment mass fractions for regional turboprop (Scholz 2015)

Flight phase	take-off	climb	descent	landing	start-up	taxi
Mass fraction	0.995	0.985	0.985	0.995	0.990	0.995

The mass ratios for the flight phases of cruise and loiter will be calculated with the Breguet range factor

$$B_S = \frac{E \cdot \eta_{P,CR}}{SFC_P \cdot g} \quad (4.31)$$

With the specific fuel consumption for propeller driven aircraft  $SFC_P$ .

The mission fuel factor for the cruise is defined by

$$M_{ff,CR} = e^{-\frac{S_{CR}}{B_S}} \quad (4.32)$$

The mission fuel factor for loiter is calculated with

$$M_{ff,LOI} = e^{-\frac{t_{LOI}}{B_t}} . \quad (4.33)$$

with the Breguet factor for time

$$B_t = \frac{B_S}{V_{CR}} . \quad (4.34)$$

Now the maximum take-off mass is calculated. Now all other remaining aircraft parameters including the maximum landing weight, operating empty weight, fuel mass, wing area and the take-off power demand can be estimated.

Finally, a check of assumptions has been made to evaluate if the aircraft is finished.

$$m_{ML} > m_{OE} + m_{MPL} + m_{F,res} \quad (4.34)$$

## 5 PreSto-Classic-Prop Implementation

In this section the changes made to PreSto-Classic-Prop are shown. These changes were made to modify the existing spreadsheet for evaluating an aircraft equipped with a hydrogen-electric powertrain.

This worksheet which is shown in Figure 5.1 provides the user with the basic information and structure of the spreadsheet.

Method for preliminary sizing of hydrogen aircraft	
Author: Prof. Dr.-Ing. Dieter Scholz, MSME HAW Hamburg <a href="http://www.profscholz.de">http://www.profscholz.de</a>	Author: BA. Martin Gollnow HAW Hamburg <a href="http://Aero.ProfScholz.de">http://Aero.ProfScholz.de</a>
These worksheets show the method and example calculation for the <b>preliminary sizing of large propeller driven aircrafts</b> certified with respect to CS-25.	
The basic method of the preliminary sizing of the aircraft is shown in the worksheets "Preliminary Sizing I", "Max. Glide Ratio in Cruise", "Preliminary Sizing II". To meet the special requirements these already existing worksheets have been modified and the worksheets "Wetted Area", "Fuel consumption", "Fuel Containment System", "Fuel Cell System", "Heat Exchanger", "Electric Propulsion System", "Thrust Device", "Mass H2 Powertrain" have been added	
The calculation is illustrated with modified data from the Airbus A320-200.	

**Figure 5.1** Worksheet "Abstract"

### 5.1 Preliminary Sizing I

This worksheet covers the calculation for the flight phases approach, landing, take-off and missed approach. It starts with a user guide to inform about the different colors being used throughout the spreadsheet to make the user aware of how to manage the input and the results. The main modification is the calculation of the propeller efficiency which is now being done automatically utilizing an iteration loop with the worksheet "thrust devices."

## 5.2 Maximum Glide Ratio in Cruise

This worksheet which is shown in Figure 5.2 will calculate the maximum glide ratio during cruise flight. This value is important for any further calculations as the glide ratio during cruise flight affects the drag and therefore the range of the plane. The main issue concerning a hydrogen-electric aircraft is the additional fuselage length needed due to the hydrogen storage tanks. This additional fuselage length results due to the location of the tanks inside the fuselage. This additional length may influence the relative wetted area which makes a calculation of the wetted area necessary. Another issue which had to be implemented into the worksheet is the additional drag due to the heat exchanger of the thermal management system.

Max. Glide Ratio in Cruise			
Estimation of $k_E$ by means of 1.), 2.) or 3.)			
1.) From theory			
Oswald efficiency factor for $k_E$	e	0,75	
Equivalent surface friction coefficient	$C_{f,eqv}$	0,003	Roskam / Raymer (see FE-Script)
Factor	$k_E$	14,01	
2.) Acc. to RAYMER			
Factor	$k_E$	11,07	for retractable propeller aircraft
3.) From own statistics			
Factor	$k_E$	11,22	for large propeller driven aircraft: statistics give a value 11,22
Estimation of max. glide ratio in cruise, $E_{max}$			
Factor	$k_E$ chosen	14,20	<<<< Choose according to task
Relative wetted area	$S_{wet} / S_w$	7,932084377	from sheet 2.1.
Aspect ratio	A	16	from sheet 1
Max. glide ratio first iteration	$E_{max,I}$	20,17	
Oswald eff. factor, clean, example plan	e	0,85	
zero lift drag coefficient	$C_{D0}$	0,026261495	
calculation max. glide ratio with additional drag due to the heat exchanger			
drag coefficient heat exchanger	$C_{D,hex}$	0,03	drag coefficient heat exchanger hoerner
total drag coefficient	$C_{D,total}$	0,056261495	
max. glide ratio	$E_{max}$	13,78	max. glide with the external drag from the heat exchanger

Figure 5.2 Worksheet "Max. Glide in Cruise"

The maximum glide ratio is defined by

$$E_{max} = k_E \cdot \sqrt{\frac{A}{S_{wet} / S_w}} \quad (5.1)$$

With  $S_{wet} / S_w$  being calculated on the worksheet "Wetted Area" and A being provided from the worksheet "Preliminary Sizing I".

To estimate the modified glide ratio which takes the additional external drag due to the heat exchangers in account the zero lift drag coefficient is calculated by

$$C_{D0} = \frac{\pi \cdot A \cdot e}{4 \cdot E_{max}^2} . \quad (5.2)$$

The modified drag coefficient which includes the drag of the heat exchanger is defined by

$$C_{D,total} = C_{D0} + C_{D,hex} . \quad (5.3)$$

With  $C_{D,hex} = 0.06$  according to Hoerner 1965.

Finally, the maximum glide ration is estimated by

$$E_{max} = \frac{1}{2} \cdot \sqrt{\frac{\pi \cdot A \cdot e}{C_{D,total}}} . \quad (5.4)$$

### 5.3 Wetted Area

Due to the changes in the fuselage length the relative wetted area must be calculated. The necessary inputs are the dimensions of the example plane. The worksheet is shown in Figure 5.3.

The wetted area of the fuselage is defined by

$$S_{wet,F} = d_F \cdot l_f \cdot \left(1 - \frac{2}{\lambda_F}\right)^{\frac{2}{3}} \cdot \left(1 + \frac{1}{\lambda_F^2}\right) . \quad (5.5)$$

With  $l_f$  composed of the example plane fuselage length and the additional length of the hydrogen storage tanks, the slenderness ratio  $\lambda_F$ .

The wetted area of the wings is estimated by

$$S_{wet,W} = 2 \cdot S_{exp,W} \cdot \left(1 + 0.25 \cdot (t/c)_r \frac{1 + \tau \cdot \lambda}{1 + \lambda}\right) . \quad (5.6)$$

The wetted area of the horizontal tail, the nacelles and the vertical tail should be provided by the example plane or by statistics.

The total wetted of the airplane is estimated by

$$S_{wet} = S_{wet,F} + S_{wet,W} + S_{wet,H} + S_{wet,V} + N_E \cdot S_{wet,nacelle} \quad (5.7)$$

The relative wetted area is defined by

$$S_{wet}/S_w = \frac{S_{wet}}{S_w} \quad (5.8)$$

Calculation of the wetted area of the plane			
Fuselage			
length fuselage example plane	$l_{Fex}$	37,57 m	Airbus 2023
diameter of the fuselage	$d_F$	3,95 m	Airbus 2023
length of the fuselage h2 plane	$l_{F,hydrogen}$	56,5557115 m	tank and cabin combined
slenderness ratio	$\lambda_F$	14,3179017	
wetted area fuselage	$S_{wet,F}$	637,932918 m <sup>2</sup>	
Wing			
exposed wing area	$S_{exp,W}$	124,138089 m <sup>2</sup>	according to preliminary sizing II
	$t/c_t$	0,1347	Butterworth-Heinemann 2000
	$t/c_r$	0,1347	Butterworth-Heinemann 2000
	$\tau$	1	
	$\lambda$	0,24	Butterworth-Heinemann 2000
wetted area wing	$S_{wet,W}$	256,636878 m <sup>2</sup>	
horizontal tail			
wetted area horizontal tail	$S_{wet,H}$	31 m <sup>2</sup>	Butterworth-Heinemann 2000
vertical tail			
wetted area vertical tail	$S_{wet,V}$	21,5 m <sup>2</sup>	Butterworth-Heinemann 2000
nacelle			
wetted area nacelle	$S_{wet,nacelle}$	18,802 m <sup>2</sup>	
wetted area h2 plane	$S_{wet}$	984,673796	
Relative wetted area	$S_{wet}/S_w$	7,93208438	

**Figure 5.3** Worksheet "Wetted Area"

## 5.4 Preliminary Sizing II

This worksheet starts with the calculations needed for the flight phase. The worksheet also calculates the fuel mass and the different weights and the wing area of the plane. Finally, the results were checked in accordance with the “first law of aircraft design.”

Due to the change in propulsion the calculation of the cruise altitude is now calculated using the wing loading to estimate the pressure in cruise

$$p_{CR} = \frac{2 \cdot g \cdot m_{MTO} / S_W}{C_L \cdot M^2 \cdot \gamma} . \quad (5.9)$$

For the prop plane the cruise altitude can be calculated with the pressure. Due to the expected maximum cruising altitude below 11 km the cruising altitude is defined by

$$h_{CR} = \frac{T_0}{L} \cdot \left( 1 - \left( \frac{p_{CR}}{p_0} \right)^{\frac{1}{5.925588}} \right) . \quad (5.10)$$

Another change is the specific fuel consumption is now being calculated by the following worksheet “Fuel consumption” Also, iterations to calculate the maximum take-off mass and the take-off power have been implemented. These iteration loops are linked with the following worksheets which calculate all subsystems of the hydrogen-electric powertrain. These iteration loops affect each other to optimize the final result.

## 5.5 Matching Chart

The Matching Chart is the only worksheet which is unmodified. This worksheet is important to visualize the results and to check for the design point which is essential in the results.

## 5.6 Fuel Consumption

This worksheet shown in Figure 5.4 calculates the specific fuel consumption during cruise and take-off, it also calculates the fuel flow during taxiing.

In a first step the efficiency of the hydrogen-electric powertrain during take-off is defined as the product of the various efficiencies of the powertrain, which are  $\eta_{FC}$  for the fuel cell,  $\eta_{EL}$

for the electric motor,  $\eta_{P,CR}$  for the propeller during cruise and  $\eta_{P,TO}$  during take-off,  $\eta_{CONV}$  for the electric converter and  $\eta_{GEAR}$  for the gearbox.

$$\eta_{CR} = \eta_{FC} \cdot \eta_{EL} \cdot \eta_{P,CR} \cdot \eta_{CONV} \cdot \eta_{GEAR} \quad (5.11)$$

and

$$\eta_{TO} = \eta_{FC} \cdot \eta_{EL} \cdot \eta_{P,TO} \cdot \eta_{CONV} \cdot \eta_{GEAR} \quad (5.12)$$

The specific fuel consumption during cruise flight is estimated by

$$SFC_{CR} = \frac{1}{H_{LH2} \cdot \eta_{CR}} \quad (5.13)$$

With  $H_{LH2}$  as the lower heating value of the hydrogen and  $\eta_{CR}$  as the overall powertrain efficiency during cruise flight.

Calculating the efficiency and fuel consumption				
Efficiency of the powertrain				
lower heating value hydrogen	$H_{LH2}$	33 kWh/kg		
efficiency fuel cell	$\eta_{FC}$	0,6		from Hepperle 2012
efficiency electric motor	$\eta_{EL}$	0,95		from Gesell et al.
efficiency propeller cruise	$\eta_{P,CR}$	0,88130446		from sheet 8.1
efficiency propeller take-off	$\eta_{P,TO}$	0,53141214		from sheet 1
efficiency electric converter	$\eta_{CONV}$	0,989		from Gesell et al.
efficiency gear box	$\eta_{GEAR}$	0,995		from Gesell et al.
efficiency power propulsion system cruise	$\eta_{CR}$	0,49433368		
efficiency power propulsion system takeoff	$\eta_{TO}$	0,2980751		
power demand cruise	$P_{CR}$	13201,4521 kW		calculated power demand during cruise flight
additional drag power condensers cruise	$P_{CORE,CRUISE}$	3443,81021 kW		additional core drag power of the heat exchanger
total power demand cruise	$P_{CR,total}$	16645,2623 kW		total power demand during cruise
fuel flow cruise	$m_{F,CR}$	0,28062905 kg/s		hydrogen fuel flow during cruise
specific fuel consumption cruise	$SFC_{CR}$	1,6859E-08 kg/N/s		specific fuel consumption during cruise
propulsive power demand takeoff	$P_{S,TO,I}$	22339 kW		from sheet 3
additional power demand condensers TO	$P_{CORE,TO}$	366,5791 kW		from sheet 7.1
total power demand takeoff	$P_{TO,total}$	22705,4891 kW		
fuel flow takeoff	$m_{FF,TO}$	0,63484448 kg/s		
friction coefficient	$\mu_{concrete}$	0,02		
taxi speed	$V_{taxi}$	10 m/s		
power demand taxiing	$P_{taxi}$	170,527928 kW		
fuel flow taxiing	$m_{FF,taxi}$	0,00476795 kg/s		

Figure 5.4 Worksheet "Fuel consumption"

The total power demand during take-off is defined as

$$P_{TO,total} = P_{S,TO,I} + P_{CORE,TO} \quad (5.14)$$

With  $P_{S,TO,I}$  as the first iteration of the total power demand during takeoff taken from the Preliminary Sizing and  $P_{CORE,TO}$  as the additional power demand due to the heat exchangers from the worksheet "Heat Exchanger".

Additionally for the sizing of the water management system the fuel flow during take-off and taxiing is calculated by

$$\dot{m}_{FF,TO} = \frac{P_{TO,total}}{H_{LH2} \cdot \eta_{TO}} \quad (5.15)$$

and

$$\dot{m}_{FF,TO} = \frac{\mu_{concrete} \cdot v_{TAXI} \cdot m_{MTO} \cdot g}{H_{LH2} \cdot \eta_{TO}} \quad (5.16)$$

With  $\mu_{concrete}$  as the friction coefficient of the concrete pavement of the taxiway and  $v_{TAXI}$  as the taxiing speed of the aircraft.

## 5.7 Fuel Containment System

This worksheet shown in Figure 5.5 calculates the weight of the fuel containment system. The information which are provided by the user are the number and the radius of the tank. Both numbers influence the weight of this system. It should be mentioned that the radius of the tank has to be in accordance with the diameter of the aircraft's fuselage.

Dimension and weight of the fuel containment system						
number of tanks	N <sub>TANK</sub>	2	the minimum number are two tanks			
Radius of the tank	R <sub>TANK</sub>	1,5 m	chosen according to the diameter of the fuselage of the plane			
Length cylindric part of ONE tank	l <sub>TANK,CY</sub>	6,2 m				
overall lenght of ONE tank	l <sub>TANK</sub>	9,5 m	thickness of the insulation	th <sub>INS</sub>	0,15 m	
Surface of the ONE tank	S <sub>TANK</sub>	86,6 m <sup>2</sup>				
mass of ONE tank	m <sub>TANK</sub>	259,9 kg	mass tank per surface	m <sub>TANK</sub> /S <sub>TANK</sub>	3 kg/m <sup>2</sup>	Seekt 2010
mass insulation ONE tank	m <sub>INS</sub>	433,2 kg	mass insulation per surface	m <sub>INS</sub> /S <sub>TANK</sub>	5 kg/m <sup>2</sup>	Seekt 2010, foam insulation of the tank
mass attachments ONE tank	m <sub>ATTACH</sub>	694,9 kg	mass attachments per volume	m <sub>ATTACH</sub> /V <sub>TANK</sub>	12 kg/m <sup>3</sup>	Westenberger 2003, includes all attachments to the tank
mass of ONE tank system	m <sub>ts</sub>	1388,1 kg				
mass of fuel containment system	m <sub>FCS</sub>	2776,1 kg				

Figure 5.5 Worksheet "Fuel Containment System"

In a first step the length of the cylindrical part of the tank will be estimated by

$$l_{TANK,CY} = \frac{\frac{V_{F,erf}}{N_{TANK}} - \frac{4 \cdot \pi \cdot r_{TANK}^3}{3}}{\pi \cdot r_{TANK}^2} . \quad (5.17)$$

With  $V_{F,erf}$  as the required fuel volume,  $N_{TANK}$  as the number of fuel tanks, and the radius of the fuel tank  $r_{TANK}$ .

The overall length of one tank is defined by

$$l_{TANK} = l_{TANK,CY} + 2 \cdot (r_{TANK} + th_{INS}) . \quad (5.18)$$

With  $th_{INS}$  as the insulation thickness of the fuel tank.

The surface of one tank can be calculated with

$$S_{TANK} = 2 \cdot \pi \cdot r_{TANK} \cdot l_{TANK,CY} + 4 \cdot \pi \cdot r_{TANK}^2 . \quad (5.19)$$

The mass of one tank is

$$m_{TANK} = S_{TANK} \cdot m_{TANK}/S_{TANK} . \quad (5.20)$$

According to Seekt 2010 the mass tank per surface  $m_{TANK}/S_{TANK}$  is set at 3 kg/m<sup>2</sup>.

The mass of the insulation is

$$m_{INS} = S_{TANK} \cdot m_{INS}/S_{TANK} . \quad (5.21)$$

According to Seekt 2010 the mass insulation per surface  $m_{INS}/S_{TANK}$  is set at 5 kg/m<sup>2</sup> while using foam insulation.

The mass of the attachments of the tank is defined by

$$m_{ATTACH} = V_{TANK} \cdot m_{ATTACH}/V_{TANK} . \quad (5.22)$$

The tank volume which is also needed will be provided by the worksheet ‘‘Preliminary Sizing II.’’ According to Westenberger 2003 the mass of the attachments to the tank per volume  $m_{ATTACH}/V_{TANK}$  is set at 12 kg/m<sup>3</sup>.

Finally, the mass of the fuel containment system can be calculated with

$$m_{FCS} = N_{TANK} \cdot (m_{TANK} + m_{INS} + m_{ATTACH}) \quad . \quad (5.23)$$

## 5.8 Fuel Cell

The aim of this worksheet shown in Figure 5.6 is to calculate the weight of the fuel cell system with its subsystems. These subsystems include the fuel cell thermal management system, the air thermal management system and the water management system.

Mass of the fuel cells					
mass fuel cells	$m_{FC}$	3349,05964 kg	power density fuel cell future	$\Phi_{FC,ft}$	8 Kadyk et al. 2018
			power density fuel cell current	$\Phi_{FC,ct}$	1,6 Kadyk et al. 2018
			oversizing factor fuel cell	$of_{FC}$	1,18 Flyzero 2022f
Amount of waste heat					
fuel cell efficiency	$\eta_{FC}$	0,6			
waste heat	$P_{WH}$	9082,19563 kW	total waste heat of the fuel cell system		
specific heat capacity hydrogen	$c_{p,H_2}$	14,3 kJ/kg/K			
storage temperature hydrogen	$T_{LH_2store}$	20,15 K			
temperature fuel cell feed	$T_{FCF}$	283,15 K			Flyzero 2022f
temperature waste water	$T_{WW}$	353,15 K			
isobaric mass heat capacity water liquid	$c_{p,water}$	4,2 kJ/kg/K			
latent heat vaporisation	$\Delta H_{v,water}$	334 kJ/kg			
Energy line heater fuel cell	$P_{LH}$	2387,5866 kW	waste heat utilized for preconditioning the hydrogen fuel feed		
Energy waste water	$P_{WW}$	1559,81288 kW	waste heat disposed by emitting water to the atmosphere or water storage		
excessive waste heat	$P_{EWH}$	5134,79615 kW	remaining waste heat to emitted to the ambient air		
fuel cell thermal managment system					
condenser	$m_C$	513,479615 kg	rejected heat/weight condensor	10 kW/kg	Flyzero 2022f
refrigerant compressor	$m_{RC}$	154,198083 kg	rejected heat/weight refrigerant compressor	33,3 kW/kg	Flyzero 2022f
compressor electric motor	$m_{CEL}$	107,647718 kg	rejected heat/weight compressor electric motors	47,7 kW/kg	Flyzero 2022f
refrigerant tank	$m_{RT}$	30,2046832 kg	rejected heat/weight refrigerant tank	170 kW/kg	Flyzero 2022f
refrigerant and pipes	$m_{RP}$	9,56200401 kg	rejected heat/weight refrigerant and pipes	53,7 kW/kg	Flyzero 2022f
heat exchanger H2-Refrigerant	$m_{HX,LH_2}$	90,5607787 kg	rejected heat/weight heat exchanger H2-Refrigerant	56,7 kW/kg	Flyzero 2022f
Expansion valves	$m_{EV}$	3,02046832 kg	rejected heat/weight expansion valves	1700 kW/kg	Flyzero 2022f
total mass fuel cell tms	$m_{FC,TMS}$	908,67335 kg			
air system TMS					
heat exchanger air pre-cooler	$m_{HX,air}$	93,5299846 kg	rejected heat/weight heat exchanger air pre-cooler	54,9 kW/kg	Flyzero 2022f
heat exchanger hydrogen pre-cooler	$m_{HX,LH_2p}$	37,2626716 kg	rejected heat/weight refrigerant heat exchanger hydrogen pre-cooler	137,8 kW/kg	Flyzero 2022f
coolant pumps	$m_{CP}$	74,5253433 kg	rejected heat/weight coolant pumps	68,9 kW/kg	Flyzero 2022f
coolant tanks	$m_{CT}$	37,2626716 kg	rejected heat/weight coolant tanks	137,8 kW/kg	Flyzero 2022f
pipes and coolant	$m_{PC}$	30,2046832 kg	rejected heat/weight pipes and coolant	170 kW/kg	Flyzero 2022f
total mass air system tms	$m_{ASTMS}$	272,785354 kg			
water system					
water tank take-off and climb					
water pump	$m_{WP}$	70 kg			Flyzero 2022f
water tank	$m_{WT}$	419,262232 kg	time for takeoff run and reaching 1000 m over ground	70 sec	
air water seperator	$m_{AWS}$	50 kg	time for taxxing	450 sec	Flyzero 2022f
total mass water system	$m_{WS}$	539,262232 kg			
total mass tms	$m_{TMS}$	1720,72094 kg			
total mass fuel cell system	$m_{FCS}$	5069,78058 kg			

Figure 5.6 Worksheet "Fuel Cell"

The calculation for the mass of the fuel cell anticipates the take-off power  $P_{TO,total}$  from the worksheet “Fuel consumption”, the fuel cell oversizing factor  $of_{FC}$ , and the power density of the fuel cells  $\Phi_{FC}$ .

$$m_{FC} = \frac{P_{TO,total}}{\Phi_{FC} \cdot of_{FC}} \quad (5.24)$$

The power density of the fuel cell is also a major mass contributor to the overall mass of the powertrain. In the worksheet are two values to choose from, one value represents the current situation and the other one represents a value in the near future. By switching between those values, the complete system mass of the aircraft changes due to the iteration loops. In this way it is possible to evaluate the enabling technology of the hydrogen powered aircraft.

In the next step the waste heat during peak power demand is being calculated by

$$P_{WH} = P_{TO,total} \cdot \eta_{FC} \quad (5.25)$$

With  $\eta_{FC}$  as the fuel cell efficiency.

To minimize the load on the thermal management system and therefore the weight of this system the waste heat will be used to transfer energy from the waste heat to the hydrogen fuel feed. This is necessary as the hydrogen is being stored in cryogenic state and needs to be conditioned to the needs of the fuel cell.

$$P_{LH} = c_{p,LH2} \cdot (T_{FCF} - T_{LH2store}) \cdot \dot{m}_{FF,TO} \quad (5.26)$$

With  $c_{p,LH2}$  as the specific heat capacity of the hydrogen propellant,  $T_{FCF}$  as the fuel feed temperature of the fuel cells,  $T_{LH2store}$  as the storage temperature of the hydrogen propellant and  $\dot{m}_{FF,TO}$  as the fuel flow during take-off.

Due to the release of excess water produced by the fuel cells to the ambient air the containing heat is released.

$$P_{WW} = c_{p,water} \cdot \dot{m}_{FF,TO} \cdot (T_{WW} - T_0) \quad (5.27)$$

With  $c_{p,water}$  as the specific heat capacity of liquid water,  $T_{WW}$  as the temperature of the wastewater,  $T_0$  as the temperature of the ambient air.

The remaining waste heat is the load of the thermal management system

$$P_{EWH} = P_{WW} - P_{LH} \quad (5.28)$$

Now the different subsystems of the fuel cell will be calculated using the rejected heat to weight ratio of FlyZero 2022f. Starting with the components of the fuel cell thermal management system.

The weight of the condenser will be estimated according to FlyZero 2022f with the ratio of rejected heat to weight  $sr_C$  set at 10 kW/kg.

$$m_c = \frac{P_{EWH}}{sr_C} \quad (5.29)$$

The weight of the refrigerant compressor will be estimated according to FlyZero 2022f with the ratio of rejected heat to weight  $sr_{RC}$  set at 33.3 kW/kg.

$$m_{RC} = \frac{P_{EWH}}{sr_{RC}} \quad (5.30)$$

The weight of the compressor electric motor will be estimated according to FlyZero 2022f with the ratio of rejected heat to weight  $sr_{CEL}$  set at 47.7 kW/kg.

$$m_{CEL} = \frac{P_{EWH}}{sr_{CEL}} \quad (5.31)$$

The weight of the refrigerant tank will be estimated according to FlyZero 2022f with the ratio of rejected heat to weight  $sr_{RT}$  set at 170 kW/kg.

$$m_{RT} = \frac{P_{EWH}}{sr_{RT}} \quad (5.32)$$

The weight of the refrigerant and pipes will be estimated according to FlyZero 2022f with the ratio of rejected heat to weight  $sr_{RP}$  set at 53.7 kW/kg.

$$m_{RP} = \frac{P_{EWH}}{sr_{RP}} \quad (5.33)$$

The weight of the heat exchanger LH2-refrigerant will be estimated according to FlyZero 2022f with the ratio of rejected heat to weight  $sr_{HX,LH2}$  set at 56.7 kW/kg.

$$m_{HX,LH2} = \frac{P_{EWH}}{sr_{HX,LH2}} \quad (5.34)$$

The weight of the expansion valves will be estimated according to FlyZero 2022f with the ratio of rejected heat to weight  $sr_{EV}$  set at 1700 kW/kg.

$$m_{EV} = \frac{P_{EWH}}{sr_{EV}} \quad (5.35)$$

The total mass of the fuel cell thermal management system is the sum of its components.

$$m_{FC,TMS} = m_C + m_{RC} + m_{CEL} + m_{RT} + m_{RP} + m_{HX,LH2} + m_{EV} \quad (5.36)$$

Continuing with the components of the air systems thermal management system.

The weight of the heat exchanger air pre-cooler will be estimated according to FlyZero 2022f with the ratio of rejected heat to weight  $sr_{HX,air}$  set at 54.9 kW/kg.

$$m_{HX,air} = \frac{P_{EWH}}{sr_{HX,air}} \quad (5.37)$$

The weight of the heat exchanger hydrogen pre-cooler will be estimated according to FlyZero 2022f with the ratio of rejected heat to weight  $sr_{HX,LH2p}$  set at 137.8 kW/kg.

$$m_{HX,LH2p} = \frac{P_{EWH}}{sr_{HX,LH2p}} \quad (5.38)$$

The weight of the coolant pumps will be estimated according to FlyZero 2022f with the ratio of rejected heat to weight  $sr_{CP}$  set at 68.9 kW/kg.

$$m_{CP} = \frac{P_{EWH}}{sr_{CP}} \quad (5.39)$$

The weight of the coolant tank will be estimated according to FlyZero 2022f with the ratio of rejected heat to weight  $sr_{CT}$  set at 137.8 kW/kg.

$$m_{CT} = \frac{P_{EWH}}{sr_{CT}} \quad (5.40)$$

The weight of the pipes and coolant will be estimated according to FlyZero 2022f with the ratio of rejected heat to weight  $sr_{PC}$  set at 170 kW/kg.

$$m_{PC} = \frac{P_{EWH}}{sr_{PC}} \quad (5.41)$$

The total mass of the air system thermal management system is the sum of its components.

$$m_{AS,TMS} = m_{HX,air} + m_{HX,LH2p} + m_{CP} + m_{CT} + m_{PC} \quad (5.42)$$

The third subsystem is the water system which consists of the water pump, the water tank, and the air-water separator. According to FlyZero 2022f the weight of the water pump  $m_{WP}$  will be set at 70 kg, the weight of the air-water separator  $m_{AWS}$  will be estimated with 50 kg. The weight of the water tank can be calculated by

$$m_{WT} = t_{TO} \cdot \dot{m}_{FF,TO} + t_{TAXI} \cdot \dot{m}_{FF,taxi} \quad (5.43)$$

With  $t_{TO}$  as the time for the takeoff and for reaching a height of 1000 meter,  $\dot{m}_{FF,TO}$  as the fuel flow during take-off,  $t_{TAXI}$  as the time for taxiing and  $\dot{m}_{FF,taxi}$  as the fuel flow during taxiing.

The total mass of the water system can be calculated by

$$m_{WS} = m_{WP} + m_{AWS} + m_{WT} \quad (5.44)$$

The total mass of the thermal management systems consists of the sum of its subsystems.

$$m_{TMS} = m_{FC,TMS} + m_{AS,TMS} + m_{WS} \quad (5.45)$$

The mass of the fuel cell system consists of the mass of the fuel cell and the mass of the thermal management system.

$$m_{FCS} = m_{FC} + m_{TMS} \quad (5.46)$$

## 5.9 Heat Exchanger

This worksheet shown in Figure 5.7 contains the sizing considerations of the heat exchanger which are a part of the fuel cell thermal management system. Based on the vapor compression cycle of the FlyZero regional plane concept the dimension of the heat exchanger is calculated under ISA+40 conditions.

sizing considerations heat exchanger			
Isobaric mass heat capacity air	$c_{p,air}$	1,004 kJ/kg/K	
density air sea-level	$\rho_{air}$	1,225 kg/m <sup>3</sup>	
Isobaric mass heat capacity R1233 liquid	$c_{p,r1233,liquid}$	1,243 kJ/kg/K	Climalife 2014
latent heat vaporisation	$\Delta H_{v,R1233}$	195,35 kJ/kg	Climalife 2014
Isobaric mass heat capacity R1233 vapour	$c_{p,r1233,vapour}$	0,825 kJ/kg/K	Climalife 2014
boiling temperature 11 bar	$T_{B,r1233}$	373,15 K	Climalife 2014
temperature ambient air	$T_{air,in}$	328,15 K	ISA +40 conditions
temperature inlet coolant	$T_{cool,in}$	380,15 K	FlyZero
total temperature difference	$\Delta T_{all}$	52 K	maximum Temperature that could emitted to the ambient air
needed mass flow air	$\dot{m}_{air}$	98,3526692 kg/s	
needed mass flow water	$\dot{m}_{water}$	24,4716868 kg/s	
needed air inlet	$A_{inlet}$	1,31510154 m <sup>2</sup>	important for the drag considerations, sized for take-off speed
core drag cruise	$D_{core,CR}$	18404,0193 N	internal drag of the heat exchanger due to the mass flow during cruise
core drag power cruise	$P_{core,CR}$	3443,81021 kW	
core drag take-off	$D_{core,TO}$	6004,50106 N	
core drag power take-off	$P_{core,TO}$	366,5791 kW	

**Figure 5.7** Worksheet "Heat Exchanger"

In a first step the temperature difference between the temperature of the ambient air  $T_{air,in}$  and the coolant inlet  $T_{cool,in}$  will be calculated by

$$\Delta T_{all} = T_{cool,in} - T_{air,in} \quad (5.47)$$

Now the needed mass flow of air can be calculated by

$$\dot{m}_{air} = \frac{P_{EWH}}{c_{p,air} \cdot \Delta T_{all}} \quad (5.48)$$

As well as the need mass flow of the coolant

$$\dot{m}_{air} = \frac{P_{EWH}}{c_{p,vp} \cdot (T_{cool,in} - T_{B,r1233}) + \Delta H_{v,r1233} + c_{p,liq} \cdot (T_{B,r1233} - T_{air,in})} \quad (5.49)$$

With  $c_{p,vp}$  as the isobaric mass heat capacity of the R1233 vapor,  $T_{B,r1233}$  as the boiling temperature at 11 bar and  $c_{p,liq}$  in liquid state as well as  $\Delta H_{v,r1233}$  as the latent heat vaporization.

Due to the initial climb being the critical phase because of the highest power demand the needed air inlet area will be calculated

$$A_{inlet} = \frac{\dot{m}_{air}}{\rho_{air} \cdot V_2} \quad (5.50)$$

This value is used to calculate the modified glide ratio of the hydrogen plane in the worksheet “Maximum Glide Ratio in Cruise.”

In the next step the core drag power of the heat exchanger during cruise and take-off is being calculated by

$$D_{core,CR} = \dot{m}_{air} \cdot V_{CR} \tag{5.51}$$

$$D_{core,TO} = \dot{m}_{air} \cdot V_2 \tag{5.52}$$

The core drag during cruise and take-off is being calculated by

$$P_{core,CR} = D_{core,CR} \cdot V_{CR} \tag{5.53}$$

$$P_{core,TO} = D_{core,TO} \cdot V_2 \tag{5.54}$$

Which is used to modify the fuel consumption during cruise in the worksheet “Fuel consumption” to determine the fuel consumption of the hydrogen powered plane.

The additional core drag power due to the heat exchangers during take-off is used to determine the fuel consumption during take-off and modifies the take-off power in the worksheet “Preliminary Sizing II” to calculate the take-off power with the additional drag power caused by the heat exchangers.

## 5.10 Electric Propulsion System

This worksheet which is shown in Figure 5.8 will calculate the weight of the electric propulsion system

mass electric propulsion system							
mass of the electronic motor	m <sub>ELEM</sub>	2270,54891 kg	mass to power ratio future	ϕ <sub>ELEM,FT</sub>	10 kW/kg	Kadyk et al. 2018	
			mass to power ratio current	ϕ <sub>ELEM,CT</sub>	5.2 kW/kg	Kadyk et al. 2018	
mass power electronics	m <sub>PEL</sub>	1587,79644 kg	mass to power ratio power electronics	ϕ <sub>PEL</sub>	14.3 kW/kg	Gesell et al 2018	
mass DC-DC converter	m <sub>CONV</sub>	366,217566 kg	mass to power ratio DC-DC converter	ϕ <sub>CONV</sub>	62 kW/kg	Gesell et al 2018	
mass cooling electric motor	m <sub>ELEMcool</sub>	1513,69927 kg	mass to power ratio cooling electric motor	ϕ <sub>ELEMcool</sub>	15 kW/kg	Gesell et al 2018	
total mass electric propulsion system	m <sub>ELEPS</sub>	5738,26218 kg					

**Figure 5.8** Worksheet "Electric Propulsion System"

This worksheet utilizes the take-off power calculated in the worksheet “Fuel consumption” as input value for the sizing of the electrical propulsion system.

The power-to-weight ratio of the electronic motor has been identified to be the main weight contributor in this part of the drivetrain. Due to its effect on the overall weight of the system and new upcoming technology which significantly affects both the weight of the electronic motor itself but also the powertrain a value of the near future has been added. This gives the opportunity to analyze these changes and their effect on the whole aircraft system.

The weight of the electric motor will be estimated according to Kadyk 2018 with the ratio of power to mass  $\phi_{ELM,CT}$  for the current technology set at 5.2 kW/kg and  $\phi_{ELM,FT}$  for the future technology set at 10 kW/kg.

$$m_{ELM} = \frac{P_{TO,total}}{\phi_{ELM}} \quad (5.55)$$

The weight of the power electronics will be estimated according to Gesell 2018 with the ratio of power to mass  $\phi_{PEL}$  set at 14.3 kW/kg.

$$m_{PEL} = \frac{P_{TO,total}}{\phi_{PEL}} \quad (5.56)$$

The weight of the DC-DC converter will be estimated according to Gesell 2018 with the ratio of power to mass  $\phi_{CONV}$  set at 62 kW/kg.

$$m_{CONV} = \frac{P_{TO,total}}{\phi_{CONV}} \quad (5.57)$$

The weight of the electric motor cooling will be estimated according to Gesell 2018 with the ratio of power to mass  $\phi_{ELMcool}$  set at 15 kW/kg.

$$m_{ELMcool} = \frac{P_{TO,total}}{\phi_{ELMcool}} \quad (5.58)$$

The total mass of the electric propulsion system is the sum of its components.

$$m_{ELPS} = m_{ELM} + m_{PEL} + m_{CONV} + m_{ELMcool} \quad (5.59)$$

## 5.11 Thrust Device

This worksheet which is shown in Figure 5.9 calculates the mass of the propeller and the gearbox attached to it.

<b>Estimation of the propeller size</b>			
Propeller Disc Area	$S_D$	18,5641778	<b>m<sup>2</sup></b>
Propeller Disc Diameter	$d_D$	4,86175331	<b>m</b>
Rotational speed propeller	$\omega_{prop}$	779,841945	<b>rpm</b>
number of main rotors	$N_{rotor}$	2	
Propeller disc loading	$L$	499,216645	<b>kWm/kg</b>
<b>Propeller efficiency</b>			
takeoff	$\eta^{P_{TO}}$	0,53141214	-
2nd segment	$\eta^{P_{2ndS}}$	0,64536042	-
missed approach	$\eta^{P_{MA}}$	0,64161265	-
cruise	$\eta^{P_{CR}}$	0,88130446	-
<b>mass estimation</b>			
Number of blades	$B$	6	FlyZero
mass estimation ONE propeller	$m_{prop,s}$	357,240905	<b>kg</b> Teeuwen 2011
mass estimation ALL propeller	$m_{prop}$	714,481809	<b>kg</b>
rotational speed electrical engine	$\omega_{eng}$	15000	<b>rpm</b> FlyZero
mass estimation gearbox ALL Gearbox	$m_{gb,s}$	1264,66681	<b>lb</b> W. Johnson 2

**Figure 5.9** Worksheet "Thrust Devices"

The mass estimation for one propeller  $m_{prop,Single}$  in kg can be calculated with the following equation according to Teeuwen 2017

$$m_{prop,Single} = 1.1 \cdot (d_D \cdot P_{S,TO} / N_E \cdot \sqrt{B})^{0.52} . \quad (5.60)$$

With  $B$  as the number of blades of each propeller,  $d_D$  as the propeller diameter in m,  $P_{S,TO}/n_E$  as the take-off power of one engine in kW.

The propeller disc diameter  $d_D$  can be calculated by

$$d_D = \sqrt{\frac{4 \cdot S_D}{\pi}} . \quad (5.61)$$

The Propeller disc area  $S_D$  can be calculated by

$$S_D = \frac{P_{S,TO}/N_E}{L_D \cdot \rho_0} \quad (5.62)$$

With  $P_{S,TO}$  as the take-off power and  $N_E$  as the number of engines and  $\rho_0$  as the density of the air at sea level and  $L_D$  as the disk loading which is provided by an iteration loop with the worksheet “Preliminary Sizing 1”

The mass estimation for one gearbox in lb can be calculated according to Johnson 2015 by

$$m_{gb,S} = 95.7634 \cdot N_{rotor}^{0.38553} \cdot P_{S,TO}/n_E^{0.78137} \cdot \frac{\omega_{engine}^{0.09899}}{\omega_{prop}^{0.80866}} \quad (5.63)$$

With  $N_{rotor}$  as the number of main rotors,  $P_{S,TO}/n_E$  as the take-off power of one engine in hp and  $\omega_{engine}$  as the rotational speed of the electrical motor is set at 15000 rpm according to FlyZero 2022g and  $\omega_{prop}$  as the rotational speed of the propeller.

According to Johnson 2015 the rotational speed of the propeller can be empirical estimated by

$$\omega_{prop} = 1986.3 \text{ rpm} - 1.3267 \cdot \frac{\text{rpm} \cdot \text{s}}{\text{m}^2} \cdot d_D \cdot V_{CR} \quad (5.64)$$

Now the propeller disc loading during take-off can be calculated by

$$L_{TO} = \frac{P_{S,TO}}{\sigma \cdot \rho_0 \cdot S_D \cdot N_{rotor}} \quad (5.65)$$

With  $N_{rotor}$  as the number of the main rotors.

The propeller efficiency for the different flight phases can be calculated by three different methods which could be selected in the worksheet “Propeller Efficiency” of the spreadsheet “PreSTo-Classic-Prop\_final2\_SLZ”. See Scholz 2020 for more details on that topic.

For the calculations the method from Wolf has been chosen. The results of the propeller efficiencies during take-off, second segment and missed approach will be provided in an iteration loop to the worksheet “1.) Preliminary Sizing I” and the propeller efficiency during cruise will be provided to the worksheet “3.) Preliminary Sizing II”.

Finally, the total mass of the thrust device can be estimated by

$$m_{gb,prop} = N_{rotor} \cdot (m_{prop,S} + m_{gb,S}) \quad (5.66)$$

## 5.12 Mass of the Hydrogen Powertrain

This worksheet shown in Figure 5.10 calculates the coefficient of the operating empty mass and the maximum take-off mass of the hydrogen aircraft. The result is being provided to the worksheet “Preliminary Sizing II” in an iterative loop.

Mass of the hydrogen propulsion system	$m_{HPS}$	16828 kg	weight of the hydrogen-electric powertrain	
Check operating empty weight length A320	$l_{A320}$	37,57 m	overall length A320 CFM56	Airbus 2023
Maximum take-off weight A320	$m_{MTO,A320}$	78000 kg	maximum take-off weight A320 CFM56	Airbus 2023
operating empty weight a320	$m_{OE,A320}$	42600 kg	operating empty weight A320	Airbus 2023
Percentage fuselage to Maximum take-off weight	$r_F$	12,1 %		Siewert 2000
Mass fuselage A320 CFM 56	$m_{F,A320}$	9438 kg		
Operating empty weight, excluding the fuselage	$m_{OEEF,A320}$	33162 kg	to calculate the weight of the remaining system and structure	
fuselage length stretched aircraft	$L_{F,stretch}$	56,55571152 m	cabin length including the hydrogen storage tanks	
Mass fuselage stretched aircraft	$m_{F,stretch}$	14207,42096 kg		
operating empty weight stretched plane without the hydrogen propulsion system	$m_{OE,stretch}$	47369,42096		
Mass of CFM56	$m_{OP,ex}$	2500 kg	weight of the conventional propulsion	Airbus 2023
number of engine example plane	$N_{E,ex}$	2		Airbus 2023
operating empty weight H2 plane including the hydrogen propulsion system	$m_{OE,LH2}$	59197,41437 kg	operating empty weight of the hydrogen plane (excluding the conventional propulsion)	
maximum zero fuel weight H2 plane	$m_{MZF}$	78453 kg		
maximum take-off weight H2 plane	$m_{MTO}$	86915 kg		
	$m_{OE}/m_{MTO}$	0,681092699	coefficient of operative empty mass of the hydrogen plane and the max take-off mass	

**Figure 5.10** Worksheet "Mass H2 Powertrain"

In a first step the masses of the systems which make up the hydrogen-electric powertrain were summarized in  $m_{HPS}$ . This contains the masses of the fuel containment system  $m_{FCS}$ , the fuel cell system  $m_{FCSYS}$ , the electrical propulsions system  $m_{ELPS}$  and the thrust devices  $m_{TDS}$ .

$$m_{HPS} = m_{FCS} + m_{ELPS} + m_{FCSYS} + m_{TDS} \quad (5.67)$$

In order to calculate the operating empty weight of the stretched aircraft the additional weight of the stretched fuselage has to be determined. The fuselage itself needs to be stretched due to placement of the hydrogen storage tanks inside the fuselage. This enlargement in length of the fuselage comes with additional weight of the fuselage which results in an increase of the operating empty weight. The weight of the fuselage of the reference aircraft A320 is calculated by

$$m_{F,A320} = m_{MTO,A320} \cdot r_F \quad (5.68)$$

With the maximum take-off mass of the A320  $m_{MTO,A320}$  set at 78000 kg according to Airbus 2023 and the weight ratio of the fuselage  $r_F$  which is set to 12.1% according to Siewert 2000.

To determine the mass of the remaining structure and systems which is not influenced by the stretching of the fuselage. This mass can be calculated by

$$m_{OE,exf,A320} = m_{OE,A320} - m_{F,A320} \quad (5.69)$$

With  $m_{OE,A320}$  set at 42600 kg according to Airbus 2023.

Now the length of stretched fuselage  $l_{F,stretch}$  can be calculated by

$$l_{F,stretch} = l_{F,A320} + N_{TANK} \cdot l_{TANK} \quad . \quad (5.70)$$

With  $l_{F,A320}$  as the length of the cabin of the A320 set at 37.57 m according to Airbus2023, the number of the fuel tanks  $N_{TANK}$  and the length of one fuel tank  $l_{TANK}$  will be provided by the worksheet “Fuel Containment System”.

The mass of the stretched fuselage  $m_{F,stretch}$  can be calculated with

$$m_{F,stretch} = \frac{l_{F,stretch} \cdot m_{F,A320}}{l_{F,A320}} \quad . \quad (5.71)$$

Now the operating empty weight of the stretched A320  $m_{OE,stretch}$  will be calculated. Note that only the fuselage has been stretched without further changes to the aircraft.

$$m_{OE,stretch} = m_{OE,exf,A320} + m_{F,stretch} \quad (5.72)$$

Now the operating empty weight of hydrogen aircraft  $m_{OE,LH2}$  will be calculated by

$$m_{OE,LH2} = m_{oe,stretch} - (N_{E,CFM56} \cdot m_{cp,CFM56}) + m_{HPS} \quad . \quad (5.73)$$

With  $N_{E,CFM56}$  as the number of engine set to 2 according to Airbus 2023 and  $m_{cp,CFM56}$  as the mass of one of the propulsion devices of the reference aircraft.

The maximum zero fuel weight of the hydrogen plane  $m_{MZF}$  can now be calculated with

$$m_{MZF} = m_{OE,H2} + m_{MPL} \quad . \quad (5.74)$$

The maximum payload  $m_{MPL}$  will be provided by the worksheet “Preliminary Sizing II”

In the next step the maximum take-off weight can be calculated by

$$m_{MTO} = m_{MZF} + m_{F,erf} \quad . \quad (5.75)$$

The needed fuel mass  $m_{F,erf}$  will be provided by the worksheet “Preliminary Sizing II”

Finally, the coefficient of operating empty mass and the maximum take-off mass can be calculated with

$$m_{OE}/m_{MTO} = \frac{m_{OE,H2}}{m_{MTO}} . \quad (5.76)$$

This result will be provided to the worksheet “Preliminary Sizing II” in an iteration loop.

## 6 Evaluation of the Hydrogen-Electric Aircraft

This section aims at comparing the hydrogen-electric aircraft to an aircraft equipped with a conventional powertrain.

### 6.1 Aircraft Requirements

The design of a new aircraft is based on the requirements which the aircraft must achieve. These requirements must be met by the redesigned plane to make a reliable comparison to the reference plane. The requirement can be seen in the Table 6.1.

**Table 6.1** Basic requirements of the aircraft

Parameter	Symbol	Unit	Value
Payload	$m_{MPL}$	kg	19256
Design Range	$R_{MPL}$	NM	1510
Mach number, cruise	$M_{CR}$		0.648
Take-off field length	$S_{TOFL}$	m	1768
Landing field length	$S_{LFL}$	m	1448
Number of passengers	$m_{PAX}$		180

### 6.2 Aircraft with Conventional Propulsion

In a first step an Airbus A320 with its conventional propulsion system will be introduced. In the next step an Aircraft will be introduced which keeps most of the basic requirements of the conventional A320 excluding the propulsion system which will be converted to turboprop.

#### 6.2.1 Conventional Airbus A320

The characteristics of the conventional A320 are shown in the Table 6.2.

**Table 6.2** Parameter of the conventional A320

Parameter	Symbol	Unit	Value
Landing field length	$S_{LFL}$	m	1448
Take-off field length	$S_{TOFL}$	m	1768
Max. lift coefficient, landing	$C_{L,max,L}$		3.408
Max. lift coefficient, take-off	$C_{L,max,TO}$		2.584
Mass ratio, max. landing to max. take-off	$m_{ML}/m_{MTO}$		0.56
Aspect ratio	$A$		9.5
Number of engines	$n_E$		2
Number of passengers	$n_{PAX}$		180
Number of seats abreast	$n_{SA}$		6
Cargo mass	$m_{CARGO}$	kg	2516
Mach number, cruise	$M_{CR}$		0.76
Design Range	$R_{MPL}$	NM	1510
Specific fuel consumption	$SFC$	kg/N/s	$1.65 \cdot 10^{-5}$

The matching chart of the conventional A320 can be seen in Appendix A.

### 6.2.2 Turboprop A320

In order to reduce the emissions of the civil aviation a lot of approaches have been taken, one of the most promising ones is to switch to a turboprop propulsion due to the better efficiency compared to a jet. But this also comes with some drawbacks which comes in form of lower cruising speed which results in longer flight times when flying over the same distance.

During the Airport 2030 study various replacement concepts for the Airbus A320 have been made including the Smart Turboprop concept. This concept retains the narrowbody fuselage of the Airbus A320 and combines it with a turboprop propulsion and a high wing instead of the jet propulsion and low wing of the A320. The parameters for this variant set up in PreSTo can be seen in the Table 6.3.

**Table 6.3** Parameter of the turboprop aircraft (Johanning 2014)

Parameter	Symbol	Unit	Value
Landing field length	$S_{LFL}$	m	1448
Take-off field length	$S_{TOFL}$	m	1768
Max. lift coefficient, landing	$C_{L,max,L}$		3
Max. lift coefficient, take-off	$C_{L,max,TO}$		2.34
Mass ratio, max. landing to max. take-off	$m_{ML}/m_{MTO}$		0.85
Aspect ratio	$A$		16
Number of engines	$n_E$		2
Number of passengers	$n_{PAX}$		180
Number of seats abreast	$n_{SA}$		6
Cargo mass	$m_{CARGO}$	kg	2516
Mach number, cruise	$M_{CR}$		0.648
Design Range	$R_{MPL}$	NM	1510
Specific fuel consumption	$SFC_p$	kg/W/s	$5.83 \cdot 10^{-8}$

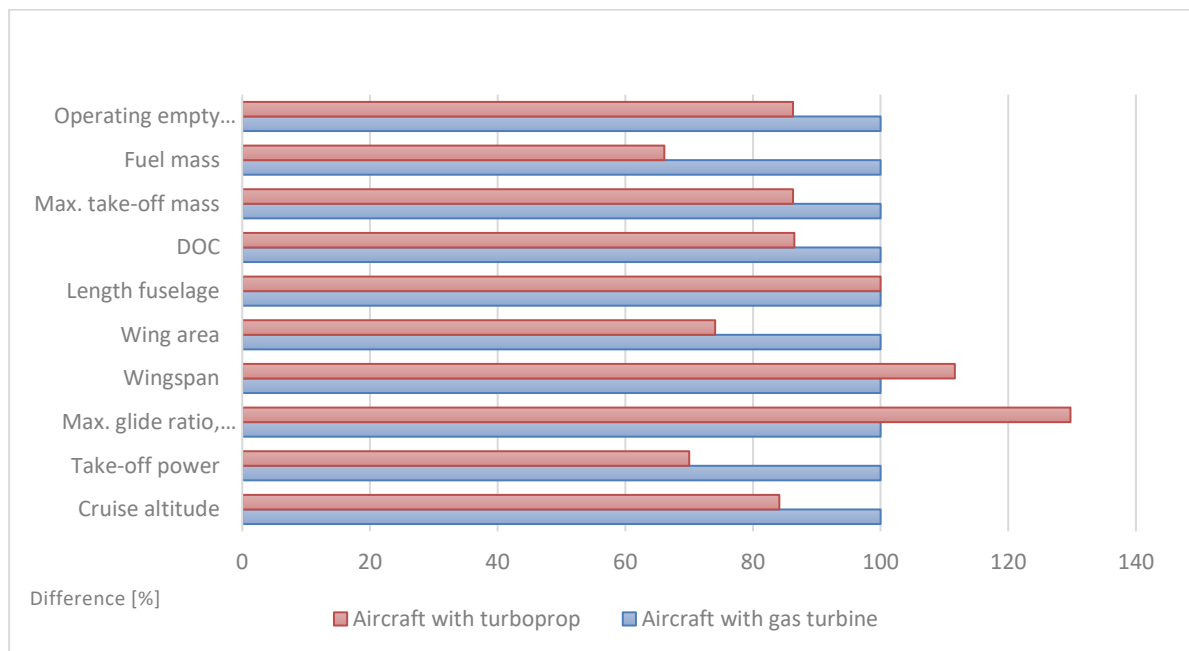
The matching chart of the turboprop aircraft can be seen in Appendix B.

### 6.2.3 Comparison of the Conventional Aircraft

The values of the conventional aircraft were calculated with the spreadsheet “A-C\_Preliminary\_SizingA320\_CFM562”. The values of the turboprop aircraft have been calculated with the spreadsheet “PreSTo-Classic-Prop-final2”. These results are compared in the Table 6.4.

**Table 6.4** Parameter of the conventional aircraft and the turboprop aircraft

Parameter	Symbol	Unit	Conventional A320	Turboprop A320	Variation [%]
Operating empty mass	$m_{OE}$	kg	41183	35533	-13.7
Fuel mass	$m_F$	kg	13102	8663	-33.9
Max. take-off mass	$m_{MTO}$	kg	73540	63452	-13.7
Seat-mile cost	DOC (AEA)	\$/NM/seat	0.111	0.096	-13.5
Length fuselage	$l_F$	m	37.57	37.57	0
Wing area	$S_W$	m <sup>2</sup>	122.3	90.6	-25.96
Wingspan	$b_W$	m	34.13	38.1	11.6
Max. glide ratio, cruise	$E_{MAX}$		17.48	22.68	29.7
Take-off power	$P_{S,TO}$	kW	17290	12106	-30
Cruise altitude	$h_{CR}$	ft	38773	32623	-15.9

**Figure 6.1** Comparison of the results of the preliminary sizing between the conventional and the turboprop version

The specific fuel consumption of the conventional A320 and the turboprop version cannot be compared directly. Nevertheless, the turboprop version is more fuel efficient. This is one of the reasons besides the increase of the maximum glide ratio in cruise that led to a significant drop in fuel mass which also equals the needed energy for the flight mission. The reduced fuel mass of the turboprop version combined with the reduction of the operating empty weight leads to a reduction of the maximum take-off mass. The reduced maximum take-off weight itself contributes to a lower take-off power and wing area compared to the conventional aircraft. What might become an issue is the increase in wingspan due to the higher aspect ratio of the turboprop version, this could be addressed by including winglets in the design.

### 6.3 Input Data Hydrogen Aircraft

For the calculation of the hydrogen-electric aircraft the input data of the reference plane has been used except the values shown in Table 6.5. All other input data has been explained in the previous section. Due to the significance of certain parts of the hydrogen-electric powertrain the values for the electric motor and the fuel cells were used in two different versions shown in Table 6.6. One value is the current state of the art the other one is the value expected to become real in the near future. This alternation aims at underlining what the most important technologies in the field of hydrogen-electric aircraft are.

**Table 6.5** Adjusted values of the different aircraft version

Parameter	Symbol	Unit	Conventional A320	Turboprop A320	LH2 aircraft current technology	LH2 aircraft future technology
Factor	$k_L$	kg/m <sup>2</sup>	0.107	0.137	0.137	0.137
Max. lift coefficient landing	$C_{L,max,L}$	-	3.4077	3	3.4077	3.4077
Mass ratio landing - take-off	$m_{ML}/m_{TO}$	-	0.878	0.85	0.93	0.93
Ratio	$V/V_{md}$	-	0.9484	1	1	1
Mach number cruise	$M_{CR}$	-	0.76	0.648	0.5	0.5

**Table 6.6** Values of the different hydrogen aircraft version (Kadyk 2018)

Parameter	Symbol	Unit	Current technology	Future technology
Power density fuel cell	$\Phi_{FC}$	kW/kg	1.6	8
Power density electric propulsion motor	$\Phi_{ELM}$	kW/kg	5.2	10

In Table 6.5 the adjustments needed to the hydrogen-electric aircraft were shown. The fuel cell and the electric motor are modelled such that they do not see a power reduction with altitude. The cruise line in the matching chart is matched with the design point by power reduction of the engines (using the throttle).

A very important issue is to comply with (4.34). This means that the landing mass has to be sufficiently high to allow landing of the aircraft with maximum payload plus fuel reserves.

For this reason, the mass ration  $m_{ML}/m_{TO}$  has to be adjusted. The value can be set to a maximum of 1.0 but has been set to 0.93 after a number of adjustments. Also the ration  $V/V_{md}$  has been set to 1.0 to get the best results. Both of these changes affect lift coefficient during cruise.

As already mentioned, the cruise altitude should be lower compared to the conventional aircraft due to the likeliness of contrails which rises with increasing altitude. To calculate the cruise altitude the pressure in cruise is needed.

$$p_{CR} = \frac{2 \cdot g \cdot m_{MTO}/S_W}{C_L \cdot M^2 \cdot \gamma} \quad (6.1)$$

To get a lower cruising altitude the pressure in cruise must be set to maximum. In a first step the wing loading at maximum take-off mass  $m_{MTO}/S_W$  which is calculated in the worksheet “Preliminary Sizing I” needs to be maximized. The factor  $k_L$  needs to be as large as possible so it will be set at the figure of the turboprop variant due to the more favorable certification conditions. The maximum lift coefficient during landing  $C_{L,max,L}$  will be set at the maximum value, which is the value of the conventional A320. Also, a larger  $S_{LFL}$  would be beneficial because it enlarges  $m_{MTO}/S_W$  but it is limited by the TLAR. In a last step to maximize  $m_{MTO}/S_W$  the mass ratio  $m_{ML}/m_{TO}$  should be addressed. This ratio should be set at the lowest value possible which could interfere with the settings above to comply with (4.34) where this ratio needs to be maximized. In this case a compromise is needed which is found by investigating the various results.

Another value which has to be addressed is the Mach number during cruise. At first the TLAR of the aircraft introduced the cruising Mach number at 0.648 this would lead to a cruising altitude of about 41000 feet for both versions of the hydrogen aircraft which would drastically increase the likeliness of contrails and is unrealistic for a fuel cell as well as for a propeller aircraft. To address this issue the Mach number in cruise for the hydrogen aircraft has to be reduced to 0.5 in violation of the TLAR. This Mach number complies with Johanning 2014 and also reduces the maximum take-off mass. With the assumed aspect ratio of 16, the wingspan is at 52 m for current technology and 44 m for the future technology scenario. This is a considerable violation of the 36 m wingspan limitation (ICAO Class C) observed by the conventional A320 and the turboprop version.

The difference of the technological level is being introduced by a variation of the power density of the fuel cell and the electric motor. According to Kadyk 2018 the improvements in the field of the fuel cell is due to the improvement of the bipolar plates and peripheral components, which contribute the biggest share of weight to the overall weight of the fuel cell. With new material from better performing, lightweight materials the weight of the fuel cell can be significantly reduced and also the power density. Another improvement can be achieved with

improved catalyst design. These improvements combined make the estimate for the power density of the future technology a reasonable estimate according to Kadyk 2018.

Regarding the improvements of the electric motor the values also have been provided by Kadyk. The amount of improvement and its timespan can better be explained with Vratny 2018 who sets the specific power of the current technology at 5 kW/kg and expects values of up to 20 kW/kg until 2030. This makes the estimation of the future power density in the field of the electric motor reasonable.

## 6.4 Results

The values of the turboprop aircraft were calculated with the spreadsheet “PreSTo-Classic-Prop-final2”. The values of the hydro-electric aircraft have been calculated with the spreadsheet “PreSTo-Classic-hydrogen\_current” and “PreSTo-Classic-hydrogen\_future”. These results are now compared to the values of the turboprop aircraft. The matching charts of the version equipped with current technology can be seen in Appendix C, the version with future technology in Appendix D.

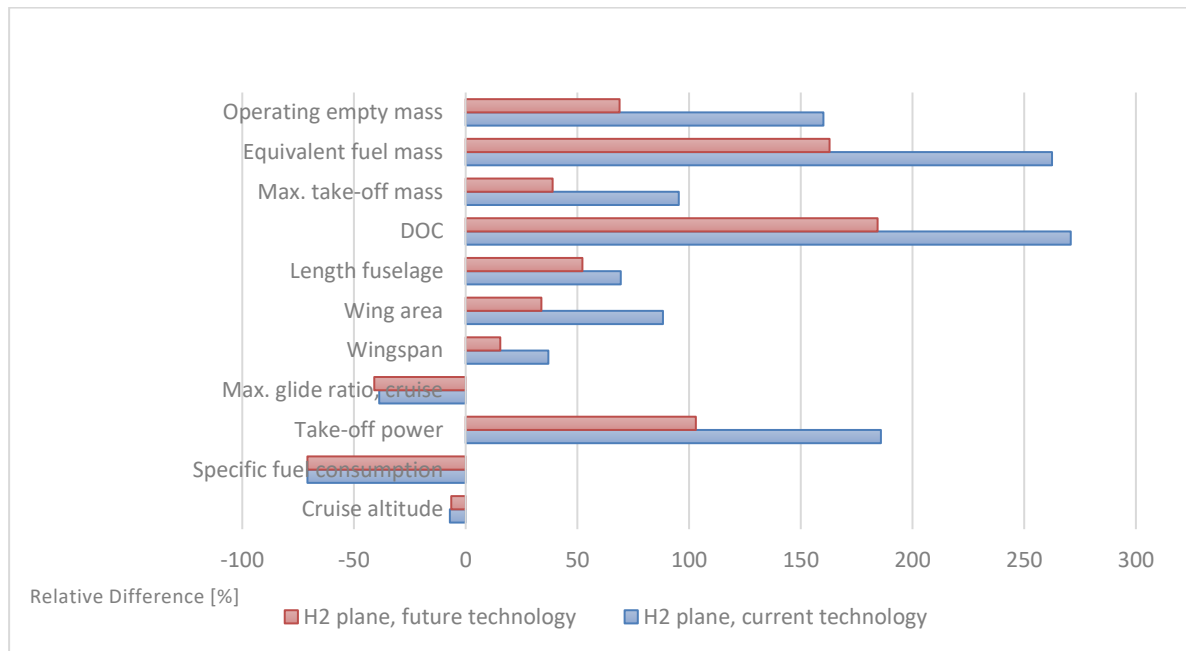
As seen in the Table 6.7 the results differ from the reference aircraft in most cases significantly. To get a better perspective of the results in the Table 6.8 and in the Figure 6.2 the relative difference of the current and the future technology to the reference aircraft is shown.

**Table 6.7** Parameter of the turboprop aircraft and the hydrogen aircraft

Parameter	Symbol	Unit	Turboprop A320	Hydrogen-electric redesign	
				Current Technology	Future technology
Operating empty mass	$m_{OE}$	kg	35533	92602	60120
Fuel mass equiv..	$m_F$	kg	8663	31399	22773
Max. take-off mass	$m_{MTO}$	kg	63452	123975	88146
Seat-mile cost	DOC (AEA)	\$/NM/seat	0.096	0.356	0.273
Length fuselage	$l_F$	m	37.57	63.65	57.2
Wing area	$S_W$	m <sup>2</sup>	90.6	170.6	121.3
Wingspan	$b_W$	m	38.1	52.2	44
Max. glide ratio, cruise	$E_{MAX}$		22.68	13.9	13.4
Take-off power	$P_{S,TO}$	kW	12106	34606	24578
Specific fuel consumption	$SFC_p$	kg/W/s	$5.83 \cdot 10^{-8}$	$1.7 \cdot 10^{-8}$	$1.7 \cdot 10^{-8}$
Cruise altitude	$h_{CR}$	ft	32649	30967	31772

**Table 6.8** Relative difference of the values of the hydrogen aircraft related to the turboprop version

Parameter	Symbol	Relative difference [%]	
		Current Technology	Future technology
Operating empty mass	$m_{OE}$	160	69
Fuel mass equiv..	$m_F$	262	163
Max. take-off mass	$m_{MTO}$	95	39
Seat-mile cost	DOC (AEA)	271	184
Length fuselage	$l_F$	69	52
Wing area	$S_W$	88	33
Wingspan	$b_W$	37	15
Max. glide ratio, cruise	$E_{MAX}$	-39	-41
Take-off power	$P_{S,TO}$	186	103
Specific fuel consumption	$SFC_p$	-71	-71
Cruise altitude	$h_{CR}$	-7	-7

**Figure 6.2** Comparison of the results of the preliminary sizing between both versions of the hydrogen aircraft related to the turboprop aircraft

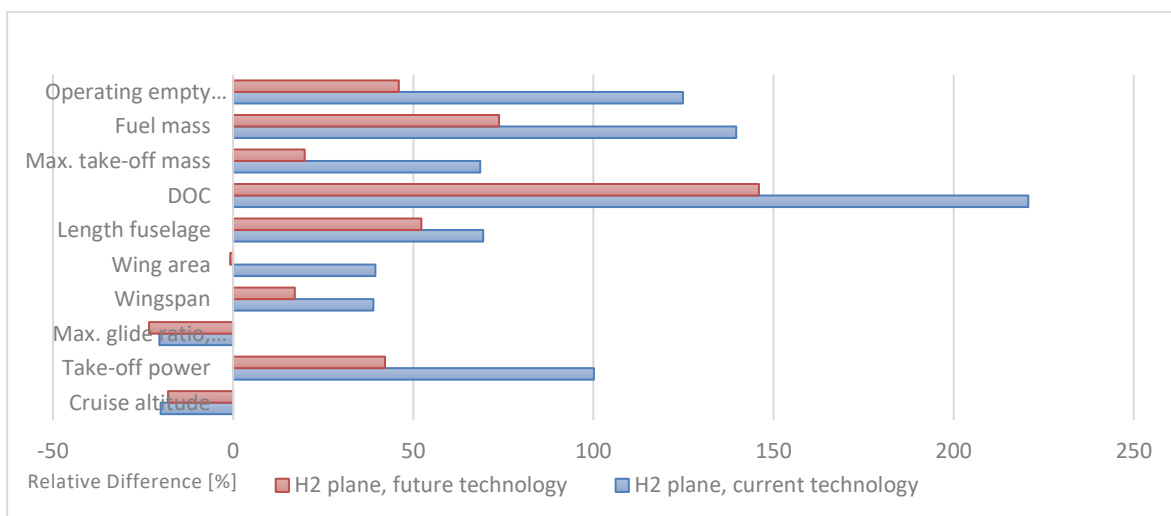
As seen in the Table 6.9, Table 6.10, and the Figure 6.2 the hydro-electric aircraft especially equipped with the current technology fails to compete with the conventional A320. The fuel energy is about 140% higher and the DOC is almost 221% higher, the hydrogen aircraft equipped with the future technology is better at about 74% and 146% but is still no improvement. This makes the hydro-electric aircraft compared to the conventional aircraft only beneficial in case of emissions.

**Table 6.9** Parameter of the conventional aircraft and the hydrogen aircraft

Parameter	Symbol	Unit	conventional A320	Hydrogen-electric redesign	
				Current Technology	Future technology
Operating empty mass	$m_{OE}$	kg	41183	92602	60120
Fuel mass equiv..	$m_F$	kg	13102	31399	22773
Max. take-off mass	$m_{MTO}$	kg	73540	123975	88146
Seat-mile cost	DOC (AEA)	\$/NM/seat	0.111	0.356	0.273
Length fuselage	$l_F$	m	37.57	63.65	57.2
Wing area	$S_W$	m <sup>2</sup>	122.3	170.6	121.3
Wingspan	$b_W$	m	34.13	52.2	44
Max. glide ratio, cruise	$E_{MAX}$		17.48	13.9	13.4
Take-off power	$P_{S,TO}$	kW	17290	34606	24578
Cruise altitude	$h_{CR}$	ft	38773	30967	31772

**Table 6.10** Relative difference of the hydrogen aircraft related to the conventional version

Parameter	Symbol	Relative difference [%]	
		Current Technology	Future technology
Operating empty mass	$m_{OE}$	125	46
Fuel mass equiv..	$m_F$	140	74
Max. take-off mass	$m_{MTO}$	69	20
Seat-mile cost	DOC (AEA)	221	146
Length fuselage	$l_F$	69	52
Wing area	$S_W$	39	-1
Wingspan	$b_W$	39	17
Max. glide ratio, cruise	$E_{MAX}$	-20	-23
Take-off power	$P_{S,TO}$	100	42
Cruise altitude	$h_{CR}$	-20	-18

**Figure 6.3** Comparison of the results of the preliminary sizing between both versions of the hydrogen aircraft related to the conventional aircraft

## 6.5 Evaluation of the Results

### 6.5.1 Operating Empty Mass

The empty weight includes the structure, landing gear, fixed equipment, avionics, and anything else which is not part of the crew, payload, or fuel. Based on this the whole hydrogen-electric powertrain is to be included in the operating empty mass. This drivetrain is composed of the fuel containment system, the fuel cell system, the electric propulsion system, and the various subsystems. In a conventional aircraft the drivetrain includes the thrust devices, the fuel tanks. Because of the higher weight of the components of the hydrogen-electric powertrain the operating empty weight is significantly higher. The fuselage also contributes to the increase of the operating empty mass due to location of the hydrogen storage tanks. These tanks cannot be fitted inside the wings, they must be located inside the fuselage. This adds additional length to the fuselage which increases the weight of the fuselage and therefore the operating empty weight as seen in Figure 6.4.

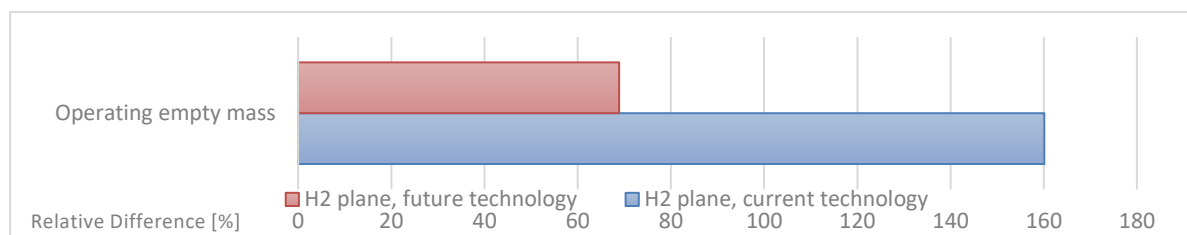


**Figure 6.4** Operating empty mass of the hydrogen aircraft related to the reference aircraft

As seen in Figure 6.4, this results in a significantly higher operating empty mass when compared to the reference plane. The increasing mass requires an increase in lift, which increases the drag and therefore the thrust and fuel consumption. This also influences the operating costs, which also increase.

To identify the major mass contributors of the hydrogen-electric powertrain the operating empty mass has been evaluated in the Figures 6.5 and 6.6. With the current technology the hydrogen-electric powertrain contributes 53% to the operating empty mass while using the values of the future technology the percentage is only 29%. This effect underlines the importance of the advancement of the enabling technologies which are the fuel cells and the electric motors.

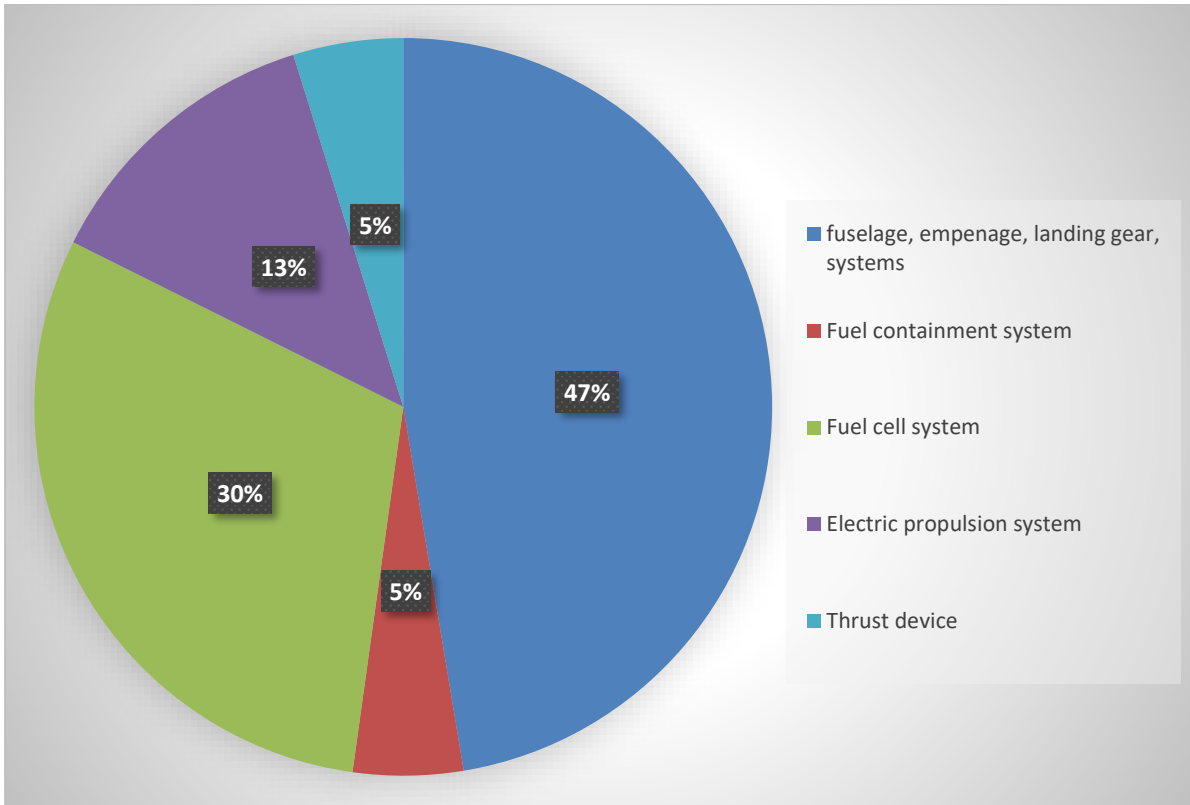


**Figure 6.5** Composition of the operating empty mass of the hydrogen aircraft with current technology

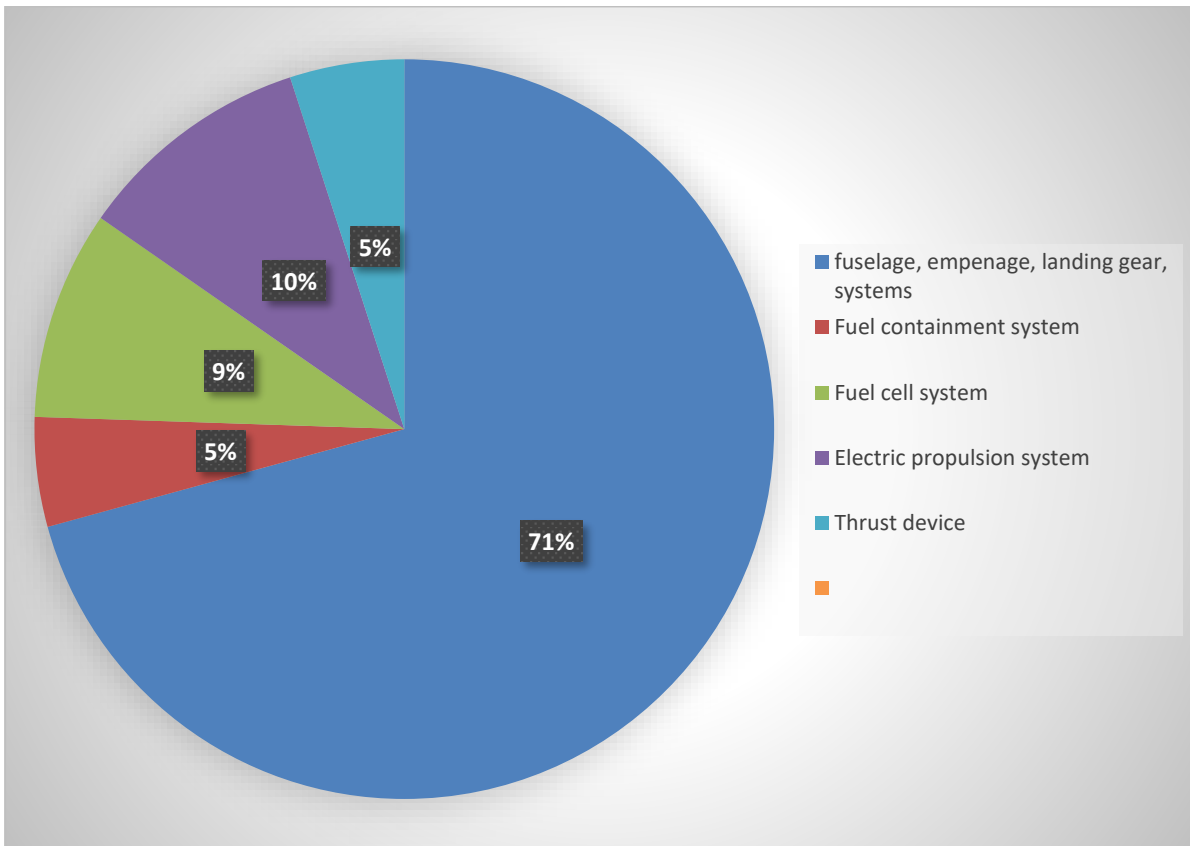


**Figure 6.6** Composition of the operating empty mass of the hydrogen aircraft with future technology

### 6.5.2 Equivalent Fuel Mass

The fuel mass of the hydrogen aircraft is influenced by the higher gravimetric energy density of the hydrogen, which is beneficial to the fuel weight. But the increase in the operating empty weight gives the need for an increase in thrust and therefore in fuel consumption. This increase in fuel mass, as seen in Figure 6.7, also influences the dimensions of the fuel containment system which directly affects the fuselage length and therefore the operating empty weight.

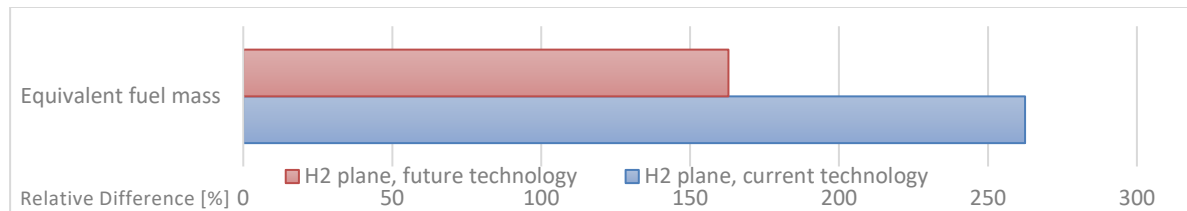


**Figure 6.7** Fuel mass of the hydrogen aircraft related to the reference aircraft

### 6.5.3 Length of the Fuselage

Besides the passenger, cargo, avionics, and fixed equipment the fuselage has to house the fuel tanks. According to Brewer 1991 the tanks are located inside the fuselage. Due to C.G. control issues one tank is in front of the fuselage behind the cockpit and the other one in the aft of the fuselage behind the passenger cabin. Both tanks add additional length to the fuselage as seen in Figure 6.8. This additional length contributes to weight of the fuselage and therefore to the operating empty weight.

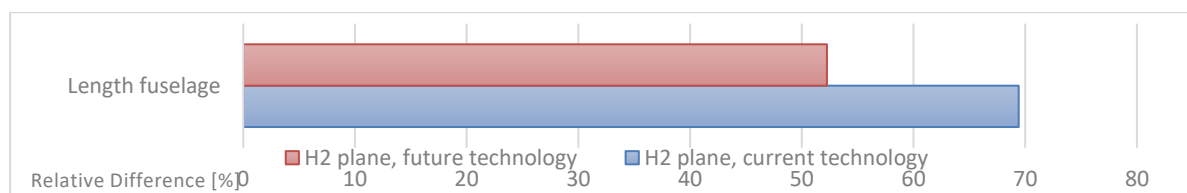


**Figure 6.8** Fuselage length of the hydrogen aircraft related to the reference aircraft

This increase in fuselage length may require adjustments to the empennage due to changes in the geometry of the plane. It also influences the geometry of the fuselage which influences the tail clearance during take-off. This could be solved by adding length to the landing gear to keep the required tail clearance. Additional length of the landing gear would also increase the operating empty weight.

### 6.5.4 Wingspan and Wing Area

As the wing area is linked to the maximum take-off weight and wing loading. The difference to the reference aircraft is mostly dependent on the increase of the maximum take-off weight. The increase in wing area, as seen in Figure 6.9, results in heavier wings. This is only slightly compensated by the absence of fuel tanks inside the wings. The wingspan also increases due to the increase in wing area. This also makes the wings heavier and limits the operability of the aircraft due to its larger dimensions.

In Element 2 of the ICAO Aerodrome Reference Code aircraft are divided into groups in regard of their wingspan. For a narrowbody aircraft like the A320 this would be code letter C, which includes wingspans from 24 m to 36 m. Both versions of the hydrogen-electric aircraft exceed these limits which makes code letter D applicable. Therefore, the hydrogen-electric aircraft will exceed the dimensions of certain airports even with the use of winglets (Skybrary 2023).

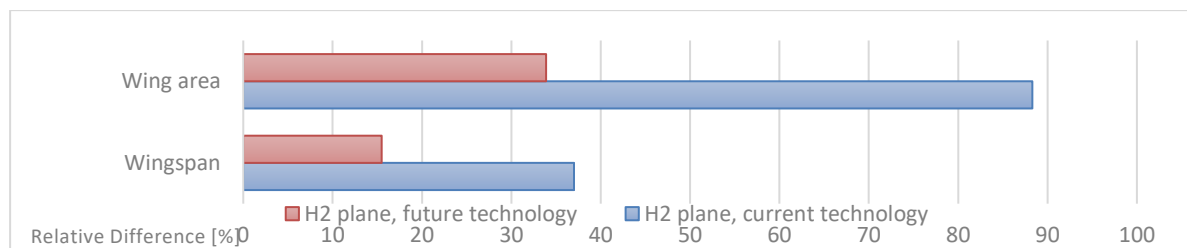


**Figure 6.9** Wingspan and Wing Area of the hydrogen aircraft related to the reference aircraft

### 6.5.5 Take-off Power

The take-off power is dependent on power-to-weight ratio of the design point and the maximum take-off weight. The increasing maximum take-off mass results in increasing take-off power. But also, the additional power demand due to the core drag power of the heat exchangers contribute to the maximum take-off power. The increasing power demand, as seen in Figure 6.10, also increases the mass of the fuel cell system and therefore the operating empty weight.

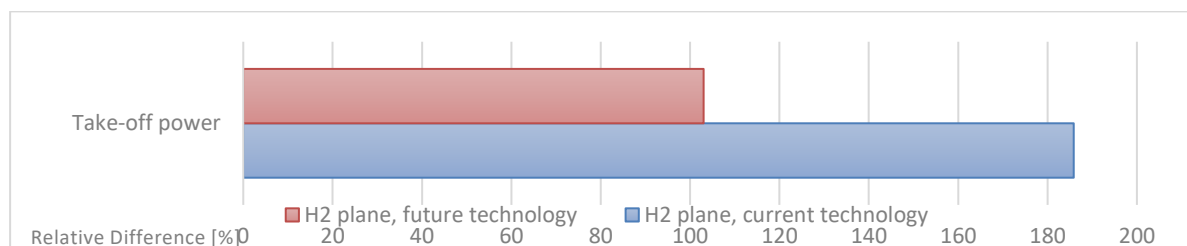


**Figure 6.10** Take-off Power of the hydrogen aircraft related to the reference aircraft

### 6.5.6 Maximum Take-off Mass

The maximum take-off mass is composed of the operating empty mass, the payload, and the fuel mass. The only mass which is constant for the reference aircraft and the hydrogen aircraft is the payload. An increase in the operating empty mass or in the fuel mass results in an increase of the maximum take-off weight as seen in Figure 6.11. This increase also affects both the operating empty weight and the fuel mass in return. When the maximum take-off mass increases the take-off power demand increases and therefore the mass of the fuel cell system increases the operating empty weight. To solve this problem during the calculation an iteration was implemented. The maximum takeoff mass also directly contributes to the DOC estimation.

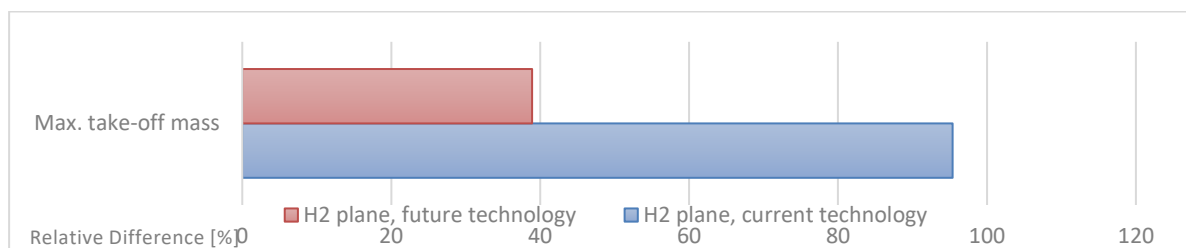


**Figure 6.11** Maximum Take-off Mass of the hydrogen aircraft related to the reference aircraft

## 6.6 Direct Operating Costs

The DOC was calculated with the method from 1989 for short and medium range aircraft of the Association of European Airlines (AEA). The direct operating cost is the sum of specific costs, which are:

- depreciation,
- interest,
- insurance,
- fuel,
- maintenance,
- crew,
- fees and charges.

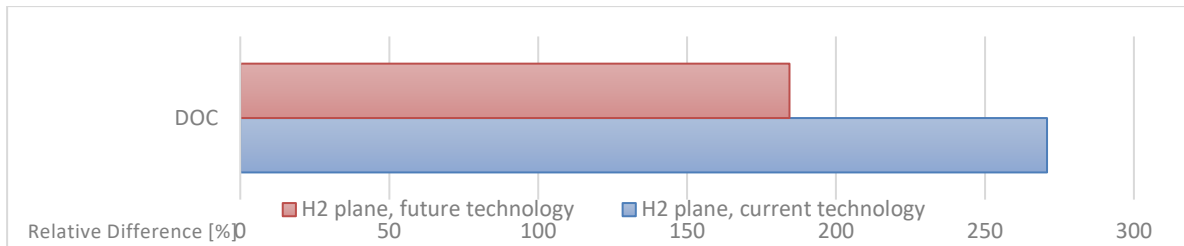


**Figure 6.12** DOC of the hydrogen aircraft related to the reference aircraft

For this calculation, all costs have been calculated except for the maintenance. As the reference aircraft features a turboprop propulsion, the hydrogen aircraft feature a hydrogen-electric powertrain. The hydrogen-electric powertrain cannot be calculated with the methods of the AEA method. Also, the price of the hydrogen-electric powertrain cannot be estimated by the AEA Method which affects the depreciation.

According to ZeroAvia's Regional Aircraft Concept Report the fuel cell must be replaced three times during the aircraft life, while the tanks and the cryogenic fuel systems must be replaced four times during the lifespan of the aircraft. This combined with the higher weight of the airframe makes it highly likely that the maintenance costs will be significantly higher compared to the reference aircraft.

As seen in Figure 6.12 the DOC for the hydrogen fueled aircraft is significantly higher compared to the reference aircraft. This result due to the higher maximum take-off weight.

## 7 Summary and Conclusions

This project aims at the benefits and challenges of a zero-emission aircraft which uses hydrogen and fuel cells. The work is based on a medium range narrowbody aircraft designed for a flight mission of 1510 NM and a payload of 19.3 t, which is equal to the Airbus A320, one of the most frequently used aircraft. The turboprop version results in 44% less fuel consumption, 14% less take-off mass, 14% less operating empty mass, and 14% less DOC.

A hydrogen-electric aircraft can be built, but only with extreme parameters. The operating empty mass is about 160% higher with current technology and 69% higher with future technology compared to the turboprop variant. This difference between the current and future technology is caused by reduction of mass of the main mass contributors. These are the fuel cells and the electric motors of the propulsion system. This reduces the mass contribution of the hydrogen-electric powertrain from 53% to 29%.

Also worth noting is the equivalent fuel mass which represents the amount of energy needed for the same flight mission which is 262% higher with current technology and 163% higher with future technology. This is one of the most important findings because it points out that the needed energy for the same flight mission is at least 163% higher than with already existing and proven technology. Especially the current technology is a massive ecological draw-back by consuming almost two and half times the fuel an improved variant of existing technology would do.

In a last step we take a look at the economical results. The DOC of the hydrogen aircraft with current technology causes 271% higher DOC than the turboprop variant, in the case of the hydrogen aircraft equipped with future technology this drops to 184%. This also makes the version using the current technology not competitive in economical view. The future version is better but still needs improvement to be beneficial under economic conditions.

Finally, the hydrogen aircraft with current technology fails in technological, ecological, and economical terms. The version equipped with the future technology is way better but still needs improvement especially in terms of energy consumption and direct operating costs. This leaves the absence of CO<sub>2</sub> and NO<sub>x</sub> emissions the only benefit remaining which the hydrogen-electric airplane has.

To become fully emission-free the hydrogen-electric plane has to avoid producing contrails which could be caused by the water vapor emissions which result due to production of water in the fuel cells. This water cannot be stored on board, because of the additional weight it would cause. To freeze the water and discard it is also not possible because of the additional weight and space the additional appliances would take. The most promising choice is storing the water being produced during critical flight phases on board and discard the stored water

and the produced water during the cruise flight phase without any treatment to the atmosphere. To reduce the likeliness of contrails a lower cruising altitude should be chosen. It might be beneficial to monitor the surroundings during flight to choose the right altitude and weather conditions.

In the long term, hydro-electric aircraft might become competitive when new and improved technology is emerging. But this does not solve the challenges of today which are lying in the emissions and energy consumption caused by the aviation industry. If we remember the comparison between the conventional and the turboprop version of the aircraft, we already noticed the significant drop in fuel mass combined with a drop in DOC. Less burned fuel means less emissions and because the flight level is lower, contrails are less likely to happen. The reduction of contrails also means an additional reduction of emissions caused by the aircraft. These benefits only come at one expense which is a lower cruising speed. Maybe this compromise could make flying more eco-friendly for the time until the hydro-electric aircraft might be improved and is finally competitive.

## 8 Recommendation

The aim of this work was to evaluate the feasibility of an aircraft using hydrogen and fuel cells as part of its propulsion. This was done by comparing the hydrogen-electric aircraft to a conventional fueled aircraft. In return most of the variables of the reference aircraft were imposed upon the hydrogen-electric aircraft. While these values were optimized for a conventional fueled aircraft, some of values proved to be unbeneficial for the hydrogen-electric aircraft. For example, the dimension of the hydrogen storage tanks was limited to the cabin diameter of the reference plane. A wider fuselage would contribute to the efficiency of the hydrogen storage tank. This would result in a reduction of the additional fuselage length and therefore reduce the operating empty mass of the plane. The solution would be a clean-sheet study which takes the requirements of the hydrogen-electric powertrain in account from the beginning of the design process.

The installation and evaluation of the heat exchangers as part of the fuel cell system seems unsatisfying. Because of being a major contributor to the drag and the power demand of the aircraft. Further studies are needed to provide hydrogen-electric aircraft with a better solution to reduce the drag and power demand caused by the heat exchangers.

Regarding the DOC estimations a method should be implemented to evaluate hydrogen-electric aircraft. The existing methods are limited to combustion engines. This takes away the possibility of comparing hydrogen fueled aircraft to conventional fueled aircraft.

The effects of the production and distribution of hydrogen should be investigated. Zero-emission aviation is only possible if the production and the distribution of the hydrogen propellant is done without environmental impact. Therefore, the means of production and its environmental impact should be investigated further.

The hydrogen infrastructure should also be investigated. The change from conventional propellant to hydrogen as a propellant would result in the need of new ways distributing the fuel. This includes the fuel delivery to airports and airport refueling infrastructure.

## List of References

- AIRBUS, 2023. *A320 - Aircraft Characteristics Airport and Maintenance Planning*. Blagnac Cedex: Airbus S.A.S. Customer Services.  
 Available from: <https://bit.ly/3HKd6wY>  
 Archived at: <https://perma.cc/BYK9-4YHL>
- AVIATION WEEK, 2020. *ZeroAvia Prepares For Hydrogen Fuel-Cell Propulsion Flight Tests*. New York: Aviation Week Network.  
 Available from: <https://bit.ly/3LbOGyt> (Closed Access)  
 Archived at: <https://perma.cc/JR6N-RWV5>
- BOATMAN, Julie, 2019. *ZeroAvia Breaks Silence on Hydrogenpowered Matrix*. Chattanooga: FLYING Media Group.  
 Available from: <https://www.flyingmag.com/zeroavia-hydrogen-powered-matrix/>  
 Archived at: <https://perma.cc/82S6-6A8N>
- BREWER, G. Daniel, 1991. *Hydrogen Aircraft Technology*. Boca Raton: CRC Press.
- CAMBRIDGE DICTIONARY, 2022.  
 Available from: <https://dictionary.cambridge.org/>
- COLOZZA, Anthony J., 2002. *Hydrogen Storage for Aircraft Applications Overview*. NASA: Hanover. Report: NASA/CR-2002-211867, Glenn Research Center.  
 Available from: <https://ntrs.nasa.gov/citations/20020085127>
- CRANFIELD AEROSPACE SOLUTIONS, 2022. *Project Fresson*.  
 Available from: <https://cranfieldaerospace.com/investors/>  
 Archived at: <https://perma.cc/9LX6-2P6P>
- DEUTSCHES ZENTRUM FÜR LUFT- UND RAUMFAHRT, 2021. *Auf dem Weg zu einer emissionsfreien Luftfahrt*. Köln: DLR.  
 Available from: <https://bit.ly/3ozLVhM>  
 Archived at: <https://perma.cc/5DKF-939N>
- DICKS, Andres L., et al., 2018. *Fuel Cell Systems Explained*. West Sussex: Wiley.
- EASA, 2021. *Certification Specifications and Acceptable Means of Compliance for Large Aeroplanes (CS-25)*.  
 Available from: <https://www.easa.europa.eu/en/downloads/134259/en>  
 Archived at: <https://perma.cc/4MS6-9RSV>

ENERGY EDUCATION, 2023. *Gravimetric Energy Density*.

Available from: <https://bit.ly/3LRqNf3>

Archived at: <https://perma.cc/HSU3-Q8WE>

EYERER, Sebastian, 2019. Experimental investigation of modern ORC working fluids R1224yd(Z) and R1233zd as replacements for R245fa. In: *Applied Energy*, vol. 240, pp. 946-963. Amsterdam: Elsevier.

Available from: <https://doi.org/10.1016/j.apenergy.2019.02.086>

FLYZERO, 2022a. *Zero-Carbon Emission Aircraft Concepts*. Aerospace Technology Institute, Martell House, University Way, Cranfield, United Kingdom. Report: FZO-AIN-REP-0007.

Available from: <https://bit.ly/3N2dwm6>

Archived at: <https://perma.cc/E79F-JB2E>

FLYZERO, 2022b. *Regional Aircraft Concept Report*. Aerospace Technology Institute, Martell House, University Way, Cranfield, United Kingdom. Report: FZO-AIN-REP-0008.

FLYZERO, 2022c. *Narrowbody Aircraft Concept Report*. Aerospace Technology Institute, Martell House, University Way, Cranfield, United Kingdom. Report: FZO-AIN-REP-0009.

FLYZERO, 2022d. *Midsize Aircraft Concept Report*. Aerospace Technology Institute, Martell House, University Way, Cranfield, United Kingdom. Report: FZO-AIN-REP-00010.

FLYZERO, 2022e. *Fuel Cell Technical Report*. Aerospace Technology Institute, Martell House, University Way, Cranfield, United Kingdom. Report: FZO-PPN-REP-00031.

FLYZERO, 2022f. *Thermal Management Technical Report*. Aerospace Technology Institute, Martell House, University Way, Cranfield, United Kingdom. Report: FZO-PPN-REP-00017.

FLYZERO, 2022g. *Propulsion Integration Report*. Aerospace Technology Institute, Martell House, University Way, Cranfield, United Kingdom. Report: FZO-PPN-REP-00011.

FLYZERO, 2022h. *Thrust Devices Technical Report*. Aerospace Technology Institute, Martell House, University Way, Cranfield, United Kingdom. Report: FZO-PPN-REP-00021.

FUHS, Allen E., 2016. *Zero-Emissions Electric Aircraft: Theory vs Reality*. New York, SAE Media Group.

Available from: <https://bit.ly/3n07BTE>

Archived at: <https://perma.cc/3665-AE74>

GESELL, Hendrik, et al., 2018. System Analysis of Turbo Electric and Hybrid Electric Propulsion Systems on a Regional Aircraft. In: *31st Congress of the International Council of the Aeronautical Sciences, Belo Horizonte, Brazil; September 09-14, 2018*. Bonn: Deutsche Gesellschaft für Luft- und Raumfahrt. Report: ICAS2018\_0831.

Available from: <https://bit.ly/41kAkAK>

Archived at: <https://perma.cc/M7Z3-DTJ9>

GIERENS, Klaus, 2021. Theory of Contrail Formation for Fuel Cells. In: *Aerospace*, vol. 8, no. 6, art. 164.

Available from: <https://doi.org/10.3390/aerospace8060164>

GKN AEROSPACE, 2021. *Zero Emission Propulsion*.

Available from: <https://bit.ly/40HG33z>

Archived at: <https://perma.cc/R9H3-4AFH>

GKN AEROSPACE, 2022. *GKN AEROSPACE'S Cryogenic Hyperconducting Technology Unlocks Hydrogen Electric Propulsion for Large Aircraft*. Shirley, GKN Aerospace.

Available from: <https://bit.ly/3N1Gbaz>

Archived at: <https://perma.cc/TD4G-NEZS>

GULLERS, Anna, 2022. *An EleFanT in the Air*. Stockholm: KTH Royal Institute of Technology. News ITM; Feb 02, 2022.

Available from: <https://www.kth.se/en/itm/nyheter/en-elephant-ovan-molnen-1.1139490>

Archived at: <https://perma.cc/S5SQ-EP6A>

HARTMANN, Johannes, 2022. Neue Flugzeugkonzepte für den klimaneutralen Luftverkehr. In: *Flugzeugbau der Zukunft*. Berlin, Neun Zeichen GmbH.

Available from: <https://bit.ly/3H08DG0> (Closed Access)

Archived at: <https://perma.cc/X2HV-XE66>

HEPPERLE, Martin, 2012. Electric Flight – Potential and Limitations. In: *Energy Efficient Technologies and Concepts of Operations*. Brüssel: NATO. Report: MP-AVT-209-09.

Available from: <https://elib.dlr.de/78726/>

HM GOVERNMENT, 2021. *UK Hydrogen Strategy*. Report: CP 475.

Available from: <https://www.gov.uk/government/publications/uk-hydrogen-strategy>

Archived at: <https://perma.cc/MPN2-SCJ9>

HOERNER, Siegfried F., 1965. *Practical Information on Aerodynamic Drag and Hydrodynamic Resistance*. Bakersfield: Hoerner Fluid Dynamics.

Available from: <https://archive.org/details/FluidDynamicDragHoerner1965>

HOIDIS, Jana, 2020. A Creative Drive For The Future Of Flight. In: *DLRmagazine*. Köln, DLR, No. 164, pp. 16-19.

Available from: <https://bit.ly/41CZfjI>

Archived at: <https://perma.cc/2A4P-P77S>

ICEMAC, 2023. *Catalog*. Istanbul

Available from: <https://www.icemac.net/wp-content/uploads/2016/12/catalog.pdf>

Archived at: <https://perma.cc/XD8N-SV7B>

INNOVATUS, 2020. *Scottish Hydrogen Fuel Tank - SHYFT*. Monkton: Innovatus Technologies Ltd.

Available from: <https://innovatustech.co.uk/product>

Archived at: <https://perma.cc/XUW3-YEK2>

JANSEN, Ralph H., et al., 2018. Overview of NASA Electrified Aircraft Propulsion Research for Large Subsonic Transports. IN: *53rd AIAA/SAE/ASEE Joint Propulsion Conference, Atlanta, 10-12 July 2017*. Atlanta, AIAA, pp. 1-20.

Available from: <https://doi.org/10.2514/6.2017-4701> (Closed Access)

Archived at: <https://perma.cc/9M5D-G7XN>

JENKINSON, Lloyd, 2000. *Aircraft Data File*.

Available from: <https://bit.ly/41dKJy0>

Archived at: <https://perma.cc/B3XT-R93L>

JOHANNING, Andreas, 2014. *Configuration for Scenario 2015 (Possible A320 Successor)*.

Available from: <https://www.fzt.haw-hamburg.de/pers/Scholz/Airport2030.html>

Archived at: <https://perma.cc/5GRH-BPYQ>

JOHNSON, Wayne, 2015. *NDARC – NASA Design and Analysis of Rotorcraft*. NASA: Moffett Field. Report: NASA/TP-2015-218751, Ames Research Center.

Available from: <https://ntrs.nasa.gov/citations/20150021267>

KADYK, Thomas, et al., 2018. Analysis and Design of Fuel Cell Systems for Aviation. In: *Energies*, No. 11, Nr. 2.

Available from: <https://doi.org/10.3390/en11020375>

KELLERMANN, Hagen, et al., 2019. Assessment of Aircraft Surface Heat Exchanger Potential. In: *9th EASN International Conference on Innovation in Aviation & Space*, Athens, 03-06 September 2019. Basel: MDPI, pp. 99-118.

Available from: <https://doi.org/10.3390/aerospace7010001>

- KHANDELWAL, Bhupendra, et al., 2013. Hydrogen Powered aircraft: The Future of Air Transport. In: *Progress in Aerospace Sciences*, vol. 60, July 2013, pp. 45-59.  
Available from: <https://doi.org/10.1016/j.paerosci.2012.12.002> (closed access)  
Archived at: <https://perma.cc/46L9-7CJK>
- KHANG, Daehoon, et al., 2022. Review of the Liquid Hydrogen Storage Tank and Insulation System for the High-Power Locomotive. In: *Selected Papers from the 10 th Asia-Pacific Forum on Renewable Energy (AFORE 2021)*. Basel: MDPI.  
Available from: <https://doi.org/10.3390/en15124357>
- KIM, Jeong Hwan, et al., 2022. Thermal-Structural Characteristics of Multi-Layer Vacuum-Insulated Pipe for the Transfer of Cryogenic Liquid Hydrogen. In: *Metals*, vol. 12, Nr. 549. Basel: MDPI.  
Available from: <https://doi.org/10.3390/met12040549>
- KOZULOVIC, Dragan, 2020. Heat Release of Fuel Cell Powered Aircraft. In: *Proceedings of Global Power and Propulsion Society*, Chania, 7-9 September 2020. Zug: GPPS.  
Available from: <https://bit.ly/3H2M3Na>  
Archived at: <https://perma.cc/C7HT-WFCT>
- LOFTIN, Laurence, 1980. *Subsonic Aircraft: Evolution and the Matching of Size to Performance*, Hampton, Virginia: National Aeronautics and Space Administration.  
Available from: <https://ntrs.nasa.gov/citations/19800020744>
- NOLAND, Dominic, 2021. Hydrogen Electric Airplane. A Disruptive Technological Path to Clean Up the Aviation Sector. In: *IEEE Electrification Magazine*, vol. 9, no. 1, pp. 92-102. ISSN 2325-5897.  
Available from: <https://doi.org/10.1109/MELE.2020.3047173> (Closed Access)  
Open Access at: <https://perma.cc/HNY9-W3P4>
- O'HAYRE, Ryan, et al., 2016. *Fuel Cell Fundamentals*. West Sussex: Wiley.
- PERRY, Dominic, 2021a. *ZeroAvia Says 'Hybrid' Flights of Modified Do 228 Will Begin in Late 2021*.  
Available from: <https://bit.ly/3LjYmHy>  
Archived at: <https://perma.cc/ZR5A-VVWT>
- PERRY, Dominic, 2021b. *ZeroAvia Pushes First Flight of Converted Do 228 into Early 2022, but Says Project Still on Track*.  
Available from: <https://bit.ly/3H3n2B1> (closed access)  
Archived at: <https://perma.cc/GD2E-V8NA>

PERRY, Dominic, 2022a. *Cranfield Aerospace Powers Towards First Flight of Converted Islander under Project Fresson*.

Available from: <https://bit.ly/3H51Taa> (closed access)

Archived at: <https://perma.cc/UJ7Z-KNSK>

PERRY, Dominic, 2022b. *GKN Confident Fuel Cells Could Power 96-seat aircraft as H2GEAR Project Advances*.

Available from: <https://bit.ly/40uka7J> (closed access)

Archived at: <https://perma.cc/G78K-UXKL>

PROJECT FRESSON, 2021. *Why Hydrogen?*

Available from: <https://projectfresson.co.uk/why-hydrogen>

Archived at: <https://perma.cc/4AK8-BD7S>

REACTION ENGINES, 2022. *Project Fresson Update – Phase 1 Underway*.

Available from: <https://reactionengines.co.uk/project-fresson-update-phase-1-underway/>

Archived at: <https://perma.cc/LAF4-97SC>

Renouard-Vallet, Gwenaëlle, et al., 2012. Fuel Cells for Civil Aircraft Application: On-Board Production of Power, Water, and Inert Gas. In: *Chemical Engineering Research and Design*, vol. 09, no. 1, pp. 3-10. ISSN 0263-8962.

Available from: <https://doi.org/10.1016/j.cherd.2011.07.016> (closed access)

Archived at: <https://perma.cc/93M9-8RGH>

RITCHIE, Hannah, 2022. *Climate Change and Flying: What Share of Global CO<sub>2</sub> Emissions Comes from Aviation?*

Available from: <https://ourworldindata.org/co2-emissions-from-aviation>

Archived at: <https://perma.cc/3XFP-HV74>

SAMPSON, Ben, 2021. GKN to Develop Nested Fan Technology for Electric Aircraft. In: *Aerospace Testing International*. Kent: Mark Allen Group.

Available from: <https://bit.ly/3AkVvYr>

Archived at: <https://perma.cc/47CJ-3KDN>

SCHOLZ, Dieter, 2015. *Aircraft Design*. Lecture Notes. Hamburg University of Applied Sciences.

Available from: <http://LectureNotes.AircraftDesign.org>

SCHOLZ, Dieter, 2020. *Der Propellerwirkungsgrad – Einfache Berechnungen*. Memo. Hamburg University of Applied Sciences.

Available from: <https://www.fzt.haw-hamburg.de/pers/Scholz/Aero/>

Archived at: <https://perma.cc/RK36-UC7S>

SCHOLZ, Dieter, 2022. *Aviation and Climate – An Overview*. Presentation. Hamburg University of Applied Sciences.

Available from: <https://bit.ly/42CKE8y>

Archived at: <https://perma.cc/QM9H-W8EV>

SEBAYANG, Andreas, 2022. Das DLR als Virtueller Flugzeugbauer für Emissionsfreies Fliegen. In: *Airliners.de*. Berlin: Neun Zeichen GmbH.

Available from: <https://bit.ly/40xkX7V> (closed access)

Archived at: <https://perma.cc/MGW8-4G6N>

SEEKT, Kolja, 2010. *Conceptual Design and Investigation of Hydrogen-Fueled Regional Freighter Aircraft*.

Available from: <https://www.fzt.haw-hamburg.de/pers/Scholz/GF/>

Archived at: <https://perma.cc/5EKU-XBM9>

SIEWERT, Axel, 2000. *Bewertung von Rumpfquerschnitten Großer Passagierflugzeuge*. Thesis. Hamburg University of Applied Sciences.

Available from: <https://www.fzt.haw-hamburg.de/pers/Scholz/arbeiten/>

Archived at: <https://perma.cc/J26H-27V8>

SKYBRARY, 2023. *ICAO Aerodrome Reference Code*.

Available from: <https://www.skybrary.aero/articles/icao-aerodrome-reference-code>

Archived at: <https://perma.cc/BT7E-ACJK>

SPIEGEL, Colleen, 2017. Water Management for PEM Fuel Cells. In: *Fuel Cell Store*. Bryan: Fuel Cell Store.

Available from: <https://bit.ly/3V2au2X>

Archived at: <https://perma.cc/D9EU-72KE>

STROMAN, Richard O., et al., 2010. *Cooling System Design for PEM Fuel Cell Powered Air Vehicles*. Washington: Navel Research Laboratory. Report: NRL/MR/6110—10-9253, Department: Chemical Dynamics and Diagnostics Branch, Chemistry Division.

Available from: <https://bit.ly/3UVyBR1>

Archived at: <https://perma.cc/XBK2-GPKK>

SVENSSON, Fredrik, et al., 2004. Reduced Environmental Impact by Lowered Cruise Altitude for Liquid Hydrogen-Fueled Aircraft. In: *Aerospace Science and Technology*. Paris: Elsevier, vol. 8, no. 4, pp. 307-320.

Available from: <https://doi.org/10.1016/j.ast.2004.02.004> (Closed Access)

Open Access at: <https://perma.cc/TM2G-Q5Q8>

TEEUWEN, Yorick, 2017. *Propeller Design for Conceptual Turboprop Aircraft*. Master Thesis. Delft University of Technology.

Available from: <https://bit.ly/3pjEnQG>

Archived at: <https://perma.cc/M8YN-6UR6>

THOMSON, Roland, et al., 2020. *Hydrogen. A Future Fuel for Aviation?* Munich: Roland Berger GMBH.

Available from: <https://bit.ly/3ozPBQp>

Archived at: <https://perma.cc/XZQ2-QWFY>

UNITED NATIONS, 2022. *What is Climate Change?*

Available from: <https://www.un.org/en/climatechange/what-is-climate-change>

Archived at: <https://perma.cc/532K-82JQ>

U.S. DEPARTMENT OF ENERGY, 2022. *Hydrogen Storage*. Washington: U.S. Department of Energy, Energy Efficiency & Renewable Energy.

Available from: <https://www.energy.gov/eere/fuelcells/hydrogen-storage>

Archived at: <https://perma.cc/SZU5-84ZE>

VERSTRAETE, Dries, et al., 2010. Hydrogen Fuel Tanks for Subsonic Transport Aircraft. In: *International Journal of Hydrogen Energy*. Miami: International Association for Hydrogen Energy, vol. 35, no. 20, pp. 11085-11098.

Available from: <https://doi.org/10.1016/j.ijhydene.2010.06.060> (Closed Access)

Archived at: <https://perma.cc/TH5A-9934>

VRATNY, Patrick Christoph, 2018. *Conceptual Design Methods of Electric Power Architectures for Hybrid Energy Aircraft*. PhD Thesis. Technische Universität München.

Available from: <https://mediatum.ub.tum.de/1445695>

Archived at: <https://perma.cc/86EJ-2CQJ>

WESTENBERGER, Andreas, 2003. *Liquid Hydrogen Fuelled Aircraft – System Analysis*. Final Technical Report. Hamburg: Airbus Deutschland GmbH.

Available from: <https://bit.ly/3B3yWbh>

Archived at: <https://perma.cc/DY79-ENPS>

WIKIMEDIA, 2022. *Storage Density of Hydrogen under Certain Pressure and Temperature Conditions*.

Available from: <https://bit.ly/3Lp1iTm>

Archived at: <https://perma.cc/RMF4-5TDR>

WIKIPEDIA, 2022. *Zero-Emission*.

Available from: [https://en.wikipedia.org/wiki/Zero\\_emission](https://en.wikipedia.org/wiki/Zero_emission)

Archived at: <https://perma.cc/8MET-M9VF>

WIKIPEDIA, 2023a. *Balance of Plant*.

Available from: [https://en.wikipedia.org/wiki/Balance\\_of\\_plant](https://en.wikipedia.org/wiki/Balance_of_plant)

Archived at: <https://perma.cc/6P9S-AYC2>

WIKIPEDIA, 2023b. *Drivetrain*.

Available from: <https://en.wikipedia.org/wiki/Drivetrain>

Archived at: <https://perma.cc/B3YR-29VX>

WIKIPEDIA, 2023c. *Airframe*.

Available from: <https://en.wikipedia.org/wiki/Airframe>

Archived at: <https://perma.cc/3EPY-D5HX>

WIKIPEDIA, 2023d. *Ducted Fan*.

Available from: [https://en.wikipedia.org/wiki/Ducted\\_fan](https://en.wikipedia.org/wiki/Ducted_fan)

Archived at: <https://perma.cc/4PR4-8WBN>

WIKIPEDIA, 2023e. *Turboprop*.

Available from: <https://en.wikipedia.org/wiki/Turboprop>

Archived at: <https://perma.cc/8E6Y-WMG2>

WIKIPEDIA, 2023f. *Heat Exchanger*.

Available from: [https://en.wikipedia.org/wiki/Heat\\_exchanger](https://en.wikipedia.org/wiki/Heat_exchanger)

Archived at: <https://perma.cc/HE8C-2DSW>

WINNEFELD, Christopher, et al., 2018. Modelling and Designing Cryogenic Hydrogen Tanks for Future Aircraft Applications. In: *Towards a Transformation to Sustainable Aviation Systems*. Basel: MDPI.

Available from: <https://doi.org/10.3390/en11010105>

ZEROAVIA, 2020a. *ZeroAvia Conducts UK's First Commercial-Scale Electric Flight*.

Available from: <https://www.zeroavia.com/press-release-23-06-2020>

Archived at: <https://perma.cc/U9S4-TNL3>

ZEROAVIA, 2020b. *ZeroAvia Completes World First Hydrogen-Electric Passenger Plane Flight*.

Available from: <https://www.zeroavia.com/press-release-25-09-2020>

Archived at: <https://perma.cc/ND9R-ZF3D>

ZEROAVIA, 2021a. ZeroAvia Expand its Hydrogen-Electric Aviation program to 19-Seat Aircraft and Raises Addition \$13 Million in Funding for Large Engine Development.

Available from: <https://www.zeroavia.com/19-seater-release>

Archived at: <https://perma.cc/YKX8-KJR6>

ZEROAVIA, 2021b. De Havilland and ZeroAvia Announce Memorandum of Understanding (MOU) to Develop Hydrogen-Electric Engine Program for Dash 8-400 Aircraft.

Available from: <https://www.zeroavia.com/de-havilland>

Archived at: <https://perma.cc/7SUG-BXFY>

ZEROAVIA, 2021c. MHIRJ and ZeroAvia to collaborate on the design & development of Zero Emission propulsion technology for Regional Jets.

Available from: <https://www.zeroavia.com/mhirj>

Archived at: <https://perma.cc/F447-RVPF>

ZEROAVIA, 2022a. Ravn Alaska Orders 30 Hydrogen-Electric Engines from ZeroAvia.

Available from: <https://www.zeroavia.com/ravn-alaska>

Archived at: <https://perma.cc/Q2GK-F72D>

ZEROAVIA, 2022b. American Airlines Announces Investment in Hydrogen-Electric Engine Developer ZeroAvia.

Available from: <https://www.zeroavia.com/aa-investment>

Archived at: <https://perma.cc/L4N9-BYUC>

ZULAWSKI, Piotr, et al., 2021. Thermal Management Phase 4 Deliverables. Abingdon: Reaction Engines.

All online resources have been accessed on 2023-05-02 or later.

## Appendix A – Matching Chart Conventional A320

This section present the matching chart which has been made with the spreadsheet “A-C\_Preliminary\_SizingA320\_CFM56”.

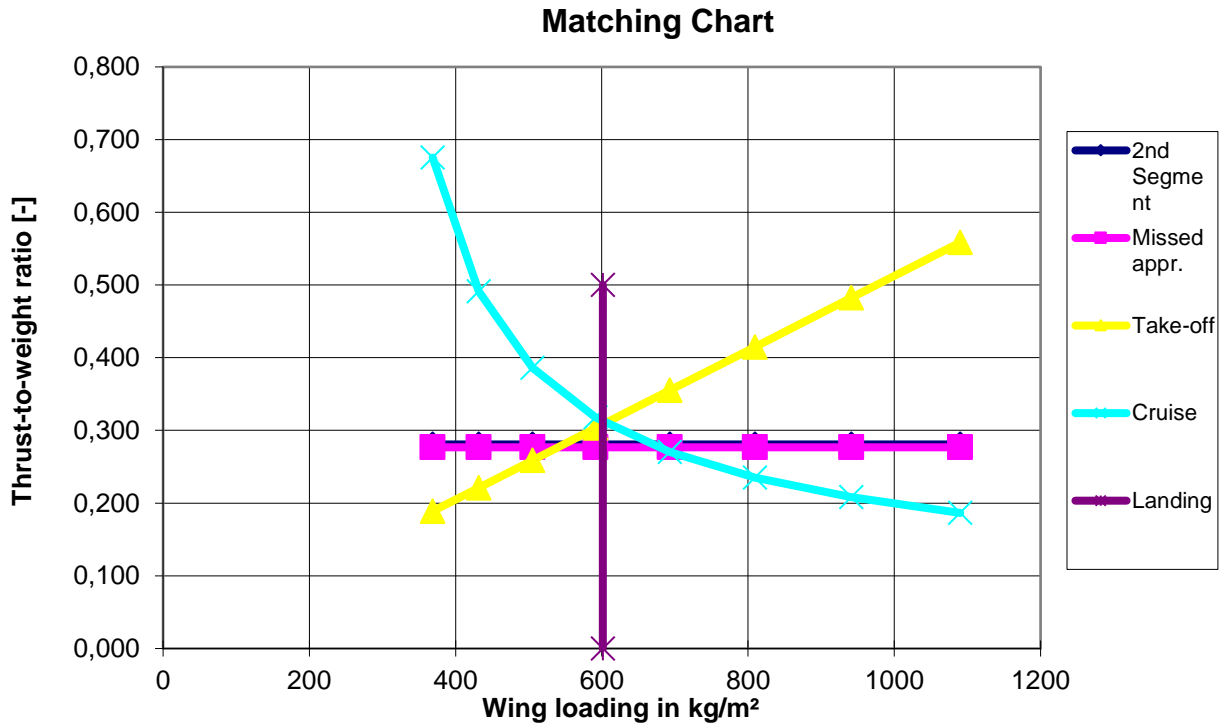


Figure A.1 Matching Chart conventional A320

## Appendix B – Matching Chart Turboprop A320

This section present the matching chart which has been made with the spreadsheet “PreSTo-Classic-Prop\_final2\_SLZ”.

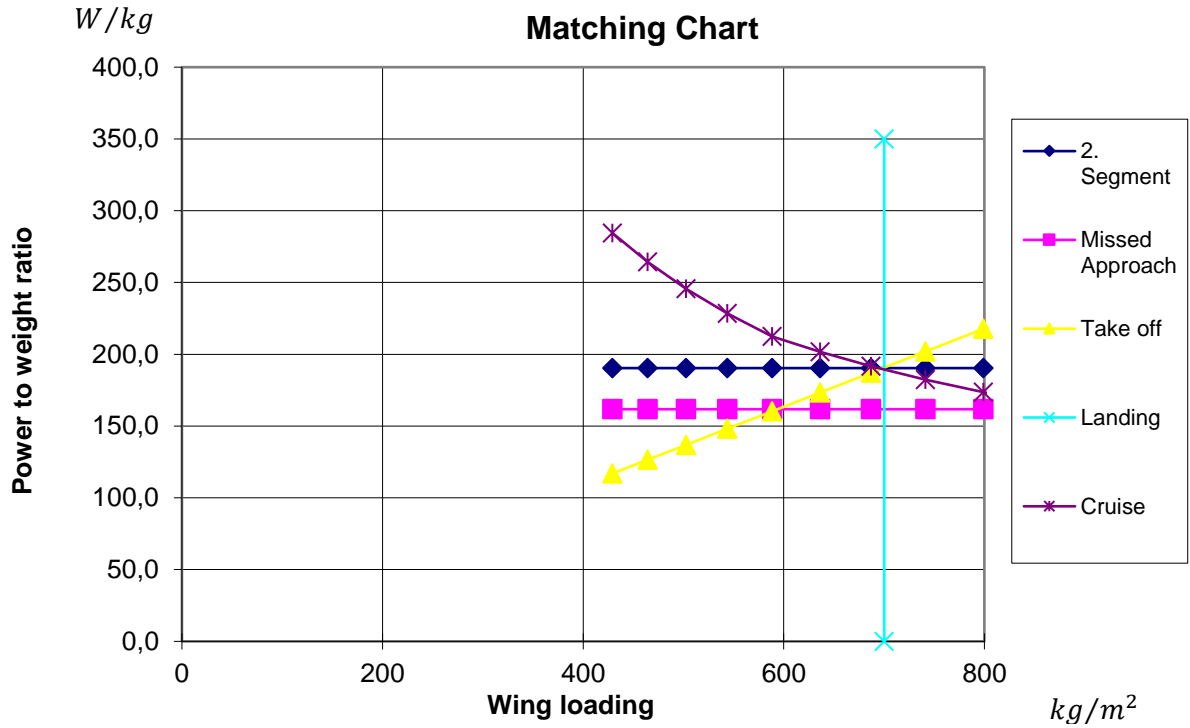
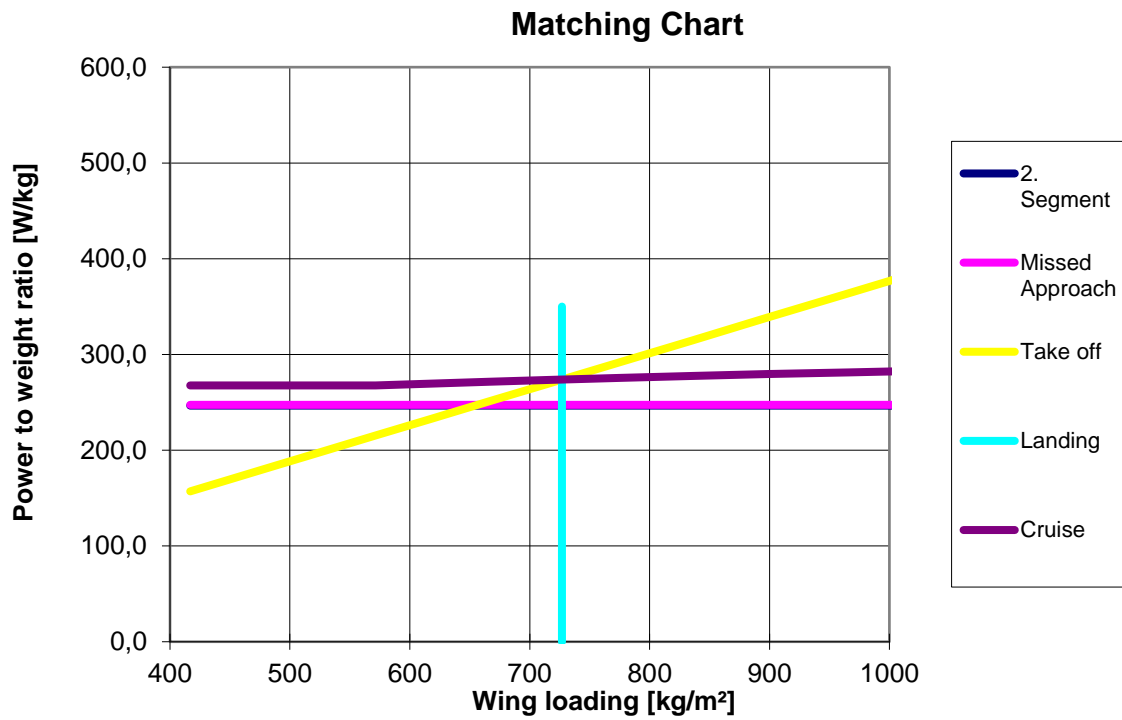


Figure B.1 Matching Chart conventional A320

## Appendix C – Matching Chart Hydrogen-Electric A320 Current Technology

This section present the matching chart which has been made with the spreadsheet “PreSTo-Classic-hydrogen\_final\_current\_technology”.



**Figure C.1** Matching Chart hydrogen A320 with current technology

## Appendix D – Matching Chart Hydrogen-Electric A320 Future Technology

This section present the matching chart which has been made with the spreadsheet “PreSTo-Classic-hydrogen\_final\_future\_technology”.

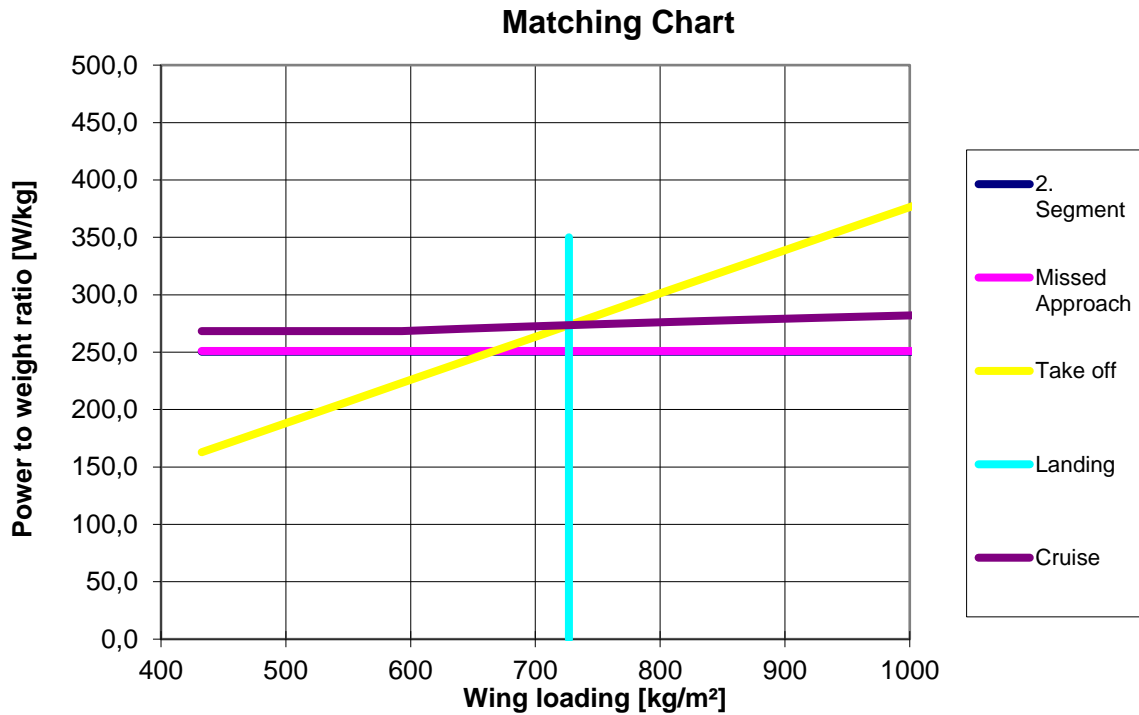


**Figure D.1** Matching Chart hydrogen A320 with future technology